

## **Response to SC1 - Michael Henehan**

We wish to thank Michael Henehan for his helpful comments on the manuscript and previous help with the code. We believe that we addressed all of the major comments as indicated in the discussion below and the updated document.

The updated manuscript and figures can be found at the end after this response.

**Comment SC1 1:** The authors on several occasions highlight the difference between their *G. ruber* data and the slope obtained by our culture experiments (Lines 385-387; 422-425; lines 525-526; 537-538; 563). In lines 422-425 the picture as presented is particularly confusing, since the authors first suggest “there is a difference in calibrations”, then say “this is particularly notable for *G. ruber*”, but then say “the sensitivity of the species analysed are not statistically different”. In truth, only the final sentence is true (with the exception of the clause “and are close to unity”. A slope of  $1.12 \pm 1.67$  is within uncertainty of our culture slope (0.6), and could technically allow a slope as low as  $-0.55$ : i.e. there is no significant difference between the slope they suggest and the slope that we observe in culture.

Framing this as a difference seems even more odd given the authors do not draw any distinction between their *T. sacculifer* slope and that of previous calibrations, because their bounds of uncertainty do not allow it- so it seems logically inconsistent to draw distinctions for *ruber* where the statistical difference is equally unfounded. I would suggest the authors go through the manuscript and revise their phrasing to reflect this lack of statistically significant difference. Including “the sensitivity of  $\delta^{11}B$  to pH is not statistically different from unity for *G. ruber*” as a main conclusion in line 563, for example, implies this study is in disagreement with cultures (which it isn't), and that we should consider a slope of 1 to be potentially suitable for this species. In reality, were we to calculate  $pCO_2$  with the slope and intercept that the authors suggest ( $m=1.12$ ,  $c=-1.23$ ), the fit of the downcore record of *G. ruber* from Chalk et al. 2017 with ice-core  $pCO_2$  would be considerably worse (see attached Fig. 1). The magnitude of  $pCO_2$  change between glacial and interglacials (i.e. the parameter that is driven by the slope of the calibration) is underestimated, with  $pCO_2$  too high in glacial by  $\sim 50$  ppm. The improved fit of the down-core record with  $pCO_2$  from ice-cores when our *ruber* calibration is used, however (see Chalk et al. 2017), offers support for the shallower-than-unity slope we observed in this species. Incidentally, also, an R-squared of 0.98 for the *ruber* core-top data presented in this study seems anomalously high relative to the scatter/uncertainty bounds in the dataset- can the authors be clear how this R-squared is computed? Is it the average R-squared of Monte Carlo regressions plotted through datapoints randomly subsampled from within the x- and y-uncertainties? Or is this simply a least-squares linear regression through the central tendencies of the datapoints? The former might be more representative, but as long as the authors are clear about what they are describing that is the main thing.

**Response 1:** *We have mitigated our discussion, especially because our dataset is too limited and our trend driven by two datapoints (WP07-1 and FC01-a). The results presented for the sensitivity > 1 of  $\delta^{11}B$  carbonate to  $\delta^{11}B$  borate have been clearly written as speculative in the text; first of all because when doing the bootstrap on all compiled data the regression is similar to Raitzsch et al., (2018), sensitivity of  $0.46 \pm 0.34$  (updated table 3) compared to  $0.45 \pm 0.16$  for Raitzsch et al., (2018) and as highlighted the uncertainties based on 5 points is important and finally  $pCO_2$  reconstructions would not be consistent with the Vostok  $pCO_2$  record.*

*The  $R^2$  were calculated with R doing a linear regression not taking into account all simulated values of the Monte Carlo Simulation. Because we did not find a way to extract those data, we decided to not present the  $R^2$  and p-value.*

**Comment SC1 2:** The authors report our generic culture intercept for *ruber* in their Table 3 (9.52), but erroneously list the size fraction as  $\sim 250 \mu\text{m}$ . I would like to point them to Fig. 6 of this 2013 paper, where we give the average size fraction of our cultures to be  $\sim 380 \mu\text{m}$ . A suggested size fraction correction on the intercept is given, such that for 300-355  $\mu\text{m}$  it would be 8.87. On this same note, the authors also combine a wide size fraction (250-400  $\mu\text{m}$ ) for *G. ruber*, which given size-related offsets from the culture calibration (as shown in Fig. 6 of Henehan et al. 2013) has the potential over such a large range to skew the data, due to size-related changes in  $\delta^{11}\text{B}$ . Can the authors give some estimate as to the distribution of test sizes within their broad sample range, so as to make them more easily comparable to published data?

**Response 2:** *I changed the size fraction in Table 3, I missed this information in your paper.*

*Most of the samples have been picked in the 250-300 size fraction (average weight/ shell of  $11 \pm 4 \mu\text{g}$  ( $n=4$ , SD) only when measurements were realized), we chose a restrained size fraction to avoid this size-related variability (at least in our calibration), we also chose this lower size fraction because some of the sites did not present shells in the higher size fractions and we wanted to stay consistent. Now, when compiling all the data this variability is not constrained.*

*From your paper, our weight/ shell variability could lead to an offset up to  $\sim 1\%$  that we acknowledged can explain most of the variability for our *G. ruber* data.*

*I have added line 582 “Henehan et al., (2013) reported a lighter  $\delta^{11}\text{B}$  with smaller test size, our sample add a weight/shell of  $11 \pm 4 \mu\text{g}$  ( $n=4$ , SD) which could also explain this variability.”*

**Comment SC1 3:** The authors screened for clay contamination using Ti/Ca ratios, as Al/Ca values were difficult to measure with their introduction system. However, they do not provide these data. Clay may carry isotopically-light sorbed  $\delta^{11}\text{B}$  with it, and introduce bias towards lighter values. To allow maximum confidence in the data, and see which datapoints if any might have some influence of clay, can the authors please provide the Ti/Ca ratios in Table 2?

**Response 3:** *We only had a contamination at one site which is not presented in the paper (site E035), with high Mn/Ca of  $79 \mu\text{mol/mol}$  and high Fe/Ca of  $3.0 \text{ mmol/mol}$ . We have added the Mn/Ca and Fe/Ca in Table 2. We didn't add the Ti/Ca ratios as we monitored it with the raw ratios and do not have the absolute values. However, a minor correlation was found between Ti/Ca and B/Ca ( $R^2=0.0887$ ). Some of our samples have elevated Fe/Ca concentration but no high Mn/Ca, we don't suspect contamination from those samples since this high Fe can potentially come from  $\text{MnCO}_3$  overgrowth and this over growth will have negligible quantity of Mg and B unlike the Fe-Mn oxide and hydroxides.*

**Comment SC1 4:** In Section 4.2.3 (note the paper skips 4.2.4 and goes straight on to 4.2.5?), the authors pool ‘deeper-dwelling’ foraminiferal species together, but this seems a bit unfounded since these foraminifera don't even have the same symbiont types (chrysophyte vs. dinoflagellate), and have quite different ecologies. I'm not convinced there's enough of an a priori reason to even do this in the first place. However, I see that the authors do already concede this may be unfounded.

**Response 4:** *We developed the discussion about the symbionts type/photosynthesis, lines 485-543.*

*Even if the data are limited, we don't want to reject a chrysophytes/insolation limiting threshold resulting in a respiration-driven environment where this calibration can make sense. I have tried to reply to this comment for reviewer 2:*

*“I have tried to improve the discussion, focusing on the symbionts/photosynthesis, because the story is of course more complex.*

*From what I see in the literature is that *T. sacculifer*, *G. ruber*, *O. universa* have mostly dinoflagellates symbionts (can have chrysophyte as well) where *G. tumida*, *G. menardii*, *P. obliquiloculata* and *N. dutertrei* will have chrysophyte algal symbionts. The photosynthesis is dependent of the nature of the host/symbionts interactions, symbionts type (pigment associated for light absorption efficiency), symbionts*

density. The recent study from Tagaki et al., (2019) is really helpful as he constrained the photosynthesis activity, light absorption efficiency and the symbiont density of those species.

*Fv/Fm* (photosynthetic activity) *T. sacculifer* > *G. menardii* > *O. universa* > *G. ruber* (white) > *N. dutertrei* > *P. obliquiloculata*

$\sigma_{psi}$  (light absorption efficiency) *N. dutertrei* > *P. obliquiloculata* > *G. menardii* > *G. ruber* > *T. sacculifer* > *O. universa*

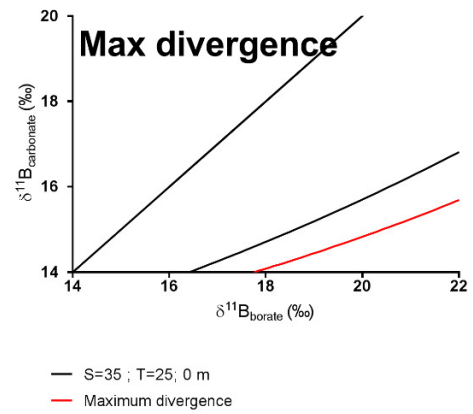
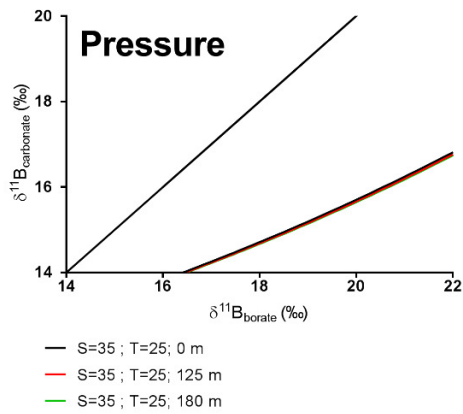
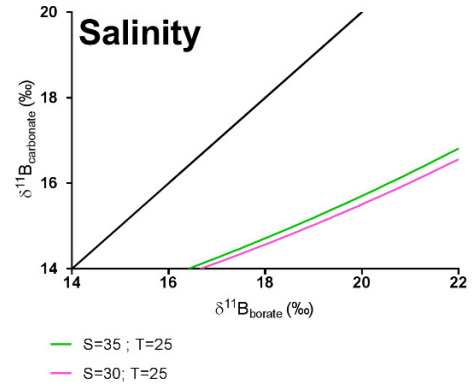
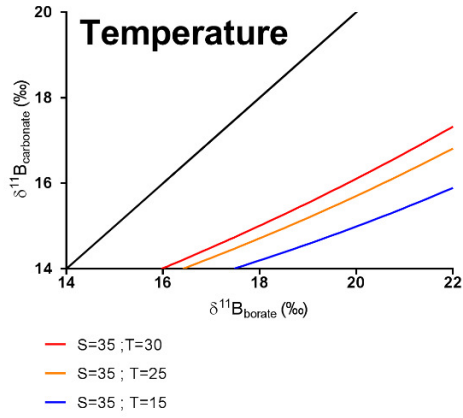
*Chla/biomass* *T. sacculifer* > *O. universa* > *G. ruber* > *N. dutertrei* > *G. menardii* > *P. obliquiloculata*

What I assume is that *T. sacculifer*, *O. universa* and *G. ruber* photosynthesis are likely to be more affected by changes in insolation than other species due to their symbiont density, high photosynthetic capacity and their light absorption efficiency. Which is still in line with the argumentation we are giving. Also, the fact that the deeper dwellers have this low boron isotopic signature is likely due to a lower symbiont density, lower photosynthetic activity and a reduced insolated environment. *P. obliquiloculata* has the lowest density and photosynthetic activity, which would translate in a respiration driven environment the fact that most of the species are following this trend would go in the sense of a respiration driven environment.

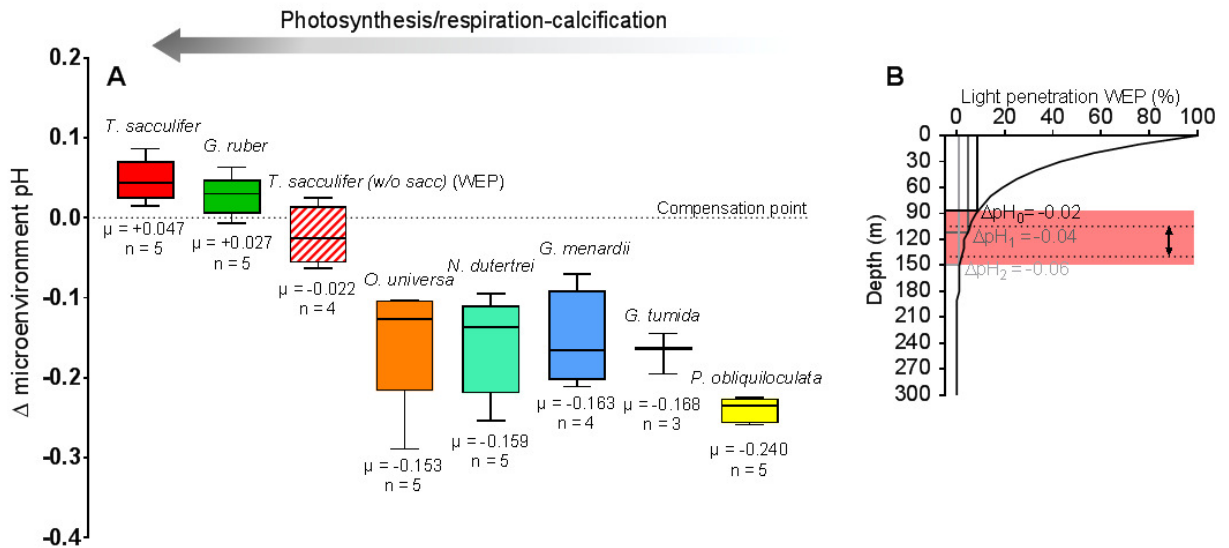
Also the fact that *O. universa* is following this trend would, I think, whether be due light limitation and/or a different symbiont due to its deeper depth.”

**Comment SC1 5:** In section 3.9, the authors make no mention of how they calculated  $pK^*B$  for each foraminifera. I take it they did indeed account for changes in  $pK^*B$  with temperature, salinity and pressure? It may sound blindingly obvious, but I'm constantly amazed at how many people make this error. On a similar theme Fig S3 the pH lines are no doubt helpful, but I'm not sure how the authors managed to calculate them, given the  $pK^*B$  is different for each foram. Is this calculated using the mean  $pK^*B$  of each of the forams plotted? This figure makes me worry that the authors just chose a single value of  $pK^*B$  for all forams in all calculations of the paper, which would be wrong.

**Response 5:** The  $pKB^*$  were calculated taking into account temperature, salinity and pressure in all calculations of the paper except in Fig S3 to draw the  $\Delta$ microenvironment pH line. We agree that individually, the parameters can significantly influence the calculations, especially temperature, then salinity and a minor effect for pressure. Maximum divergence was observed for site CD107-a due to colder temperature however for the other sites due to our uncertainties, the results were still consistent with our discussion.



However, I have directly calculated the pH difference from the microenvironment for each of the species (every calculations taking into account, P, T and S). Results are shown in Figure 7 (or below).



**Comment SC1 6:** I think the decision to group ‘shallow-dwelling’ foraminifera (note it is not clearly defined what species this includes in any caption) in Fig. S4 (and in the text where this is referenced) is I think unfounded. It produces a correlation between B/Ca and Borate/DIC, sure, but it’s entirely driven by the interspecies difference between *ruber* and *sacculifer*, and we know from Kat Allen’s work for example that these species have fundamentally different B/Ca-Borate/DIC relationships.. they shouldn’t be lumped together in one group. As it is, it makes this look like a carbonate system relationship when on an intra-species level there is no significant correlation with the carbonate system (as we also observed elsewhere).

**Response 6:** *We group G. ruber and T. sacculifer data in the “shallow-dwelling” foraminifera. It is true that this calibration can be driven by interspecific differences. Then, I have added calibrations for T. sacculifer and G. ruber.*

*Line 429-432: “B/Ca ratios are presented in Table 2. Values are species specific consistent with previous work (e.g., compiled in Henehan et al., 2016) with ratios higher for G. ruber > T. sacculifer > T. sacculifer (w/o sacc) > P. obliquiloculata > O. universa > > G. menardii > N. dutertrei > G. tumida > G. inflata > N. pachyderma > G. bulloides (Fig. 7). This study supports interspecific B/Ca ratios (Allen and Hönisch, 2012; Henehan et al., 2016).”*

*Line 565-568: “Those interspecific differences still remain to be explained, however, part of this variability is likely due to changes of the carbonate chemistry of the microenvironment resulting in changing competition between borate and bicarbonate ion, but we can’t exclude specific biological processes, and for the mixed-dweller (e.g. non respiration-driven microenvironment) day/night calcification ratios.”*

1 Seawater pH reconstruction using boron isotopes in multiple planktonic foraminifera species with  
2 different depth habitats and their potential to constrain pH and pCO<sub>2</sub> gradients  
3

4  
5 Maxence Guillermic<sup>1,2</sup>, Sambuddha Misra<sup>3,4</sup>, Robert Eagle<sup>1,2</sup>, Alexandra Villa<sup>2,5</sup>, Fengming Chang<sup>6</sup>,  
6 Aradhna Tripathi<sup>1,2</sup>  
7  
8  
9

10  
11 <sup>1</sup> Department of Earth, Planetary, and Space Sciences, Department of Atmospheric and Oceanic  
12 Sciences, Institute of the Environment and Sustainability, UCLA, University of California – Los  
13 Angeles, Los Angeles, CA 90095 USA

14 <sup>2</sup> Laboratoire Géosciences Océan UMR6538, UBO, Institut Universitaire Européen de la Mer, Rue  
15 Dumont d'Urville, 29280, Plouzané, France

16 <sup>3</sup> Indian Institute of Science, Centre for Earth Sciences, Bengaluru, Karnataka 560012, India

17 <sup>4</sup> The Godwin Laboratory for Palaeoclimate Research, Department of Earth Sciences, University of  
18 Cambridge, UK

19 <sup>5</sup> Department of Geology, University of Wisconsin-Madison, Madison, WI 53706 USA

20 <sup>6</sup> Key Laboratory of Marine Geology and Environment, Institute of Oceanology, Chinese Academy of  
21 Sciences, Qingdao 266071, China  
22  
23  
24  
25  
26  
27  
28  
29  
30  
31  
32  
33  
34  
35  
36

37 Submitted to Biogeosciences  
38  
39  
40

41 \*Corresponding author:

42 E-mail address: maxence.guillermic@gmail.com  
43

44 **ABSTRACT**

45

46 Boron isotope systematics of planktonic foraminifera from core-top sediments and culture experiments have  
47 been studied to investigate the sensitivity of  $\delta^{11}\text{B}$  of their calcite tests to seawater pH. However, our knowledge  
48 of the relationship between  $\delta^{11}\text{B}$  and pH remains incomplete for many taxa. Thus, to expand the potential scope  
49 of application of this proxy, we report  $\delta^{11}\text{B}$  data for 7 different species of planktonic foraminifera from sediment  
50 core-tops. We utilize a method for the measurement of small samples of foraminifera and calculate the  $\delta^{11}\text{B}$ -  
51 calcite sensitivity to pH for *Globigerinoides ruber*, *Trilobus sacculifer* (sacc or w/o sacc), *Orbulina universa*,  
52 *Pulleniatina obliquiloculata*, *Neogloboquadrina dutertrei*, *Globorotalia menardii* and *Globorotalia tumida*,  
53 including for unstudied core-tops and species. The sensitivity of  $\delta^{11}\text{B}_{\text{carbonate}}$  to  $\delta^{11}\text{B}_{\text{borate}}$  (eg.  
54  $\Delta\delta^{11}\text{B}_{\text{carbonate}}/\Delta\delta^{11}\text{B}_{\text{borate}}$ ) in core-tops is consistent with previous studies for *T. sacculifer* and *G. ruber* and close  
55 to unity for *N. dutertrei*, *O. universa* and combined deep-dwelling species. Deep-dwelling species closely follow  
56 the core-top calibration for *O. universa*, which is attributed to respiration-driven microenvironments, likely  
57 caused by light limitation and/or symbiont/host interactions. These taxa have diverse ecological preferences and  
58 are from sites that span a range of oceanographic regimes, including some that are in regions of air-sea  
59 equilibrium and others that are out of equilibrium with the atmosphere. Our data support the premise that  
60 utilizing boron isotope measurements of multiple species within a sediment core can be utilized to constrain  
61 vertical profiles of pH and  $\text{pCO}_2$  at sites spanning different oceanic regimes, thereby constraining changes in  
62 vertical pH gradients and yielding insights into the past behavior of the oceanic carbon pumps.

## 63 1. Introduction

64 The oceans are absorbing a substantial fraction of anthropogenic carbon emissions resulting in declining  
65 surface ocean pH (Fig. 1; IPCC, 2014). Yet there is a considerable uncertainty over the magnitude of future pH  
66 change in different parts of the ocean and the response of marine biogeochemical cycles to physio-chemical  
67 parameters (T, pH) caused by climate change (Bijma et al., 2002; Ries et al., 2009). Therefore, there is an  
68 increased interest in reconstructing past seawater pH (Hönisch and Hemming, 2005; Liu et al., 2009; Wei et al.,  
69 2009; Douville et al., 2010), in understanding spatial variability in aqueous pH and carbon dioxide ( $p\text{CO}_2$ )  
70 (Foster et al., 2008; Martinez-Boti et al., 2015b; Raitzsch et al., 2018), and in studying the response of the  
71 biological carbon pump utilizing geochemical proxies (Yu et al., 2007, 2010, 2016).

72 Although proxies for carbon cycle reconstruction are complex in nature (Pagani et al., 2005; Tripathi et  
73 al., 2009, 2011; Allen and Hönisch, 2012), the boron isotope composition of foraminiferal tests is emerging as  
74 one of the more robust candidates (Hönisch et al., 2005, 2009; Ni et al., 2007; Foster et al., 2008, 2012; Bartoli et  
75 al., 2011; Henehan et al., 2013; Martinez-Boti et al., 2015b; Chalk et al., 2017). The study of laboratory cultured  
76 foraminifera has demonstrated a systematic dependence of the boron isotope composition of tests on ambient pH  
77 (Sanyal et al., 1996, 2001; Henehan et al., 2013, 2016). Core-top measurements on globally distributed samples  
78 also show a  $\delta^{11}\text{B}$  sensitivity to pH with taxa-specific offsets from the theoretical fractionation line of borate ion  
79 (Rae et al., 2011; Henehan et al., 2016; Raitzsch et al., 2018).

80 Knowledge of seawater pH, in conjunction with constraints on one other carbonate system parameter  
81 (Total Alkalinity (TA), DIC (dissolved inorganic carbon),  $[\text{HCO}_3^-]$ ,  $[\text{CO}_3^{2-}]$ ), can be utilized to constrain aqueous  
82  $p\text{CO}_2$ . Application of empirical calibrations for boron isotopes, determined for select species of foraminifera  
83 from core-tops and laboratory cultures, has resulted in accurate reconstructions of  $p\text{CO}_2$  utilizing downcore  
84 samples from sites that are in quasi-equilibrium with the atmosphere at present.  $\delta^{11}\text{B}_{\text{carbonate}}$  based reconstructed  
85 values of  $p\text{CO}_2$  are analytically indistinguishable from ice core  $\text{CO}_2$  records (Hönisch et al., 2005, 2009; Foster et  
86 al., 2008; Henehan et al., 2013; Chalk et al., 2017).

87 Therefore, the last decade has produced several studies aiming at reconstructing past seawater pH using  
88 boron isotopes to constrain atmospheric  $p\text{CO}_2$  in order understand the changes in the global carbon cycle  
89 (Hönisch et al., 2005, 2009; Foster et al., 2008, 2012, 2014; Seki et al., 2010; Bartoli et al., 2011; Henehan et al.,  
90 2013; Martinez-Boti et al., 2015a, 2015b; Chalk et al., 2017). In addition to reconstructing atmospheric  $p\text{CO}_2$ , in  
91 a few studies, the  $\delta^{11}\text{B}$  proxy has been applied to mixed-layer planktonic foraminifera at sites out of equilibrium  
92 with the atmosphere to constrain past air-sea fluxes (Foster et al., 2014; Martinez-Boti et al., 2015b). A small  
93 body of work has examined whether data for multiple species in core-top (Foster et al., 2008) and down-core  
94 samples could be used to constrain vertical profiles of pH through time (Palmer et al., 1998; Pearson and Palmer,  
95 1999).

96 In this study, we make critical additions to the emerging pool of boron isotope data of core-top  
97 planktonic foraminifera from different oceanographic regimes, including data for species that have not  
98 previously been examined. We utilize a low-blank (15 pg B to 65 pg B), high precision (2sd on the international  
99 standard JCP-1 is 0.20 ‰, n=6)  $\delta^{11}\text{B}_{\text{carbonate}}$  analysis method (down to  $\sim 250 \mu\text{g CaCO}_3$ ), modified after Misra et  
100 al. (2014), to study multiple species of planktonic foraminifera from sediment core-tops that span a range of  
101 oceanographic regimes, including open-ocean oligotrophic settings and marginal seas. We constrain calibrations  
102 for different species, and compare results to published work (Foster et al., 2008; Henehan et al., 2013; Henehan



103 et al., 2016; Martinez-Boti et al., 2015b; Raitzsch et al., 2018). We also test whether these data support the  
104 application of boron isotope measurements of multiple species within a sediment core as a proxy for constraining  
105 vertical profiles of pH and pCO<sub>2</sub>.

106

## 107 **2. Background**

### 108 **2.1 Planktonic foraminifera as archives of seawater pH**

109 Planktonic foraminifera are used as archives of past environmental conditions within the mixed layer  
110 and thermocline, as their chemical composition is correlated with the physio-chemical parameters of their  
111 calcification environment (Ravelo and Fairbanks, 1992; Elderfield and Ganssen, 2000; Dekens et al., 2002;  
112 Anand et al., 2003; Sanyal et al., 2001; Ni et al., 2007; Henehan et al., 2013, 2015, 2016; Howes et al., 2017;  
113 Raitzsch et al., 2018). The utilization of geochemical data for multiple planktonic foraminifera species with  
114 different ecological preferences to constrain vertical gradients has been explored in several studies. The  
115 framework for such an approach was first developed using modern samples of planktonic foraminifera for  
116 oxygen isotopes, where it was proposed as a tool to constrain vertical temperature gradients and study physical  
117 oceanographic conditions during periods of calcification (Ravelo and Fairbanks, 1992).

118 Because planktonic foraminifera species complete their lifecycle in a particular depth habitat due to  
119 their ecological preference (Ravelo and Fairbanks, 1992; Farmer et al., 2007), it is theoretically possible to  
120 reconstruct water column profiles of pH using data from multiple taxa (Palmer and Pearson, 1998; Anagnostou  
121 et al., 2016). The potential use of an analogous approach to reconstruct past profiles of seawater pH was first  
122 highlighted by Palmer and Pearson (1998) on Eocene samples to constrain pH-depth gradients. However, in  
123 these boron isotope-based studies, it was assumed that boron isotope offset from seawater and foraminiferal  
124 carbonate were constant, which is an assumption not supported by subsequent studies (e.g., Hönisch et al., 2003;  
125 Foster et al., 2008; Henehan et al., 2013, 2016; Raitzsch et al., 2018; Rae, 2018). Furthermore, δ<sup>11</sup>B differences  
126 between foraminifera species that inhabit waters that are the same pH makes the acquisition of more core-top  
127 and culture data essential for applications of the proxy.

128

### 129 **2.2 Boron systematics in seawater**

130 Boron is a conservative element in seawater with a long residence time (τ<sub>B</sub> ~ 14 Myr) (Lemarchand et  
131 al., 2002a). In seawater, boron exists as trigonal boric acid B(OH)<sub>3</sub> and tetrahedral borate ion B(OH)<sub>4</sub><sup>-</sup> (borate).  
132 The relative abundance of boric acid and borate ion is a function of the ambient seawater pH. At standard open  
133 ocean conditions (T = 25 °C and S = 35), the dissociation constant of boric acid is 8.60 (Dickson, 1990),  
134 implying that boron mainly exists in the form of boric acid in seawater. Since the pK<sub>B</sub> and seawater pH (e.g.,  
135 ~8.1, NBS) values are similar, it implies that small changes in seawater pH will induce strong variations in the  
136 abundance of the two boron species (Fig. 2).

137 Boron has two stable isotopes, <sup>10</sup>B and <sup>11</sup>B, with average relative abundances of 19.9 and 80.1 %,  
138 respectively. Variations in B isotope ratio are expressed in conventional delta (δ) notation:

139

$$140 \quad \delta^{11}\text{B} (\%) = 1000 \times \left( \frac{{}^{11}\text{B}/{}^{10}\text{B}_{\text{Sample}}}{{}^{11}\text{B}/{}^{10}\text{B}_{\text{NIST 951-a}}} - 1 \right) \quad (1)$$

141

142 where positive values represent enrichment in the heavy isotope  $^{11}\text{B}$ , and negative values enrichment in the light  
143 isotope  $^{10}\text{B}$ , relative to the standard reference material. Boron isotope values are reported versus the NIST SRM  
144 951 (Cantazaro et al., 1970).

145  $\text{B}(\text{OH})_3$  is enriched in  $^{11}\text{B}$  compared to  $\text{B}(\text{OH})_4^-$  with a constant offset between the two chemical  
146 species, within the range of physio-chemical variation observed in seawater, given by the fraction factor ( $\alpha$ ). The  
147 fractionation ( $\epsilon$ ) between  $\text{B}(\text{OH})_3$  and  $\text{B}(\text{OH})_4^-$  of  $27.2 \pm 0.6 \text{ ‰}$  has been empirically determined by Klochko et  
148 al., (2006) in seawater. Note, Nir et al., (2015) calculate this fractionation, using an independent method, to be  
149  $26 \pm 1 \text{ ‰}$ , which is within the analytical uncertainty of the Klochko et al., (2006) value.

150

### 151 **2.3 Boron isotopes in planktonic foraminifera calcite**

152 Many biogenic carbonate-based geochemical proxies are affected by “vital effects” or biological  
153 fractionations (Urey et al., 1951). The  $\delta^{11}\text{B}_{\text{carbonate}}$  in foraminifera exhibits species-specific offsets (see Rae et al.,  
154 2018 for review) compared to theoretical predictions for the boron isotopic composition of  $\text{B}(\text{OH})_4^-$  ( $\alpha=1.0272$ ,  
155 Klochko et al., 2006). As the analytical and technical aspects of boron isotope measurements have improved  
156 (Foster et al., 2008; Rae et al., 2011; Misra et al., 2014; Lloyd et al., 2018), evidence for taxonomic differences  
157 have not been eliminated, but have become increasingly apparent (Foster et al., 2008, 2018; Henehan et al 2013,  
158 2016; Noireaux et al., 2015; Foster et al., 2016; Rae et al., 2018; Raitzsch et al., 2018).

159 At present, culture and core-top calibrations have been published for several planktonic species  
160 including *Trilobatus sacculifer*, *Globigerinoides ruber*, *Globigerina bulloides*, *Neogloboquadrina pachyderma*,  
161 *Orbulina universa* (Foster et al., 2008; Henehan et al., 2013; Henehan et al., 2015; Sanyal et al., 1996; Sanyal et  
162 al., 2001). Although the boron isotopic composition of several species of foraminifera are now commonly used  
163 tools for reconstructing surface seawater pH, for other species, there is a lack of data constraining boron isotope  
164 sensitivity between foraminiferal carbonate and borate ion in seawater.

165

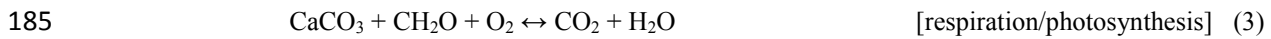
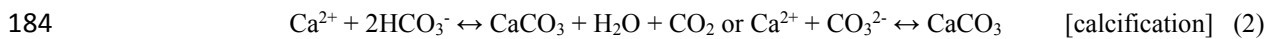
### 166 **2.4 Origin of biological fractionations in foraminifera**

167 Perforate foraminifera are calcifying organisms that maintain a large degree of biological control over  
168 their calcification space, and thus, mechanisms of biomineralization may be of significant importance in  
169 controlling the  $\delta^{11}\text{B}$  of the biogenic calcite. The biomineralization of foraminifera is based on seawater  
170 vacuolization (Erez, 2003; de Nooijer et al., 2014) with parcels of seawater being isolated by an organic matrix  
171 thereby creating a vacuole filled with seawater. Recent work has also demonstrated that even if the chemical  
172 composition of the reservoirs is modified by the organism, seawater is directly involved in the calcification  
173 process with vacuoles formed at the periphery of the shell (de Nooijer et al., 2014). Culture experiments by  
174 Rollion-Bard and Erez., (2010) have proposed that the pH at the site of biomineralization is elevated to an upper  
175 pH limit of  $\sim 9$  for the shallow-water, symbiont-bearing benthic foraminifera *Amphistegina lobifera*, which  
176 would support a pH modulation of a calcifying fluid in foraminifera. We acknowledge this is speculative as it is  
177 based upon benthic foraminifer experiments.

178 For taxa with symbionts, the microenvironment surrounding the foraminifera is chemically different  
179 from seawater due to photosynthetic activity (Jorgensen et al., 1985; Rink et al., 1998; Köhler-Rink and Kühl,  
180 2000). Photosynthesis by the symbionts elevates the pH of the microenvironment (Jorgensen et al., 1985; Rink et

181 al., 1998; Wolf-Gladrow et al., 1999; Köhler-Rink and Kühl, 2000), while calcification and respiration decrease  
182 it (Equation 2 and 3).

183



186

187  $\delta^{11}\text{B}$  in foraminifera is primary controlled by seawater pH, but is also dependent of the pH alteration of  
188 microenvironments due to calcification, respiration and symbiont photosynthesis.  $\delta^{11}\text{B}$  should therefore reflect  
189 the relative dominance of these processes and may account for species-specific  $\delta^{11}\text{B}$  offsets. Theoretical  
190 predictions from Zeebe et al. (2003) and foraminiferal data from Hönisch et al., (2003) highlighted the  
191 dominance of microenvironment pH in  $\delta^{11}\text{B}$  signature of foraminifera. Their work also suggested that for a given  
192 species, there should be a constant offset observed between the boron isotope composition of foraminifera and  
193 borate ion over a large range of pH, imparting confidence in utilizing species-specific boron isotope data as a  
194 proxy for seawater pH.

195 Comparison of boron isotope data for multiple planktonic foraminiferal species indicate that taxa with  
196 high levels of symbiont activity such as *T. sacculifer* and *G. ruber* show higher  $\delta^{11}\text{B}$  values than the  $\delta^{11}\text{B}$  of  
197 ambient borate (Foster et al., 2008, Henehan et al., 2013, Raitzsch et al., 2018). The sensitivities  
198 ( $\Delta\delta^{11}\text{B}_{\text{carbonate}}/\Delta\delta^{11}\text{B}_{\text{borate}}$  referred to as the slope) of existing calibrations suggest a different species-specific  
199 sensitivity for these species compared to other taxa (Sanyal et al., 2001; Henehan et al., 2013; Henehan et  
200 al., 2015; Raitzsch et al., 2018). For example, *Orbulina universa* exhibits a lower  $\delta^{11}\text{B}$  than *in situ*  $\delta^{11}\text{B}$  values of  
201 borate ion (Henehan et al., 2016), consistent with the species living deeper in the water column characterized by  
202 reduced photosynthetic activity.

203 It is possible that photosynthetic activity by symbionts might not be able to compensate for changes in  
204 calcification and/or respiration, leading to an acidification of the microenvironment. It is interesting to note that  
205 for *O. universa* the slope determined for the field-collected samples is not statistically different from unity ( $0.95$   
206  $\pm 0.17$ ) (Henehan et al. 2016), while culture experiments report slopes of  $\leq 1$  for multiple species including *G.*  
207 *ruber* (Henehan et al., 2013), *T. sacculifer* (Sanyal et al., 2001), and *O. universa* (Sanyal et al., 1999). More  
208 core-top and culture calibrations are needed to fully understand why different slopes are observed, which is part  
209 of the motivation for this study.

210

## 211 **2.5 Planktic foraminifera depth and habitat preferences**

212 The preferred depth habitat of different species of planktonic foraminifera depends on their ecology,  
213 which in turn relies on the hydrographic conditions. For example, *G. ruber* is commonly found in the mixed  
214 layer (Fairbanks and Wiebe, 1980; Dekens et al., 2002; Farmer et al., 2007) during the summer (Deuser et al.,  
215 1981) whereas *T. sacculifer* is present in the mixed layer until mid-thermocline depths (Farmer et al., 2007)  
216 during spring and summer (Deuser et al., 1981, 1989). Specimens of *P. obliquiloculata* and *N. dutertrei* are  
217 abundant during winter months (Deuser et al., 1989), with an acme in the mixed layer (~60m) for *P.*  
218 *obliquiloculata*, and at mid-thermocline depths for *N. dutertrei* (Farmer et al., 2007). In contrast, *O. universa*  
219 tends to record annual average conditions within the mixed layer. Specimens of *G. menardii* calcify within the  
220 seasonal thermocline (Fairbanks et al., 1982, Farmer et al., 2007, Regenberg et al., 2009), and in some regions in

221 the upper thermocline (Farmer et al., 2007), and records annual temperatures. *G. tumida* is found at the lower  
222 thermocline or below the thermocline and records annual average conditions (Fairbanks and Wiebe, 1980;  
223 Farmer et al., 2007, Birch et al., 2013).

224

### 225 3. Materials and Methods

226

#### 227 3.1 Localities studied

228 Core-top locations were selected to span a broad range of seawater pH, carbonate system parameters,  
229 and oceanic regimes. Samples from Atlantic Ocean (CD107-A), Indian Ocean (FC-01a and FC-02a), Arabian  
230 Sea (FC-13a and FC-12b) and Pacific Ocean (WP07-01, A14, and Ocean Drilling Program 806A and 807A)  
231 were analyzed; characteristics of the sites are summarized in Table 1 and S7, Fig. 3, and Fig. 4.

232 Atlantic site CD107-a (CD107 site A) was drilled in 1997 by the Benthic Boundary Layer program  
233 (BENBO) (K.S. Black et al., 1997 - cruise report RRS Charles Darwin Cruise 107). Arabian Sea sites FC-12b  
234 (CD145 A150) and FC-13a (CD145 A3200) were retrieved by the *Charles Darwin* in the Pakistan Margin in  
235 2004 (B.J. Bett et al., 2003 - cruise report n°50 RRS Charles Darwin Cruise 145). A14 was recovered by box  
236 corer in the southern area of the South China Sea in 2012. Core WP07-01 was obtained from the Ontong Java  
237 Plateau using a giant piston corer during the Warm Pool Subject Cruise in 1993. Holes 806A and 807A were  
238 retrieved on Leg 130 by the Ocean Drilling Program (ODP). The top 10 cm of sediment from CD107-A have  
239 been radiocarbon dated to be Holocene <3 ky (Thomson et al., 2000). Samples from multiple box cores from  
240 Indian Ocean sites were radiocarbon dated as Holocene <7.3 ky (Wilson et al., 2012). Samples from western  
241 equatorial Pacific Site 806B, close to site WP07-01, are dated to between 7.3-8.6 ky (Lea et al., 2000). Arabian  
242 Sea and Pacific core-top samples were not radiocarbon dated but are assumed to be Holocene.

243

#### 244 3.2 Species

245 Around 50-100 foraminifera shells were picked from the 400-500 µm fraction size for *Globorotalia*  
246 *menardii* and *Globorotalia tumida*, >500 µm for *Orbulina universa*, from the 250-400 µm fraction size for  
247 *Trilobatus sacculifer* (w/o sacc, without sacc-like final chamber), *Trilobatus sacculifer* (sacc, sacc-like final  
248 chamber), *Globigerinoides ruber* (white, sensu stricto), *Neogloboquadrina dutertrei*, *Pulleniatina*  
249 *obliquiloculata*. The samples picked for analyses were visually well preserved.

250

#### 251 3.3 Sample cleaning

252 Briefly, picked foraminifera were gently cracked open, clay removed and checked for coarse-grained  
253 silicates. The next stages of sample processing and chemical separation were performed in a class 1000 clean lab  
254 equipped with boron-free HEPA filters. Samples were then cleaned using full reductive and oxidative cleaning  
255 (Boyle and Keigwin, 1985; Barker et al., 2003). A final leaching step with 0.001N HCl was done before  
256 dissolution in 1N HCl. Each sample was divided into two aliquots: an aliquot for boron purification and one  
257 aliquot for trace element analysis.

258

#### 259 3.4 Reagents

260 Double-distilled HNO<sub>3</sub> and HCl acids (from Merck® grade) and a commercial bottle of HF Ultrapure  
261 grade were used at Brest. Double-distilled acids were used at Cambridge. All acids and further dilutions were

262 prepared using double-distilled 18.2 MΩ.cm-1 MQ water. Working standards for isotope ratio and trace element  
263 measurements were freshly diluted on a daily basis with the same acids used for sample preparation to avoid any  
264 matrix effect.

265

### 266 **32.5 Boron isotopes**

267 Boron purification for isotopic measurement was done utilizing microdistillation method developed by  
268 Gaillardet et al., (2001), for Ca-rich matrices by Wang et al., (2010) and adapted at Cambridge by Misra et al.,  
269 (2014a). 70 μL of dissolved carbonate sample was loaded on a cap of a clean fin legged 5 mL conical beaker  
270 upside down. The tightly closed beaker was put on a hotplate at 95°C for 15 hours. The beakers were taken off  
271 the hotplate and were allowed to cool for 15 min. The cap where the residue formed was replaced by a clean one.  
272 Then, 100 μL of 0.5% HF were added to the distillate.

273 Boron isotopic measurements were carried out on a Thermo Scientific @Neptune+ MC-ICP-MS at the  
274 University of Cambridge. Neptune+ was equipped with Jet interface and two 10<sup>13</sup> Ω resistors. The instrumental  
275 setup included Savillex® 50μl/min C-flow self-aspirating nebulizer, single pass Teflon® Scott-type spray  
276 chamber constructed utilizing Savillex® column components, 2.0 mm Pt injector from ESI®, Thermo® Ni ‘H’  
277 type sample cone and ‘X’ type skimmer cones. Both isotopes of boron were determined utilizing 10<sup>13</sup> Ω resistors  
278 (Misra et al., 2014a; Lloyd et al., 2018).

279 The sample size for boron isotope analyses typically ranged from 10 ppb B (~5 ng B) to 20 ppb B  
280 samples (~10 ng B). Instrumental sensitivity for <sup>11</sup>B was 17 mV/ppb B (eg. 170 mV for 10ppb B) in wet plasma  
281 at 50μl/min sample aspiration rate. Intensity of <sup>11</sup>B for a sample at 10ppb B was typically 165mV ± 5mV closely  
282 matched the 170mV ± 5mV of the standard. Due to the low boron content of the samples extreme care was taken  
283 to avoid boron contamination during sample preparation and reduce memory effect during analysis. Procedural  
284 boron blanks ranged from 15pg B to 65 pg B (contributed to less than <1% of the sample signal). The acid blank  
285 during analyses was measured at ≤ 1mV on the <sup>11</sup>B, meaning a contribution < 1% of the sample intensity, no  
286 memory effect was observed within and across sessions.

287 Analyses of external standards were done to ensure data quality. For δ<sup>11</sup>B measurements two carbonate  
288 standards were utilized: the JCP-1 (Geological Survey of Japan, Tsukuba, Japan) international standard (Gutjahr  
289 et al., 2014) and the NEP internal coral (Porites sp., δ<sup>11</sup>B = 26.12 ± 0.92 ‰, 2SD, n=33 Holcomb et al., 2015 and  
290 Sutton et al., 2018, Table S2) from University of Western Australia/Australian National University. Certified  
291 boron isotopes liquid standard, the ERM<sup>®</sup> AE121 (δ<sup>11</sup>B = 19.9 ± 0.6 ‰, SD, certified) was used to monitor  
292 reproducibility and drift during each session (Vogl and Rosner, 2011; Foster et al., 2013; Misra et al., 2014).  
293 Results for the isotopic composition of the NEP standard are shown in Table S2, average values are δ<sup>11</sup>B<sub>NEP</sub> =  
294 25.70 ± 0.93 ‰ (2SD, n=22) over different 7 analytical sessions with each number representing an ab-initio  
295 processed sample - this study). Our results are within error of published values of 26.20 ± 0.88 ‰ (2SD, n = 27)  
296 and 25.80 ± 0.89 ‰ (2SD, n = 6) by Holcomb et al. (2015) and Sutton et al. (2018) respectively. Chemically  
297 cleaned JCP<sub>1</sub> samples were measured at 24.06 ± 0.20 (2SD, n=6) and is within error of published values of 24.37  
298 ± 0.32 ‰ and 24.42 ± 0.28 ‰ by Holcomb et al. (2015) and Sutton et al. (2018) respectively.

299

### 300 **3.6 Trace elements**

301 The calcium concentration of each sample was measured on an ICP-AES ® Ultima 2 HORIBA at the  
302 Pôle spectrometrie Océan (PSO), UMR6538 (Plouzané, France). Samples were then diluted to fixed calcium  
303 concentrations (typically 10 ppm or 30 ppm Ca) using 0.1 M HNO<sub>3</sub> & 0.3 M HF matching multi-element  
304 standards Ca concentration to avoid any matrix effect (Misra et al., 2014b). Trace elements (e.g. X/Ca ratios)  
305 were analyzed on a Thermo Scientific ® Element XR HR-ICP-MS at the PSO, Ifremer (Plouzané, France).

306 Trace element analyses were done at a Ca concentration of 10 or 30 ppm. The typical blanks for a 30  
307 ppm Ca session were: <sup>7</sup>Li < 2%, <sup>11</sup>B < 7%, <sup>25</sup>Mg < 0.2% and <sup>43</sup>Ca < 0.02%. Additionally, blanks for a 10 ppm Ca  
308 session were: <sup>7</sup>Li < 2.5%, <sup>11</sup>B < 10%, <sup>25</sup>Mg < 0.4% and <sup>43</sup>Ca < 0.05%. Due to strong memory effect for boron  
309 and instrumental drift on the Element XR, long sessions of conditioning were done prior analyses. Boron blanks  
310 were driven below 5% of signal intensity usually after 4 to 5 days of continuous analyses of carbonate samples.  
311 External reproducibility was determined on the consistency standard Cam-Wuellestorf (courtesy of the  
312 University of Cambridge) (Misra et al., 2014b), Table S3. Our X/Ca ratio measurements on the external standard  
313 Cam-Wuellestorf were all the time within error of the published value (Table S3) validating the robustness of  
314 our trace elements data. Analytical uncertainty of a single measurement was calculated from the reproducibility  
315 of the Cam-Wuellestorf, measured during a particular mass spectrometry session. The analytical uncertainties  
316 on the X/Ca ratios are: 0.4 µmol/mol for Li/Ca, 7 µmol/mol for B/Ca and 0.01 mmol/mol for Mg/Ca (2SD,  
317 n=31) respectively.

318

### 319 **3.7 Oxygen isotopes**

320 Carbonate δ<sup>13</sup>C and δ<sup>18</sup>O were measured on a Gas Bench II coupled to a Delta V mass spectrometer at  
321 the stable isotope facility of Pôle spectrometrie Océan (PSO), Plouzané. Around 20 shells were weighed, crushed  
322 and clay removed. The recovered foraminifera were weighed in tubes and flushed with He gas. Samples were  
323 then digested in phosphoric acid and analyzed. Results were calibrated to the VPDB scale by international  
324 standard NBS19 and analytical precision on the in-house standard Ca21 was better than 0.11‰ for δ<sup>18</sup>O (1SD,  
325 n=5) and 0.03‰ for δ<sup>13</sup>C (1SD, n=5).

326

### 327 **3.8 Calcification depth determination**

328 We utilized two different chemo-stratigraphic methods to estimate the calcification depth in this study  
329 (Table S6 and S7). The first method, commonly used in paleoceanography, utilizes δ<sup>18</sup>O measurements of the  
330 carbonate (δ<sup>18</sup>O<sub>c</sub>) to estimate calcification depths (referred to as δ<sup>18</sup>O-based calcification depths) (Schmidt et al.,  
331 2002; Mortyn et al., 2003; Sime et al., 2005; Farmer et al., 2007; Birsh et al., 2013). The second method utilizes  
332 Mg/Ca-based temperature estimates (T<sub>Mg/Ca</sub>) to constrain calcification depths (Quintana Krupinski et al., 2017).  
333 In both cases, the postulate was that vertical profiles of seawater temperature are available for different seasons  
334 in ocean atlases and cruise reports, and that hydrographic data and geochemical proxy signatures can be  
335 compared to assess the depth in the water column that represents the species maximum abundance.

336 The two different methods to estimate calcification depth were then compared to published depth  
337 estimates for the basin, and where available, for the same site (Table S6). We chose literature values for  
338 calcification depths when available, or depths that were closest to what is known for the region or basin. As  
339 foraminifera can migrate in the water column along their ontogeny, we applied (based on uncertainties of our

340 measurements) an uncertainty of  $\pm 10$  m for calcification depths  $> 70$  m and an uncertainty of  $\pm 20$  m when  
341 calcification depths  $< 70$  m. The depth habitats utilized to derive *in situ* parameters are summarized in Table S7.

342

### 343 **3.9 $\delta^{11}\text{B}_{\text{borate}}$**

344 Two carbonate system parameters are needed to fully constrain the carbonate system. Following the  
345 approach of Foster et al., (2008) we used the GLODAP database (Key et al., 2004) corrected for anthropogenic  
346 inputs in order to estimate pre-industrial carbonate system parameters at each site. Temperature, salinity and  
347 pressure for each site are from the World ocean database 2013 (Boyer et al., 2013). We utilized the R<sup>®</sup> code in  
348 Henehan et al, (2016) (courtesy of Michael Henehan) to calculate the  $\delta^{11}\text{B}_{\text{borate}}$  and derive our calibrations.  
349 Uncertainty for  $\delta^{11}\text{B}_{\text{borate}}$  utilizing the code was similar to the one calculated by applying 2 standard deviations of  
350 the calculated  $\delta^{11}\text{B}_{\text{borate}}$  within the limits imposed by the calcification depth.

351 The Matlab<sup>®</sup> template provided by Zeebe and Wolf-Gladow, (2001) was used to calculate pCO<sub>2</sub> from  
352 TA; temperature, salinity and pressure were included into the calculations. Total boron was calculated from Lee  
353 et al., (2010), K<sub>1</sub> and K<sub>2</sub> were calculated from Mehrbach et al. (1973) refitted by Dickson and Millero (1987).

354 Statistical tests were made utilizing GraphPad<sup>®</sup> software, linear regressions for calibration were  
355 derived utilizing R<sup>®</sup> code in Henehan et al, (2016) (courtesy of Michael Henehan) with a k=500.

356

## 357 **4. Results**

358

### 359 **4.1 Depth habitat**

360 The calcification depths utilized in this paper are summarized in Tables S6 and S7, including a  
361 comparison of calcification depth determination methods. The calculated calcification depths are consistent with  
362 the ecology of each species and the hydrography of the sites. Specimens of *G. ruber* and *T. sacculifer* appear to  
363 be living in the shallow mixed layer (0-100 m), with *T. sacculifer* living or migrating deeper than *G. ruber*  
364 (down to 125 m). Specimens of *O. universa* and *P. obliquiloculata* are living in the upper thermocline; *G.*  
365 *menardii* is found in the upper thermocline until the thermocline depth specific to the location; *N. dutertrei* is  
366 living around the thermocline depth and specimens of *G. tumida* are found in the lower thermocline.

367 Data from both approaches implies that some species inhabit deeper environments in the Western  
368 Equatorial Pacific (WEP) relative to the Arabian Sea, which in turn are deeper dwelling than in the Indian  
369 Ocean. In some cases, we find evidence for differences in habitat depth of up to  $\sim 100$  m between the WEP and  
370 the Arabian Sea. This trend is observed for *G. ruber* and *T. sacculifer*, but not for *O. universa*.

371 Some differences in calcification depth are observed between the two calcification depth determination  
372 methods. These differences might be due to the choice of calibrations. Alternatively, our uncertainties for  $\delta^{18}\text{O}$   
373 implies larger uncertainties on the calcification depth determination using this approach, compared to Mg/Ca  
374 measurements.

375

### 376 **4.2 Empirical calibrations of foraminiferal $\delta^{11}\text{B}_{\text{carbonate}}$ to $\delta^{11}\text{B}_{\text{borate}}$**

377 Results for the different species analyzed in this study are presented in Fig. 5, Fig. 6 and summarized in  
378 Table 2; additionally, published calibrations for comparison are summarized in Table 3.

379

#### 380 4.2.1 *G. ruber*

381 Our results for *G. ruber* (Fig. 5) are in good agreement with published data from other core-tops,  
382 sediment traps, tows, and culture experiments for  $\delta^{11}\text{B}_{\text{borate}} > 19 \text{ ‰}$  (Foster et al., 2008, Henehan et al., 2013,  
383 Raitzsch et al., 2018). However, for  $\delta^{11}\text{B}_{\text{borate}} < 19 \text{ ‰}$  our results show lighter  $\delta^{11}\text{B}_{\text{carbonate}}$  compared to published  
384 values. Whilst this species has been widely studied previously, the sites selected in this study allow us to extend  
385 the calibration. The positive offset from the 1:1 curve has been explained by the high photosynthetic activity  
386 (Hönisch et al., 2003; Zeebe et al., 2003). Two calibrations have been derived. Utilizing only our data, the  
387 sensitivity of  $\delta^{11}\text{B}_{\text{carbonate}}$  to  $\delta^{11}\text{B}_{\text{borate}}$  of our linear regression is not statistically different from 1 and do not follow  
388 the low sensitivity trend of the culture experiments from Sanyal et al., (2001) or Henehan et al., (2013), ( $p < 0.05$ ).  
389 The uncertainty on this regression is important due to our small dataset and not inconsistent with the second  
390 calibration made compiling all data from literature. The sensitivity of this regression is similar (e.g. 0.46 ( $\pm 0.34$ )  
391 to the one recently published by Raitzsch et al., (2018) (e.g. 0.45 ( $\pm 0.16$ ), Table 3).

392

#### 393 4.2.2 *T. sacculifer*

394  $\delta^{11}\text{B}_{\text{carbonate}}$  results for *T. sacculifer* (sacc and w/o sacc) (Fig. 5) are compared to published data (Foster  
395 et al., 2008; Martinez-Boti et al., 2015b, Raitzsch et al., 2018). Results for *T. sacculifer* are in good agreement  
396 with the literature and fall above the 1:1 line. Linear regression on our data yields a slope of  $1.3 \pm 0.2$  but is not  
397 statistically different to the results from Martinez-Boti et al., (2015b) (Table 3), ( $p > 0.05$ ). However, when  
398 compiled with published data using the bootstrap method a slope of  $0.83 \pm 0.48$  is calculated, with a large  
399 uncertainty given the variability in the data. It is also noticeable that *T. sacculifer* (w/o sacc) samples from the  
400 WEP have a  $\delta^{11}\text{B}_{\text{carbonate}}$  close or below the 1:1 line and are significantly lower compared to the combined *T.*  
401 *sacculifer* of other sites ( $p = 0.01$ , unpaired t-test).

402

#### 403 4.2.3 *O. universa* and deeper dwelling species: *N. dutertrei*, *P. obliquiloculata*, *G. menardii* and *G. tumida*

404 Our results for *O. universa* (Fig. 5), *N. dutertrei*, *P. obliquiloculata*, *G. menardii* and *G. tumida* (Fig. 6)  
405 fall below the 1:1 line. These data for *O. universa* are not statistically different from the Henehan et al. (2016)  
406 calibration ( $p > 0.05$ ). Our results for *N. dutertrei* expand upon the initial measurements presented in Foster et al.,  
407 (2008). The different environments experienced by *N. dutertrei* in our study permit us to extend the range and  
408 derive a calibration for this species; the slope is close to unity ( $0.93 \pm 0.55$ ), and is similar to the ( $0.95 \pm 0.17$ )  
409 previously reported by Henehan et al., (2016) for *O. universa* and not statistically different ( $p > 0.05$ ). The data  
410 for *P. obliquiloculata* exhibits the largest offset from the theoretical line. The range of  $\delta^{11}\text{B}_{\text{borate}}$  from the samples  
411 we have of *G. menardii* and *G. tumida* is not sufficient to derive calibrations, but the points are in good  
412 agreement with the *N. dutertrei* calibration and Henehan et al. (2016) calibration for *O. universa*.

413 For all species, the slopes are not statistically different from Henehan et al. (2016) ( $p > 0.05$ ) and are  
414 close to unity. If data for deep-dwelling foraminiferal species are pooled together with each other and with data  
415 from Henehan et al., (2016) and Raitzsch et al., (2018), we calculate a slope of  $0.95 (\pm 0.13)$  ( $R^2 = 0.7987$ ,  
416  $p < 0.0001$ ); if only our data are used, we calculate a slope that is not significantly different ( $0.82 \pm 0.27$ ;  $p < 0.05$ ).  
417 However, it may remain premature to assume that a unique calibration with a slope of  $\sim 0.9$  can be used for all  
418 deeper-dwelling species; more data is needed for *P. obliquiloculata*, *G. menardii* and *G. tumida* to robustly test  
419 this assertion.



420

#### 421 4.2.4 Comparison of core-top and culture data

422 The data for *G. ruber* and *T. sacculifer* from the core-tops we measured are broadly consistent with  
423 previous published results. The calibrations between these core-top derived estimates and culture experiments  
424 are not statistically different due to small datasets and uncertainties on the linear regressions (Henehan et al.,  
425 2013; Marinez-Boti et al., 2015; Raitzsch et al., 2018; Table 3). The sensitivities of the species analyzed are not  
426 statistically different and are close to unity.

427

#### 428 4.3 B/Ca ratios

429 B/Ca ratios are presented in Table 2. Values are species specific consistent with previous work (e.g.,  
430 compiled in Henehan et al., 2016) with ratios higher for *G. ruber* > *T. sacculifer* > *T. sacculifer* (w/o sacc) > *P.*  
431 *obliquiloculata* > *O. universa* > > *G. menardii* > *N. dutertrei* > *G. tumida* > *G. inflata* > *N. pachyderma* > *G.*  
432 *bulloides* (Fig. 7). This study supports interspecific B/Ca ratios (Yu et al., 2007; Tripathi et al., 2009, 2011; Allen  
433 and Hönisch, 2012; Henehan et al., 2016). Differences between surface- and deep-dwelling foraminifera are  
434 observed, with lower values and a smaller range for the deeper dwelling taxa (58-126  $\mu\text{mol/mol}$  vs 83-190  
435  $\mu\text{mol/mol}$  for shallow dwellers). The B/Ca data for deep-dwelling taxa exhibits a significant correlation with  
436  $[\text{B}(\text{OH})_4^-]/[\text{HCO}_3^-]$  ( $p < 0.05$ ), but no correlation with  $\delta^{11}\text{B}_{\text{carbonate}}$  and temperature (Fig. S3). Surface-dwelling  
437 species have B/Ca ratios that exhibit significant correlations with  $[\text{B}(\text{OH})_4^-]/[\text{HCO}_3^-]$ ,  $\delta^{11}\text{B}_{\text{carbonate}}$  and  
438 temperature. The sensitivity of B/Ca to  $[\text{B}(\text{OH})_4^-]/[\text{HCO}_3^-]$  is lower for deep-dwelling species compared to  
439 surface dwelling species. When all the B/Ca data are compiled, significant trends are observed with  $[\text{B}(\text{OH})_4^-]$   
440  $[\text{HCO}_3^-]$ ,  $\delta^{11}\text{B}_{\text{carbonate}}$  and temperature (Fig. S3). We also observe that if we compare data from all sites together,  
441 correlations exist between B/Ca and the water depths of the cores (not significant, Fig. S4) but these correlations  
442 may also be related to the different the depth habitats of different taxa in each region, a significant trend is  
443 observed when all the data are plotted ( $R^2=0.11$ ,  $p < 0.05$ , Fig. S4).

444

### 445 5. Discussion

446

#### 447 5.1 Sources of uncertainty relating to depth habitat and seasonality at studied sites

448

##### 449 5.1.1 Depth habitats and $\delta^{11}\text{B}_{\text{borate}}$

450 Because foraminifera will record ambient environmental conditions during calcification, the accurate  
451 characterization of *in-situ* data is needed not only for calibrations, but also to understand the reconstructed record  
452 of pH or  $p\text{CO}_2$ . The species we examined are ordered here from shallower to deeper depth habitats: *G. ruber* > *T.*  
453 *sacculifer* (sacc) > *T. sacculifer* (w/o sac) > *O. universa* > *P. obliquiloculata* > *G. menardii* > *N. dutertrei* > *G.*  
454 *tumida* (this study; Birch et al., 2013; Farmer et al., 2007), although the specific water depth will vary depending  
455 on the hydrology of the site (Kemle-von and Oberhänhsl, 1999). We note that calculation of absolute  
456 calcification depths can be challenging in some cases as many species migrate during their ontogeny (Steinhardt  
457 et al., 2015).

458 We find that assumptions about the specific depth habitat a species of foraminifera is calcifying over, in  
459 a given region, can lead to differences of a few per mil in calculated isotopic compositions of borate (Fig. 4).

460 Hence this can cause a bias in calibrations if calcification depths are assumed instead of being calculated (i.e.,  
461 with  $\delta^{18}\text{O}$  and/or Mg/Ca). Factors including variations in thermocline depth can impact depth habitats for some  
462 taxa. At the sites we examined, most of the sampled species live in deeper depth habitats in the WEP relative to  
463 the Indian Ocean, which in turn is characterized by deeper depth habitats than in the Arabian Sea. In the tropical  
464 Pacific, *T. sacculifer* is usually found deeper than *G. ruber* except at sites characterized by a shallow  
465 thermocline, in which case they tend to overlap their habitat (e.g., ODP Site 806 in the WEP which has a deeper  
466 thermocline than at ODP Site 847 in the Eastern Equatorial Pacific; EEP) (Rickaby et al., 2005). The difference  
467 in depth habitats for *T. sacculifer* and *N. dutertrei* between the WEP and EEP can be as much as almost 100 m  
468 (Rickaby et al., 2005).

469

### 470 5.1.2 Seasonality and *in-situ* $\delta^{11}\text{B}_{\text{borate}}$

471 As discussed by Raitzsch et al., (2018), depending of the study area, foraminiferal fluxes can change  
472 throughout the year, so seasonality can have a major impact on hydrographic carbonate parameters calculations  
473 for any given water depth. We therefore recalculated the theoretical  $\delta^{11}\text{B}_{\text{borate}}$  using seasonal data for temperature  
474 and salinity and annual values for TA and DIC for each depth at each site. The GLODAP (2013) database does  
475 not provide seasonal TA or DIC values.

476 The low sensitivity of  $\delta^{11}\text{B}_{\text{borate}}$  to temperature and salinity means that calculated  $\delta^{11}\text{B}_{\text{borate}}$  for each  
477 water depth at our sites were not strongly impacted (Fig. S1). Thus, these findings support Raitzsch et al. (2018),  
478 who concluded that calculated  $\delta^{11}\text{B}_{\text{borate}}$  values corrected for seasonality was within error of non-corrected values  
479 for each water depth. As Raitzsch et al, (2018) highlight, seasonality might be more important at high latitude  
480 sites where seasonality is more marked, however, the seasonality of primary production will also be more tightly  
481 constrained due to the seasonal progression of winter light limitation and intense vertical mixing and summer  
482 nutrient limitation.

483 Data for our sites suggests that most  $\delta^{11}\text{B}_{\text{borate}}$  variability we observe does not come from seasonality but  
484 from the assumed water depths for calcification. With the exception of a few specific areas such as the Red Sea  
485 (Henehan et al., 2016, Raitzsch et al., 2018), at most sites examined, seasonal  $\delta^{11}\text{B}_{\text{borate}}$  at a fixed depth does not  
486 vary by more than  $\sim 0.2\%$ . We conclude that seasonality is not an important factor impacting carbonate system  
487 parameters at the sites we examined.

488

### 489 5.2 $\delta^{11}\text{B}$ , microenvironment pH and depth habitats

490 In planktonic foraminifera, algal symbiosis is the more common symbiotic relationship. For most of  
491 planktonic foraminifera, the host presents only one species of symbionts (Gast and Caron, 2001). The family  
492 Globigerinidae, including *G. ruber*, *T. sacculifer* and *O. universa*, commonly have dinoflagellates or chrysophyte  
493 algal symbionts (Anderson and Be, 1976; Spero, 1987). The families Pulleniatinidae, Globorotaliidae, including  
494 *N. dutertrei*, *P. obliquiloculata*, *G. menardii* and *G. tumida*, have chrysophyte algal symbionts (Gastrich, 1988).

495 The relationship between the symbionts and the host is complex by nature. Nevertheless, this symbiotic  
496 relationship provides energy (Hallock, 1981b) and promotes calcification of the foraminifera (Duguay, 1983;  
497 Erez et al., 1983) by providing the inorganic carbon to the host (Jorgensen et al., 1985). Also, for *T. sacculifer*  
498 and *O. universa* photosynthesis increases with higher insolation (Jorgensen et al., 1985; Rink et al., 1998).

499 Dinoflagellate-bearing foraminifera (*G. ruber*, *T. sacculifer* and *O. universa*) tend to have a higher  
500 symbiont density and photosynthesis activity while *P. obliquiloculata*, *G. menardii* and *N. dutertrei* have  
501 lowered symbiont density and *P. obliquiloculata*, *N. dutertrei* lower photosynthetic activity (Takagi et al., 2019).  
502 *P. obliquiloculata* showed the minimum symbiont density and photosynthetic activity (Takagi et al., 2019).

503 It is now accepted that the foraminifera  $\delta^{11}\text{B}$  signature comes from the microenvironment pH  
504 (Jorgensen et al., 1985; Rink et al., 1998; Köhler-Rink and Köhl, 2000; Hönisch et al., 2003; Zeebe et al., 2003).  
505 Foraminifera with high photosynthetic activity and symbiont density like *G. ruber* and *T. sacculifer* present a pH  
506 of microenvironment higher than ambient seawater,  $\delta^{11}\text{B}$  higher than 1:1 line (Foster et al., 2008, Henehan et al.,  
507 2013, Raitzsch et al., 2018). The opposite can also be true, from our study, species with lower photosynthetic  
508 activity and lower symbiont density present microenvironments lower than ambient seawater,  $\delta^{11}\text{B}$  lower than  
509 1:1 line (Martinez-Boti et al., 2015b; Henehan et al., 2016), this is the case in our data for *N. dutertrei*, *G.*  
510 *menardii* and *P. obliquiloculata* and likely *G. tumida*. Nevertheless, the low  $\delta^{11}\text{B}$  of *O. universa* and *T.*  
511 *sacculifer* (w/o sacc) from the WEP are difficult to reconcile with a high photosynthetic activity compared to *T.*  
512 *sacculifer* et *G. ruber*.

513 The photosynthetic activity is also function of the light level they received which is, in the natural  
514 system, dependent of their depth in the water column, for the purpose of this study we will not consider turbidity  
515 which also influences the light penetration in the water column. In this case, the photosynthetically active  
516 foraminifera living close to the surface should see their microenvironment pH (thus  $\delta^{11}\text{B}$ ) more sensitive to water  
517 depth changes. A deeper depth habitat will change the light intensity they received and as a consequence may  
518 lower their photosynthetic activity reducing their microenvironment pH. This thought is supported by the  
519 significant trend observed between our  $\Delta^{11}\text{B}$  and the calcification depth for *G. ruber* and *T. sacculifer* of our sites  
520 (Fig. S2). This trend basically supports the fact that the microenvironment pH decrease with calcification depth.  
521 We observe a decrease of  $\delta^{11}\text{B}$  in the WEP for *T. sacculifer* (w/o sacc), significantly different from the other sites  
522 ( $p < 0.05$ ). The  $\Delta^{11}\text{B}$  of *G. ruber*, *T. sacculifer* (w/o sacc and sacc) is also significantly lower in the WEP  
523 compared to the other sites ( $p < 0.05$ ). To test if the  $\delta^{11}\text{B}$  signature was inferred to a light driven, we have been  
524 able to independently calculate the depth of the foraminifera based on various light insolation culture  
525 experiments (Jorgensen et al., 1985) and the  $\Delta$ microenvironment pH derived from our data (Fig. 8A and B). This  
526 exercise verified that this low  $\delta^{11}\text{B}$  can be explained by the reduced light environment due to a deeper depth  
527 habitat in the WEP (Fig. 8B). Also, *T. sacculifer* has the potential to support more photosynthesis due to its  
528 higher symbiont density. Higher photosynthetic activity is observed compared to other species potentially  
529 supporting higher symbiont/host interactions. Those results could be in line with a greater sensitivity of *T.*  
530 *sacculifer* photosynthetic activity with changes in insolation/water depth. It can also be noted that this species  
531 presents the largest variations in symbiont density versus its test size. When applied to the other species *O.*  
532 *universa* data suggest a microenvironment pH 0.10 to 0.20 lower than ambient seawater pH which would be in  
533 line with species living deeper than 50m (light compensation point (Ec), Rink et al., 1998) also consistent with  
534 our calcification depth reconstructions.  $\Delta$ microenvironment pH is higher in *T. sacculifer* > *G. ruber* > *T.*  
535 *sacculifer* (w/o sacc - WEP) > *O. universa*, *N. dutertrei*, *G. menardii*, *G. tumida* > *P. obliquiloculata* in line with  
536 photosymbiosis findings from Tagazaki et al., (2019). Also, the higher  $\delta^{11}\text{B}$  data from the African upwelling  
537 published by Raitzsch et al., (2018) for *G. ruber* and *O. universa* might reflect the higher microenvironment pH  
538 due to a shallower depth habitat. This could highlight a potential issue with calibration when applied to sites with

539 different oceanic regimes as the  $\delta^{11}\text{B}$  specie-specific calibrations could be also location-specific for the mixed  
540 dweller species.

541 Microenvironment pH results for *N. dutertrei*, *G. menardii*, *G. tumida*, are similar to *O. universa* and  
542 suggest a threshold for respiration driven  $\delta^{11}\text{B}$  signature. This threshold can be driven by a change of  
543 photosynthetic activity due to lower light intensity at deeper depth and/or a change in the symbiont assemblage  
544 with non-dinoflagellate symbionts at deeper depth. We can explain this threshold because deep dweller species  
545 do not experience important changes of insolation at those depths so their microenvironments should be  
546 respiration driven and relatively stable. We can also note that *P. obliquiloculata* which has the lowest symbiont  
547 density and photosynthetic activity has the lowest microenvironment pH compared to other deeper dweller  
548 species supporting this respiration driven microenvironment.

549

### 550 **5.3 $\delta^{11}\text{B}$ sensitivity to $\delta^{11}\text{B}_{\text{borate}}$ and relationship with B/Ca signatures**

551  $\delta^{11}\text{B}_{\text{carbonate}}$  and B/Ca data have shown to be sensitive to precipitation rate with at higher precipitation  
552 rate increasing  $\delta^{11}\text{B}_{\text{carbonate}}$  (Farmer et al., 2019) and B/Ca (Farmer et al., 2019; Gabitov et al., 2014; Kaczmarek  
553 et al., 2016; Mavromatis et al., 2015; Ushikawa et al., 2015). A recent study from Farmer et al, (2019) has  
554 proposed that in foraminifera at higher precipitation rates, more borate ion is incorporated into the carbonate  
555 mineral, while at lower precipitation rates, more boric acid is incorporated. They also suggest this may explain  
556 low sensitivities of culture experiments.

557 When combining all literature data, *T. sacculifer* and *G. ruber* have sensitivities of  $\delta^{11}\text{B}_{\text{carbonate}}$  to  
558  $\delta^{11}\text{B}_{\text{borate}}$  of  $0.83 \pm 0.48$  and  $0.46 \pm 0.34$  respectively in line with previous literature and paleo- $\text{CO}_2$   
559 reconstructions. Also, if we only take into account our data, the observation that the sensitivity of  $\delta^{11}\text{B}_{\text{carbonate}}$  to  
560  $\delta^{11}\text{B}_{\text{borate}}$  are not statistically different from unity for most of the species investigated we can speculate that for  
561 these taxa, changes in precipitation rate and contributions of boric acid are not likely to be important. If  
562 considering only the data from this study, *G. ruber* ( $1.12 \pm 1.67$ ) and *T. sacculifer* ( $1.38 \pm 1.35$ ) present higher  
563 sensitivities of  $\delta^{11}\text{B}_{\text{carbonate}}$  to  $\delta^{11}\text{B}_{\text{borate}}$ . We can then again speculate that the observed high values for  $\delta^{11}\text{B}_{\text{carbonate}}$   
564 at high seawater pH can be due to higher precipitation rates. We note this could also be consistent with the  
565 higher sensitivity of B/Ca signatures in these two surface dwelling species to ambient  $[\text{B}(\text{OH})_4^-]/[\text{HCO}_3^-]$  relative  
566 to deeper dwelling species. Those interspecific differences still remain to be explained, however, part of this  
567 variability is likely due to changes in the carbonate chemistry of the microenvironment resulting in changing  
568 competition between borate and bicarbonate. A caveat is that we can not exclude specific biological processes,  
569 and that in taxa with a non respiration-driven microenvironment, changes in day/night calcification ratios also  
570 impacting observed values. As indicated by Farmer et al., (2019), studies of calcite precipitation rates in  
571 foraminifera may help to improve our understanding of the fundamental basis of boron-based proxies.

572

### 573 **5.4 Evaluation of species for pH reconstructions and water depth pH reconstructions**

574 This data set allows us to reassess the utility of boron-based proxies for the carbonate system. The main  
575 interest with utilizing boron-based proxies relates to the reconstruction of past oceanic conditions - specifically  
576 pH and  $\text{pCO}_2$ . Mixed-layer species (eg. *G. ruber* and *T. sacculifer*) are potential archives for atmospheric  $\text{CO}_2$   
577 reconstructions. Other species can shed light on other aspects of the carbon cycle including the physical and  
578 biological carbon pumps.

579 There are a few main inferences we can make. When compiled with data from the literature,  
580 sensitivities of  $\delta^{11}\text{B}_{\text{carbonate}}$  to  $\delta^{11}\text{B}_{\text{borate}}$  for *G. ruber* and *T. sacculifer* are similar to previous studies (Martinez-  
581 Boti et al., 2015b; Raitzsch et al., 2018) which is also supporting of previous paleo-reconstructions. Our data  
582 also support the observations of Henehan et al., (2016) for *O. universa*.

583 In order to derive accurate reconstructions of past ambient pH and pCO<sub>2</sub>, accurate species-specific  
584 calibrations need to be used that are constrained by core-tops or samples from similar types of settings (Fig. 9,  
585 10, S6). Lighter  $\delta^{11}\text{B}$  signatures in *T. sacculifer* (w/o sacc) are observed in the WEP, which may be explained by  
586 the deeper depth habitat for these taxa, where lower light levels might reduce symbiont photosynthetic activity.  
587 Also, correction will be needed for *T. sacculifer* (w/o sacc) in the WEP. When applying the calibrations n°2 and  
588 4 to *T. sacculifer* and *G. ruber* (compilation of all data, Table 3) our data show more variability, especially for *G.*  
589 *ruber* which lead to the larger mismatch compared to *in-situ* parameters. Henehan et al., (2013) reported a lighter  
590  $\delta^{11}\text{B}$  with smaller test size, our sample add a weight/shell of  $11 \pm 4 \mu\text{g}$  (n=4, SD) which, despite a narrow range,  
591 could still explain this variability. The higher divergence of reconstructed values from *in-situ* measurements are  
592 observed at site WPO7-01 for both *T. sacculifer* (w/o sacc) and *G. ruber*. More data would be needed to  
593 determine a proper correction for both species, coretop study will be determinant for future downcore  
594 reconstructions, especially in the WEP.

595 We also find that for two species, the boron proxy is a relatively straightforward recorder of ambient  
596 pH, with sensitivities close to unity for and *O. universa*, and *N. dutertrei*. There is also promise in using multiple  
597 species in a sample from different hydrographic regimes to reconstruct vertical profiles of pH and pCO<sub>2</sub>. We are  
598 able to reproduce pH and pCO<sub>2</sub> profiles from multiple sites with different water column structures (Fig. 9) with  
599 those reconstructions within error of the *in-situ* values, for most sites. In order to avoid circularity, to validate  
600 these calibrations, we recalculated ambient pH and pCO<sub>2</sub> by first excluding site-specific data and then  
601 recalculating species-specific calibrations, followed by application to each specific site. The comparison of the  
602 two methods does not show significant differences and validates the robustness of the calibrations (Fig. S5). We  
603 utilized the calibrations derived from our data for *G. ruber* (calibration n°1 and 2, Table 3), *T. sacculifer*  
604 (calibration n°3 and 4, Table 3), *O. universa* (calibration n°8, Table 3), for *P. obliquiloculata* (calibration n°11,  
605 Table 3), and for *N. dutertrei*, *G. tumida* and *G. menardii* the calibration made on the compilation of the deep-  
606 dweller (calibration n°13, Table 3). Results are shown in Fig. 9 and evaluated in Fig. 10. For *G. menardii*, more  
607 data would be helpful to provide additional constraints. Results for *G. ruber* are the sparsest, potentially due to  
608 difference in test sizes (Henehan et al., 2013) or undocumented diagenetic effects. Results reaffirm the  
609 importance of working with narrow size fractions (Henehan et al., 2013) and the importance of core-top study to  
610 determine corrections.

611

## 612 **6. Conclusions and future implications**

613 Our study has extended the boron isotope proxy with data for new species and sites. The work supports  
614 previous work showing that depth habitats of foraminifera vary depending on the oceanic regime, and this  
615 impacts boron isotope signatures. Low  $\delta^{11}\text{B}$  values in the WEP compared to other regions for *T. sacculifer* (w/o  
616 sacc) may be explained by a reduction in microenvironment pH due to a deeper depth habitat associated with  
617 reduced irradiance and thus photosynthetic activity. Those results might also highlight a potential need for

618 studying core-tops in order to establish what factors are important to accurately develop reconstructions in  
619 different areas.

620 The sensitivity of  $\delta^{11}\text{B}$  to pH is in line with previously published data for *T. sacculifer*, *G. ruber*. The  
621 sensitivity of  $\delta^{11}\text{B}$  to pH of *O. universa* (mixed dweller), *N. dutertrei*, *G. menardii* and *G. tumida* (deep-  
622 dwellers) are similar but more data are needed to fully determine those sensitivities. The similarity of boron  
623 isotope calibrations for deep-dwelling taxa might be related to respiration-driven microenvironments.

624 Reconstruction of seawater pH and carbonate system parameters is achievable using foraminiferal  $\delta^{11}\text{B}$   
625 but additional core-top and down-core studies reconstructing depth profiles will be needed in order to further  
626 verify those calibrations. Past pH and  $\text{pCO}_2$  water depth profiles can potentially be created by utilizing multiple  
627 foraminiferal species in concert with taxa-specific calibrations for similar settings. This approach has much  
628 potential for enhancing our understanding of the past workings of the oceanic carbon cycle, and the biological  
629 pump.

630

631 **Author contribution**

632 R.E and A.T. wrote the proposals that funded the work. A.T. and F.C. provided the samples. M.G., S.M. and  
633 A.T. contributed to the experimental design. A.V. helped for sample preparation. M.G. and S.M contributed to  
634 developing the method of boron isotope analysis. M.G. performed the measurements with assistance from S.M.  
635 M.G conducted the data analysis. M.G. drafted the paper, which was edited by all authors. Interpretation was led  
636 by M.G., A.T., S.M. with input from R.E., A.V. and F.C.

637

638 **Competing interests**

639 The authors declare that they have no conflict of interest.

640

641 **Acknowledgments:**

642 The authors wish to thank Jesse Farmer for his valuable and detailed comments on the actual and a previous  
643 version of the manuscript. We wish to thank Michael Henehan for helpful discussion, comments on the  
644 manuscript and help with the code. We also want to thank the anonymous reviewer for helpful comments. Lea  
645 Bonnin for assistance with picking samples, the IODP repository for provision of samples, the Tripathi Laboratory  
646 (UCLA) for their technical support, Mervyn Greaves, Madeleine Bohlin (University of Cambridge) for technical  
647 support and use of laboratory space, Yoan Germain, Emmanuel Ponzevera and Oanez Lebeau for technical  
648 support and use of laboratory space in Brest, Jill Sutton for helpful conversation on the manuscript. Research is  
649 supported by DOE BES grant DE-FG02-13ER16402, by the International Research Chair Program that is funded  
650 by the French government (LabexMer ANR-10-LABX-19-01), and IAGC student research grant 2017.

651

652 **References**

- 653 Allen, K. A. and Hönisch, B.: The planktic foraminiferal B/Ca proxy for seawater carbonate chemistry: A critical  
654 evaluation, *Earth Planet. Sci. Lett.*, 345–348, 203–211, 2012.
- 655 Anand, P., Elderfield, H. and Conte, M. H.: Calibration of Mg/Ca thermometry in planktonic foraminifera from a  
656 sediment trap time series. *Paleoceanography* 18, 2003.
- 657 Anderson, O. R. and Bé, A.W. H.: The ultrastructure of a planktonic foraminifer, *Globigerinoides sacculifer*  
658 (Brady), and its symbiotic dinoflagellates, *J. Foramin. Res.*, 6, 1–21, 1976.
- 659 Arbuszewski, J., DeMenocal, P., Kaplan, A. and Farmer, E. C.: On the fidelity of shell-derived  $\delta^{18}\text{O}$  seawater  
660 estimates, *Earth Planet. Sci. Lett.*, 300, 185–196, 2010.
- 661 Axelsson, M. D., Rodushkin, I., Ingri, J. and Öhlander, B.: Multielemental analysis of Mn–Fe nodules by ICP-  
662 MS: optimisation of analytical method, *Analyst*, 127, 76–82, 2002.
- 663 Babila, T.L., Rosenthal, Y., Conte, M.H.: Evaluation of the biogeochemical controls on B/Ca of *Globigerinoides*  
664 *ruber* white from the Oceanic Flux Pro-gram, Bermuda. *Earth Planet. Sci. Lett.* 404, 67–76, 2014.
- 665 Barker S., Greaves M. and Elderfield H.: A study of cleaning procedures used for foraminiferal Mg/Ca  
666 paleothermometry. *Geochemistry, Geophys. Geosystems* 4, 1–20, 2003.
- 667 Bartoli, G., Hönisch, B. and Zeebe, R. E.: Atmospheric CO<sub>2</sub> decline during the Pliocene intensification of  
668 Northern Hemisphere glaciations. *Paleoceanography* 26, 1–14, 2011.
- 669 Bemis, B. E., Spero, H. J., Bijma, J. and Lea, D. W.: Reevaluation of the oxygen isotopic composition of  
670 planktonic foraminifera: Experimental results and revised paleotemperature equations. *Paleoceanography*  
671 13, 150–160, 1998.
- 672 Bemis, B. E., Spero, H. J. and Thunell, R. C.: Using species-specific paleotemperature equations with  
673 foraminifera: a case study in the Southern California Bight, *Mar. Micropaleontol.*, 46, 405–430, 2002.
- 674 Bijma, J., Faber Jr., W.W., Hemleben, C.: Temperature and salinity limits for growth and survival of some  
675 planktonic foraminifera in laboratory cultures, *J. Foraminiferal Res.* 20 (2), 95–116, 1990.
- 676 Bijma, J., Hönisch, B. and Zeebe, R. E.: Impact of the ocean carbonate chemistry on living foraminiferal shell  
677 weight: Comment on “Carbonate ion concentration in glacial-age deep waters of the Caribbean Sea” by W.  
678 S. Broecker and E. Clark, *Geochemistry, Geophys. Geosystems*, 3, 1–7, 2002.
- 679 Birch, H., Coxall, H. K., Pearson, P. N., Kroon, D. and O’Regan, M.: Planktonic foraminifera stable isotopes and  
680 water column structure: Disentangling ecological signals, *Mar. Micropaleontol.*, 101, 127–145, 2013.
- 681 Boyer, T.P., Antonov, J. I., Baranova, O. K., Coleman, C., Garcia, H. E., Grodsky, A., Johnson, D. R., Locarnini,  
682 R. A., Mishonov, A. V., O’Brien, T.D., Paver, C.R., Reagan, J.R., Seidov, D., Smolyar, I. V., and Zweng,  
683 M. M.: *World Ocean Database*, NOAA Atlas NESDIS 72, S. Levitus, Ed., A. Mishonov, Technical Ed.,  
684 Silver Spring, MD, 209, 2013.
- 685 Boyle, E. A.: Manganese carbonate overgrowths on foraminifera tests, *Geochim. Cosmochim. Acta.*, 47, 1815–  
686 1819, 1983.
- 687 Branson, O., Kaczmarek, K., Redfern, S. A. T., Misra, S., Langer, G., Tyliszczak, T., Bijma, J. and Elderfield,  
688 H.: The coordination and distribution of B in foraminiferal calcite, *Earth Planet. Sci. Lett.*, 416, 67–72,  
689 2015.



- 690 Catanzaro, E.J., Champion, C.E., Garner, A.L., Marinenko, G., Sappenfield, K.M. and Shields, W.R.: Boric  
691 Acid; Isotopic and Assay Standard Reference Materials. U.S. Natl. Bur. Stand. Spec., Publ. 260-17, 70p,  
692 1970.
- 693 Chalk, T. B., Hain, M. P., Foster, G. L., Rohling, E. J., Sexton, P. F., Badger, M. P. S., Cherry, S. G., Hasenfratz,  
694 A. P., Haug, G. H., Jaccard, S. L., Martínez-García, A., Pälike, H., Pancost, R. D. and Wilson, P. A.:  
695 Causes of ice age intensification across the Mid-Pleistocene Transition, *Proc. Natl. Acad. Sci.*, 114,  
696 13114–13119, 2017.
- 697 Coadic, R., Bassinot, F., Dissard, D., Douville, E., Greaves, M. and Michel, E.: A core-top study of dissolution  
698 effect on B/Ca in Globigerinoides sacculifer from the tropical Atlantic: Potential bias for paleo-  
699 reconstruction of seawater carbonate chemistry, *Geochemistry, Geophys. Geosystems* 14, 1053–1068,  
700 2013.
- 701 de Nooijer, L. J., Spero, H. J., Erez, J., Bijma, J. and Reichart, G. J.: Biomineralization in perforate foraminifera.  
702 *Earth-Science Rev.*, 135, 48–58, 2014.
- 703 Dekens, P. S., Lea, D. W., Pak, D. K. and Spero, H. J.: Core top calibration of Mg/Ca in tropical foraminifera:  
704 Refining paleotemperature estimation, *Geochemistry, Geophys. Geosystems* 3, 1–29, 2002.
- 705 Deuser, W.G., Ross, E.H., Hemleben, Ch., Spindler, M.: Seasonal changes in species composition, numbers,  
706 mass, size, and isotopic composition of planktonic foraminifera settling into the deep Sargasso Sea,  
707 *Palaeogeogr., Palaeoclimat., Palaeoecol.*, 33:103-127, 1981.
- 708 Deuser, W. G. and Ross, E. H.: Seasonally abundant planktonic foraminifera of the Sargasso Sea; succession,  
709 deep-water fluxes, isotopic compositions, and paleoceanographic implications, *J. Foraminifer. Res.* 19,  
710 268–293, 1989.
- 711 Dickson, A. G.: Thermodynamics of the dissociation of boric acid in synthetic seawater from 273.15 to 318.15  
712 K., *Deep Sea Res., Part A, Oceanogr. Res. Pap.* 37, 755–766, 1990.
- 713 Dickson, A.G., Millero, F.J.: A comparison of the equilibrium constants for the dissociation of carbonic acid in  
714 seawater media, *Deep-Sea Res.*, 34, 1733–1743, 1987.
- 715 Douville, E., Paterne, M., Cabioch, G., Louvat, P., Gaillardet, J., Juillet-Leclerc, A. and Ayliffe, L.: Abrupt sea  
716 surface pH change at the end of the Younger Dryas in the central sub-equatorial Pacific inferred from  
717 boron isotope abundance in corals (*Porites*), *Biogeosciences* 7, 2445–2459, 2010.
- 718 Duguay, L.E.: Comparative laboratory and field studies on calcification and carbon fixation in foraminiferal-  
719 algal associations, *Journal of Foraminiferal Research* 13, 252-261, 1983.
- 720 Duplessy, J., Labeyrie, L., Juilletleclerc, A., Maitre, F., Duprat, J. and Sarnthein, M.: Surface salinity  
721 reconstruction of the north-atlantic ocean during the last glacial maximum, *Oceanol. Acta*, 14, 311–324,  
722 1991.
- 723 Elderfield, H., Yu, J., Anand, P., Kiefer, T. and Nyland, B.: Calibrations for benthic foraminiferal Mg/Ca  
724 paleothermometry and the carbonate ion hypothesis, *Earth Planet. Sci. Lett.*, 250, 633–649., 2006.
- 725 Elderfield, H. and Granssen, G.: Past temperatures and O18 of surface ocean waters inferred from foraminiferal  
726 Mg/Ca ratios, *Nature* 405, 442–445, 2000.
- 727 Erez J.: Calcification Rates, Photosynthesis and Light in Planktonic Foraminifera. In: Westbroek P., de Jong  
728 E.W. (eds) *Biomineralization and Biological Metal Accumulation*. Springer, Dordrecht, 1983.
- 729 Erez, J.: The Source of Ions for Biomineralization in Foraminifera and Their Implications for Paleoceanographic  
730 Proxies, *Rev. Mineral. Geochemistry*, 54, 115–149, 2003.

- 731 Fairbanks, R. G. and Wiebe, P. H.: Foraminifera and Chlorophyll Maximum: Vertical Distribution, Seasonal  
732 Succession, and Paleoceanographic Significance, *Science*, 209, 1524–1526, 1980.
- 733 Fairbanks, R. G., Sverdlow, M., Free, R., Wiebe, P. H. and Bé, A. W. H.: Vertical distribution and isotopic  
734 fractionation of living planktonic foraminifera from the Panama Basin, *Nature*, 298, 841–844, 1982.
- 735 Farmer, E. C., Kaplan, A., de Menocal, P. B. and Lynch-Stieglitz, J.: Corroborating ecological depth preferences  
736 of planktonic foraminifera in the tropical Atlantic with the stable oxygen isotope ratios of core top  
737 specimens, *Paleoceanography*, 22, 1–14, 2007.
- 738 Feely, R.: Impact of Anthropogenic CO<sub>2</sub> on the CaCO<sub>3</sub> System in the Oceans, *Science*, 305, 362–366, 2004.
- 739 Ferguson, J. E., Henderson, G. M., Kucera, M. and Rickaby, R. E. M.: Systematic change of foraminiferal  
740 Mg/Ca ratios across a strong salinity gradient, *Earth Planet. Sci. Lett.*, 265, 153–166, 2008.
- 741 Foster, G. L.: Seawater pH, pCO<sub>2</sub> and [CO<sub>3</sub><sup>2-</sup>] variations in the Caribbean Sea over the last 130 kyr: A boron  
742 isotope and B/Ca study of planktic foraminifera, *Earth Planet. Sci. Lett.*, 271, 254–266, 2008.
- 743 Foster, G. L. and Sexton, P. F.: Enhanced carbon dioxide outgassing from the eastern equatorial Atlantic during  
744 the last glacial, *Geology*, 42, 1003–1006, 2014.
- 745 Foster, G. L., Lear, C. H. and Rae, J. W. B.: The evolution of pCO<sub>2</sub>, ice volume and climate during the middle  
746 Miocene, *Earth Planet. Sci. Lett.*, 341–344, 243–254, 2012.
- 747 Foster, G. L. and Rae, J. W. B.: Reconstructing Ocean pH with Boron Isotopes in Foraminifera, *Annu. Rev.*  
748 *Earth Planet. Sci.*, 44, 207–237, 2016.
- 749 Gabitov, R. I., Rollion-bard, C., Tripathi, A. and Sadekov, A.: In situ study of boron partitioning between calcite  
750 and fluid at different crystal growth rates, *Geochim. Cosmochim. Acta*, 137, 81–92, 2014.
- 751 Gaillardet, J., Lemarchand, D., Göpel, C. and Manhès, G.: Evaporation and Sublimation of Boric Acid :  
752 Application for Boron Purification from Organic Rich Solutions, *Geostand. Newsl.*, 25, 67–75, 2001.
- 753 Gast R. J. and Caron D. A.: Photosymbiotic associations in planktonic foraminifera and radiolaria, 1–7, 2001.
- 754 Gastrich, M.D.: Ultrastructure of a new intracellular symbiotic alga found within planktonic foraminifera,  
755 *Journal of Phycology* 23, 623–632, 1988.
- 756 Gattuso, J.P. and Hansson, L.: *Ocean acidification*, Oxford University Press, 2011.
- 757 Hallock P.: *Algal Symbiosis : A Mathematical Analysis Marine Biology* 62, 249–255, 1981b.
- 758 Hemming, N. G. and Hanson, G. N. Boron isotopic composition and concentration in modern marine carbonates,  
759 *Geochim. Cosmochim. Acta*, 56, 537–543, 1992.
- 760 Hendry, K.R., Rickaby, R.E.M., Meredith, M.P., Elderfield, H.: Controls on stable isotope and trace metal  
761 uptake in *Neogloboquadrina pachyderma* (sinistral) from an Antarctic sea-ice environment. *Earth Planet.*  
762 *Sci. Lett.* 278, 67–77, 2009.
- 763 Henehan, M. J., Foster, G. L., Bostock, H. C., Greenop, R., Marshall, B. J. and Wilson, P. A.: A new boron  
764 isotope-pH calibration for *Orbulina universa*, with implications for understanding and accounting for ‘vital  
765 effects’, *Earth Planet. Sci. Lett.*, 454, 282–292, 2016.
- 766 Henehan, M. J., Foster, G. L., Rae, J. W. B., Prentice, K. C., Erez, J., Bostock, H. C., Marshall, B. J. and Wilson,  
767 P. A.: Evaluating the utility of B/Ca ratios in planktic foraminifera as a proxy for the carbonate system: A  
768 case study of *Globigerinoides ruber*, *Geochemistry, Geophys. Geosystems* 16, 1052–1069, 2015.

- 769 Henehan, M. J., Rae, J. W. B., Foster, G. L., Erez, J., Prentice, K. C., Kucera, M., Bostock, H. C., Martínez-Botí,  
770 M. A., Milton, J. A., Wilson, P. A., Marshall, B. J. and Elliott, T.: Calibration of the boron isotope proxy in  
771 the planktonic foraminifera *Globigerinoides ruber* for use in palaeo-CO<sub>2</sub> reconstruction, *Earth Planet. Sci.*  
772 *Lett.* 364, 111–122, 2013.
- 773 Holcomb, M., Decarlo, T. M., Schoepf, V., Dissard, D., Tanaka, K. and McCulloch, M.: Cleaning and pre-  
774 treatment procedures for biogenic and synthetic calcium carbonate powders for determination of elemental  
775 and boron isotopic compositions, *Chem. Geol.*, 398, 11–21, 2015.
- 776 Hönlisch, B., Hemming, N. G., Archer, D., Siddall, M. and McManus, J. F.: Atmospheric Carbon Dioxide  
777 Concentration Across the Mid-Pleistocene Transition, *Science*, 324, 1551–1554, 2009.
- 778 Hönlisch, B., Bijma, J., Russell, A. D., Spero, H. J., Palmer, M. R., Zeebe, R. E. and Eisenhauer, A.: The  
779 influence of symbiotic photosynthesis on the boron isotopic composition of foraminifera shells, *Mar.*  
780 *Micropaleontol.*, 49, 87–96, 2003.
- 781 Hönlisch, B. and Hemming, N. G.: Ground-truthing the boron isotope-paleo-pH proxy in planktonic foraminifera  
782 shells: Partial dissolution and shell size effects, *Paleoceanography* 19, 1–13, 2004.
- 783 Hönlisch, B., Bickert, T. and Hemming, N. G.: Modern and Pleistocene boron isotope composition of the benthic  
784 foraminifer *Cibicides wuellerstorfi*, *Earth Planet. Sci. Lett.*, 272, 309–318, 2008.
- 785 Howes, E. L., Kaczmarek, K., Raitzsch, M., Mewes, A., Bijma, N., Horn, I., Misra, S., Gattuso, J. P. and Bijma,  
786 J.: Decoupled carbonate chemistry controls on the incorporation of boron into *Orbulina universa*,  
787 *Biogeosciences*, 14, 415–430, 2017.
- 788 IPCC: Climate Change 2014 - The Physical Science Basis, edited by Intergovernmental Panel on Climate  
789 Change, Cambridge University Press, Cambridge., 2014.
- 790 Jørgensen, B. B., Erez, J., Revsbech, P. and Cohen, Y.: Symbiotic photosynthesis in a planktonic foraminifera,  
791 *Globigerinoides sacculifer* (Brady), studied with microelectrodes, *Limnol. Oceanogr.*, 30, 1253–1267  
792 1985.
- 793 Kaczmarek, K., Nehrke, G., Misra, S., Bijma, J. and Elderfield, H.: Investigating the effects of growth rate and  
794 temperature on the B/Ca ratio and  $\delta^{11}\text{B}$  during inorganic calcite formation, *Chem. Geol.*, 421, 81–92,  
795 2016.
- 796 Kemle-von Mücke S. and Oberhänsli H.: The Distribution of Living Planktic Foraminifera in Relation to  
797 Southeast Atlantic Oceanography, *Use Proxies Paleoceanogr.*, 91–115, 1999.
- 798 Key, R.M.: A global ocean carbon climatology: Results from Global Data Analysis Project (GLODAP), *Global*  
799 *Biogeochem. Cycles*, 18, GB4031, 2004.
- 800 Kim, S.-T. and O'Neil, J. R.: Equilibrium and nonequilibrium oxygen isotope effects in synthetic carbonates,  
801 *Geochim. Cosmochim. Acta*, 61, 3461–3475, 1997.
- 802 Klochko, K., Cody, G. D., Tossell, J. A., Dera, P. and Kaufman, A. J.: Re-evaluating boron speciation in  
803 biogenic calcite and aragonite using  $^{11}\text{B}$  MAS NMR, *Geochim. Cosmochim. Acta*, 73, 1890–1900, 2009.
- 804 Klochko, K., Kaufman, A. J., Yao, W., Byrne, R. H. and Tossell, J. A.: Experimental measurement of boron  
805 isotope fractionation in seawater, *Earth Planet. Sci. Lett.*, 248, 276–285, 2006.
- 806 Köhler-Rink, S. and Kühl, M.: Microsensor studies of photosynthesis and respiration in larger symbiotic  
807 foraminifera. I. The physico-chemical microenvironment of *Marginopora vertebralis*, *Amphistegina*  
808 *lobifera* and *Amphisorus hemrichii*, *Mar. Biol.*, 137, 473–486, 2000.

- 809 Köhler-Rink, S. and Kühl, M., Microsensor studies of photosynthesis and respiration in the larger symbiont  
810 bearing foraminifera *Amphistegina lobifera*, and *Amphisorus hemprichii*, *Ophelia*, 55, 111–122, 2001.
- 811 Lea, D. W., Pak, D. K. and Spero, H. J.: Climate impact of late quaternary equatorial Pacific sea surface  
812 temperature variations, *Science*, 289, 1719–1724, 2000.
- 813 Lemarchand, D., Gaillardet, J., Lewin, A. and Allègre, C. J.: Boron isotope systematics in large rivers:  
814 Implications for the marine boron budget and paleo-pH reconstruction over the Cenozoic, *Chem. Geol.*,  
815 190, 123–14, 2002.
- 816 Liu, Y., Liu, W., Peng, Z., Xiao, Y., Wei, G., Sun, W., He, J., Liu, G. and Chou, C.-L.: Instability of seawater  
817 pH in the South China Sea during the mid-late Holocene: Evidence from boron isotopic composition of  
818 corals, *Geochim. Cosmochim. Acta*, 73, 1264–1272, 2009.
- 819 Lloyd, N. S., Sadekov, A. Y. and Misra, S.: Application of 1013ohm Faraday cup current amplifiers for boron  
820 isotopic analyses by solution mode and laser ablation multicollector inductively coupled plasma mass  
821 spectrometry, *Rapid Commun. Mass Spectrom.*, 32, 9–18, 2018.
- 822 Martínez-Botí, M. A., Foster, G. L., Chalk, T. B., Rohling, E. J., Sexton, P. F., Lunt, D. J., Pancost, R. D.,  
823 Badger, M. P. S. and Schmidt, D. N.: Plio-Pleistocene climate sensitivity evaluated using high-resolution  
824 CO<sub>2</sub> records, *Nature*, 518, 49–54, 2015a.
- 825 Martínez-Botí M. A., Marino G., Foster G. L., Ziveri P., Henehan M. J., Rae J. W. B., Mortyn P. G. and Vance  
826 D.: Boron isotope evidence for oceanic carbon dioxide leakage during the last deglaciation. *Nature*, 518,  
827 219–222, 2015b.
- 828 Martínez-Botí, M. A., Mortyn, P. G., Schmidt, D. N., Vance, D. and Field, D. B.: Mg/Ca in foraminifera from  
829 plankton tows: Evaluation of proxy controls and comparison with core tops, *Earth Planet. Sci. Lett.*, 307,  
830 113–125, 2011.
- 831 Mavromatis, V., Montouillout, V., Noireaux, J., Gaillardet, J. and Schott, J.: Characterization of boron  
832 incorporation and speciation in calcite and aragonite from co-precipitation experiments under controlled  
833 pH, temperature and precipitation rate, *Geochim. Cosmochim. Acta*, 150, 299–313, 2015.
- 834 McCulloch, M. T., D’Olivo, J. P., Falter, J. L., Georgiou, L., Holcomb, M., Montagna, P. and Trotter, J. A.  
835 Boron Isotopic Systematics in Scleractinian Corals and the Role of pH Up-regulation, *Boron Isot. Adv.*  
836 *Isot. Geochemistry*, 2018.
- 837 Millero, F.: Speciation of metals in natural waters, *Geochem. Trans.*, 2, 57, 2001.
- 838 Millero, F., Woosley, R., DiTrollo, B. and Waters, J.: Effect of Ocean Acidification on the Speciation of Metals  
839 in Seawater, *Oceanography* 22, 72–85, 2009.
- 840 Misra, S., Greaves, M., Owen, R., Kerr, J., Elmore, A. C. and Elderfield, H.: Determination of B/Ca of natural  
841 carbonates by HR-ICP-MS, *Geochemistry, Geophys. Geosystems*, 15, 1617–1628, 2014a.
- 842 Misra, S., Owen, R., Kerr, J., Greaves, M. and Elderfield, H.: Determination of  $\delta^{11}\text{B}$  by HR-ICP-MS from mass  
843 limited samples: Application to natural carbonates and water samples, *Geochim. Cosmochim. Acta*, 140,  
844 531–552, 2014b.
- 845 Mortyn, P. G. and Charles, C. D.: Planktonic foraminiferal depth habitat and  $\delta^{18}\text{O}$  calibrations: Plankton tow  
846 results from the Atlantic sector of the Southern Ocean, *Paleoceanography*, 18, 2003.
- 847 Mulitza, S., Boltovskoy, D., Donner, B., Meggers, H., Paul, A. and Wefer, G.: Temperature: $\delta^{18}\text{O}$  relationships  
848 of planktonic foraminifera collected from surface waters, *Palaeogeogr. Palaeoclimatol. Palaeoecol.*, 202,  
849 143–152, 2003.

- 850 Ni, Y., Foster, G. L., Bailey, T., Elliott, T., Schmidt, D. N., Pearson, P., Haley, B. and Coath, C.: A core top  
851 assessment of proxies for the ocean carbonate system in surface-dwelling foraminifers, *Paleoceanography*  
852 22, 2007.
- 853 Nir, O., Vengosh, A., Harkness, J. S., Dwyer, G. S. and Lahav, O.: Direct measurement of the boron isotope  
854 fractionation factor: Reducing the uncertainty in reconstructing ocean paleo-pH, *Earth Planet. Sci. Lett.*,  
855 414, 1–5, 2015.
- 856 Noireaux, J., Mavromatis, V., Gaillardet, J., Schott, J., Montouillout, V., Louvat, P., Rollion-Bard, C. and  
857 Neuville, D. R.: Crystallographic control on the boron isotope paleo-pH proxy, *Earth Planet. Sci. Lett.*,  
858 430, 398–407, 2015.
- 859 Orr, J. C., Fabry, V. J., Aumont, O., Bopp, L., Doney, S. C., Feely, R. A., Gnanadesikan, A., Gruber, N., Ishida,  
860 A., Joos, F., Key, R. M., Lindsay, K., Maier-Reimer, E., Matear, R., Monfray, P., Mouchet, A., Najjar, R.  
861 G., Plattner, G. K., Rodgers, K. B., Sabine, C. L., Sarmiento, J. L., Schlitzer, R., Slater, R. D., Totterdell, I.  
862 J., Weirig, M. F., Yamanaka, Y. and Yool, A.: Anthropogenic ocean acidification over the twenty-first  
863 century and its impact on calcifying organisms, *Nature*, 437, 681–686, 2005.
- 864 Pagani, M.: Marked Decline in Atmospheric Carbon Dioxide Concentrations During the Paleogene, *Science*,  
865 309, 600–603, 2005.
- 866 Palmer, M. R., Pearson, P. N. and Cobb, S. J., Reconstructing Past Ocean pH-Depth Profiles, *Science*, 282,  
867 1468–1471, 1998.
- 868 Pearson, P. N. and Palmer, M. R.: Middle Eocene seawater pH and atmospheric carbon dioxide concentrations,  
869 *Science*, 284, 1824–1826, 1999.
- 870 Peeters, F. J. C. and Brummer, G.-J. a.: The seasonal and vertical distribution of living planktic foraminifera in  
871 the NW Arabian Sea, *Geol. Soc. London, Spec. Publ.*, 195, 463–497, 2002.
- 872 Quintana Krupinski, N. B., Russell, A. D., Pak, D. K. and Paytan, A.: Core-top calibration of B/Ca in Pacific  
873 Ocean *Neoglobobulimina inconstans* and *Globobulimina bulloides* as a surface water carbonate system proxy,  
874 *Earth Planet. Sci. Lett.*, 466, 139–151, 2017.
- 875 Rae, J.W.B.: Boron Isotopes in Foraminifera: Systematics, Biomineralisation, and CO<sub>2</sub> Reconstruction. In:  
876 Marschall, H., Foster, G. (eds), *Boron Isotopes. Advances in Isotope Geochemistry*. Springer, Cham, 2018.
- 877 Rae, J. W. B., Foster, G. L., Schmidt, D. N. and Elliott, T.: Boron isotopes and B/Ca in benthic foraminifera:  
878 Proxies for the deep ocean carbonate system, *Earth Planet. Sci. Lett.*, 302, 403–413, 2011.
- 879 Raitzsch, M., Bijma, J., Benthien, A., Richter, K.-U., Steinhofel, G. and Kučera, M.: Boron isotope-based  
880 seasonal paleo-pH reconstruction for the Southeast Atlantic – A multispecies approach using habitat  
881 preference of planktonic foraminifera, *Earth Planet. Sci. Lett.*, 487, 138–150, 2018.
- 882 Ravelo, A. C. and Fairbanks, R. G.: Oxygen isotopic composition of multiple species of planktonic foraminifera:  
883 recorder of the modern photic zone temperature gradient, *Palaeogeogr. Palaeoclimatol. Palaeoecol.*, 7,  
884 815–831, 1992.
- 885 Regenberg, M., Nürnberg, D., Steph, S., Groeneveld, J., Garbe-Schönberg, D., Tiedemann, R. and Dullo, W.-C.:  
886 Assessing the effect of dissolution on planktonic foraminiferal Mg/Ca ratios: Evidence from Caribbean  
887 core tops, *Geochemistry, Geophys. Geosystems*, 7, 2006.
- 888 Regenberg, M., Steph, S., Nürnberg, D., Tiedemann, R. and Garbe-Schönberg, D.: Calibrating Mg/Ca ratios of  
889 multiple planktonic foraminiferal species with  $\delta^{18}\text{O}$ -calcification temperatures: Paleothermometry for the  
890 upper water column, *Earth Planet. Sci. Lett.*, 278, 324–336, 2009.

- 891 Rickaby, R. E. M. and Halloran, P.: Cool La Nina During the Warmth of the Pliocene?, *Science*, 307, 1948–  
892 1952, 2005.
- 893 Ries, J. B., Cohen, A. L. and McCorkle, D. C.: Marine calcifiers exhibit mixed responses to CO<sub>2</sub>-induced ocean  
894 acidification, *Geology*, 37, 1131–1134, 2009.
- 895 Rink, S., Kühl, M., Bijma, J. and Spero, H. J.: Microsensor studies of photosynthesis and respiration in the  
896 symbiotic foraminifer *Orbulina universa*, *Mar. Biol.*, 131, 583–595, 1998.
- 897 Rollion-Bard, C. and Erez, J.: Intra-shell boron isotope ratios in the symbiont-bearing benthic foraminiferan  
898 *Amphistegina lobifera*: Implications for  $\delta^{11}\text{B}$  vital effects and paleo-pH reconstructions, *Geochim.*  
899 *Cosmochim. Acta*, 74, 1530–1536, 2010.
- 900 Rostek, F., Ruhland, G., Bassinot, F. C., Muller, P. J., Labeyrie, L. D., Lancelot, Y. and Bard, E.: Reconstructing  
901 Sea-Surface Temperature and Salinity Using  $\delta^{18}\text{O}$  and Alkenone Records, *Nature*, 364, 319–321, 1993.
- 902 Russell, A. D., Hönisch, B., Spero, H. J. and Lea, D. W.: Effects of seawater carbonate ion concentration and  
903 temperature on shell U, Mg, and Sr in cultured planktonic foraminifera, *Geochim. Cosmochim. Acta*, 68,  
904 4347–4361, 2004.
- 905 Sanyal, A., Bijma, J., Spero, H. J. and Lea, D. W.: Empirical relationship between pH and the boron isotopic  
906 composition of *Globigerinoides sacculifer*: Implications for the boron isotopes paleo-pH proxy,  
907 *Paleoceanography*, 16, 515–519, 2001.
- 908 Sanyal, A., Hemming, N. G., Broecker, W. S., Lea, D. W., Spero, H. J., & Hanson, G. N. Oceanic pH control on  
909 the boron isotopic composition of foraminifera: evidence from culture experiments, *Paleoceanography*,  
910 11(5), 513-517, 1996.
- 911 Schmidt, G. A. and Mulitza, S.: Global calibration of ecological models for planktic foraminifera from core-top  
912 carbonate oxygen-18, *Mar. Micropaleontol.*, 44, 125–140, 2002.
- 913 Seki, O., Foster, G. L., Schmidt, D. N., Mackensen, A., Kawamura, K. and Pancost, R. D.: Alkenone and boron-  
914 based Pliocene pCO<sub>2</sub> records, *Earth Planet. Sci. Lett.*, 292, 201–211, 2010.
- 915 Shirayama, Y.: Effect of increased atmospheric CO<sub>2</sub> on shallow water marine benthos, *J. Geophys. Res.*, 110,  
916 C09S08, 2005.
- 917 Sime, N. G., De La Rocha, C. L. and Galy, A.: Negligible temperature dependence of calcium isotope  
918 fractionation in 12 species of planktonic foraminifera, *Earth Planet. Sci. Lett.*, 232, 51–66, 2005.
- 919 Spero H. J.: Symbiosis in the planktonic foraminifer, *Orbulina universa*, and the isolation of its symbiotic  
920 dinoflagellate, *Gymnodinium beii* sp. nov., *J. Phycol.* 23, 307-317, 1987.
- 921 Sutton, J. N., Liu, Y. W., Ries, J. B., Guillemin, M., Ponzevera, E. and Eagle, R. A.:  $\delta^{11}\text{B}$  as monitor of  
922 calcification site pH in divergent marine calcifying organisms, *Biogeosciences*, 15, 1447–1467, 2018.
- 923 Takagi H., Kimoto K., Fujiki T., Saito H., Schmidt C. and Kucera M.: Characterizing photosymbiosis in modern  
924 planktonic foraminifera, *Biogeosciences*, 3377–3396, 2019.
- 925 Thomson, J., Brown, L., Nixon, S., Cook, G. T. and MacKenzie, A. B.: Bioturbation and Holocene sediment  
926 accumulation fluxes in the north-east Atlantic Ocean (Benthic Boundary Layer experiment sites), *Mar.*  
927 *Geol.*, 169, 21–39, 2000.
- 928 Tripathi, A.: Deep-Sea Temperature and Circulation Changes at the Paleocene-Eocene Thermal Maximum.  
929 *Science*, 308, 1894–1898, 2005.

- 930 Tripathi, A. K., Roberts, C. D. and Eagle, R. A.: Coupling of CO<sub>2</sub> and Ice Sheet Stability Over Major Climate  
931 Transitions of the Last 20 Million Years, *Science*, 326, 1394–1397, 2009.
- 932 Tripathi, A. K., Roberts, C. D., Eagle, R. A. and Li, G.: A 20 million year record of planktic foraminiferal B/Ca  
933 ratios: Systematics and uncertainties in pCO<sub>2</sub> reconstructions, *Geochim. Cosmochim. Acta*, 75, 2582–  
934 2610, 2011.
- 935 Uchikawa, J., Penman, D. E., Zachos, J. C. and Zeebe, R. E.: Experimental evidence for kinetic effects on B/Ca  
936 in synthetic calcite: Implications for potential B(OH)<sub>4</sub><sup>-</sup> and B(OH)<sub>3</sub> incorporation, *Geochim. Cosmochim.  
937 Acta*, 150, 171–191, 2015.
- 938 Urey, H.C., Lowenstam, H.A., Epstein, S. & McKinney, C.R.: Measurement of paleo-temperature and  
939 temperatures of the upper cretaceous of England, Denmark, and the southeastern United-States. *Geol. Soc.  
940 Am. Bull.*, 62, 399–416, 1951.
- 941 Wang, B.-S., You, C.-F., Huang, K.-F., Wu, S.-F., Aggarwal, S. K., Chung, C.-H. and Lin, P.-Y.: Direct  
942 separation of boron from Na- and Ca-rich matrices by sublimation for stable isotope measurement by MC-  
943 ICP-MS, *Talanta*, 82, 1378–1384, 2010.
- 944 Wang, G., Cao, W., Yang, D. and Xu, D.: Variation in downwelling diffuse attenuation coefficient in the  
945 northern South China Sea, *Chinese J. Oceanol. Limnol.*, 26, 323–333, 2008.
- 946 Weare, B. C., Strub, P. T. and Samuel, M. D. Annual Mean Surface Heat Fluxes in the Tropical Pacific Ocean, J.  
947 *Phys. Oceanogr.*, 11, 705–717, 1981.
- 948 Wei, G., McCulloch, M. T., Mortimer, G., Deng, W. and Xie, L.: Evidence for ocean acidification in the Great  
949 Barrier Reef of Australia, *Geochim. Cosmochim. Acta*, 73, 2332–2346, 2009.
- 950 Wilson, D. J., Piotrowski, A. M., Galy, A. and McCave, I. N.: A boundary exchange influence on deglacial  
951 neodymium isotope records from the deep western Indian Ocean, *Earth Planet. Sci. Lett.*, 341–344, 35–47,  
952 2012.
- 953 Wolf-Gladrow, D. A., Riebesell, U., Burkhardt, S. and Buma, J.: Direct effects of CO<sub>2</sub> concentration on growth  
954 and isotopic composition of marine plankton, *Tellus B Chem. Phys. Meteorol.*, 51, 461–476, 1999.
- 955 Yu, J., Menviel, L., Jin, Z. D., Thornalley, D. J. R., Barker, S., Marino, G., Rohling, E. J., Cai, Y., Zhang, F.,  
956 Wang, X., Dai, Y., Chen, P. and Broecker, W. S.: Sequestration of carbon in the deep Atlantic during the  
957 last glaciation, *Nat. Geosci.*, 9, 319–324, 2016.
- 958 Yu, J., Thornalley, D. J. R., Rae, J. W. B. and McCave, N. I.: Calibration and application of B/Ca, Cd/Ca, and δ  
959 <sup>11</sup>B in *Neogloboquadrina pachyderma* (sinistral) to constrain CO<sub>2</sub> uptake in the subpolar North Atlantic  
960 during the last deglaciation, *Paleoceanography*, 28, 237–252, 2013.
- 961 Yu, J., Foster, G. L., Elderfield, H., Broecker, W. S. and Clark, E.: An evaluation of benthic foraminiferal B/Ca  
962 and δ<sup>11</sup>B for deep ocean carbonate ion and pH reconstructions, *Earth Planet. Sci. Lett.*, 293, 114–120, 20,  
963 2010.
- 964 Yu, J., Elderfield, H., Hönisch, B.: B/Ca in planktonic foraminifera as a proxy for surface seawater pH.  
965 *Paleoceanography*22, PA2202, 2007.
- 966 Yu, J., Day, J., Greaves, M. and Elderfield, H., Determination of multiple element/calcium ratios in foraminiferal  
967 calcite by quadrupole ICP-MS, *Geochemistry, Geophys. Geosystems* 6, 2005.
- 968 Zeebe, R. E. and Wolf-Gladrow, D., CO<sub>2</sub> in Seawater: Equilibrium, Kinetics, Isotopes Elsevier Oceanography  
969 Series 65, Amsterdam, 2001.

970 Zeebe, R. E., Wolf-Gladrow, D. A., Bijma, J. and Hönisch, B., Vital effects in foraminifera do not compromise  
971 the use of  $\delta^{11}\text{B}$  as a paleo- pH indicator: Evidence from modeling, *Paleoceanography*, 18, 2003.



972 **Figure caption**

973

974 **Figure 1:** Reactions governing dissolved inorganic carbon equilibria.

975

976 **Figure 2:** (A) Speciation of  $\text{H}_3\text{BO}_3$  and  $\text{H}_4\text{BO}_4^-$  as function of seawater pH (total scale), (B)  $\delta^{11}\text{B}$  of dissolved  
977 inorganic boron species as a function of seawater pH, (C) sensitivity of  $\delta^{11}\text{B}$  of  $\text{H}_4\text{BO}_4^-$  for a pH ranging from  
978 7.6 to 8.4.  $T=25^\circ\text{C}$ ,  $S=35$ ,  $\delta^{11}\text{B}=39.61$  ‰ (Foster et al., 2010), dissociation constant  $\alpha = 1.0272$  (Klochko et al.,  
979 2006).

980

981 **Figure 3:** Map showing locations of the core-tops used in this study (white diamonds). Red open circles  
982 represent the sites used for *in-situ* carbonate parameters from GLODAP database (Key et al., 2004).

983

984 **Figure 4:** Pre-industrial data versus depth of the sites used in this study. The figure shows seasonal temperatures  
985 (extracted from World Ocean Database 2013), density anomaly ( $\text{kg/m}^3$ ), pre-industrial pH and pre-industrial  
986  $\delta^{11}\text{B}$  of  $\text{H}_4\text{BO}_4^-$  (calculated from the GLODAP database and corrected for anthropogenic inputs).

987

988 **Figure 5:** Boron isotopic measurements of mixed-layer foraminifera plotted against the  $\delta^{11}\text{B}_{\text{borate}}$ .  $\delta^{11}\text{B}_{\text{borate}}$  were  
989 characterized by determination of the calcification depth of the foraminifera, A) *G. ruber*, B) *T. sacculifer*, C) *O.*  
990 *universa*. Mono-specific calibrations are summarized in Table 3.

991

992 **Figure 6:** Boron isotopic measurements of deep-dwelling foraminifera ( $\delta^{11}\text{B}_{\text{carbonate}}$ ) plot against  $\delta^{11}\text{B}_{\text{borate}}$ .  
993  $\delta^{11}\text{B}_{\text{borate}}$  were characterized by determining the calcification depth of foraminifera, A) *P. obliquiloculata*, B) *G.*  
994 *menardii*, C) *N. dutertrei*, D) *G. tumida* and E) Compilation of deep dweller species. Mono-specific calibrations  
995 are summarized in Table 3.

996

997 **Figure 7:** Boxplots of B/Ca ratios for multiple species, *T. sacculifer* (this study; Foster et al., 2008; Ni et al;  
998 2007; Seki et al., 2010), *G. ruber* (this study; Babila et al., 2014; Foster et al., 2008; Ni et al., 2007), *G. inflata*,  
999 *G. bulloides* (Yu et al., 2007), *N. pachyderma* (Hendry et al., 2009; Yu et al., 2013), *N. dutertrei* (this study;  
1000 Foster et al., 2008), *O. universa*, *P. obliquiloculata*, *G. menardii*, *G. tumida* (this study).

1001

1002 **Figure 8:** A) Boxplot showing the calculated microenvironment pH difference ( $\Delta\text{microenvironment pH}$ )  
1003 between microenvironment and external pH based on the  $\delta^{11}\text{B}$  data. B) This figure shows that a decrease in  
1004 insolation can explain the low  $\delta^{11}\text{B}$  from the WEP. Light penetration profile in the Western Pacific, with  $E_0$   
1005 in the WEP of  $220 \text{ J}\cdot\text{s}\cdot\text{m}^{-2}$  (Weare et al., 1981) and a light attenuation coefficient of 0.028 (Wang et al., 2008).  
1006 Theoretical depths were calculated for a decrease in microenvironment pH of  $\Delta\text{pH}_1 = -0.02$  (e.g. WP07-a);  
1007  $\Delta\text{pH}_1 = -0.04$  (e.g. A14),  $\Delta\text{pH}_2 = -0.06$  (e.g. 806A). Light penetration corresponding to  $E_c$  is  $\sim 12\%$ ,  $\Delta\text{pH}_0 \sim 7\%$ ,  
1008  $\Delta\text{pH}_1 \sim 5\%$ ,  $\Delta\text{pH}_2 \sim 1\%$  respective depth are 75m, 90m, 110m and 150m. Grey band is the calcification depth of  
1009 *T. sacculifer* (w/o sacc) utilized in this study.

1010

1011 **Figure 9:** Water depth pH profiles reconstructed at every site applying the mono-specific calibrations derived  
1012 from our results (Table 3). Figure is showing measured  $\delta^{11}\text{B}_{\text{calcite}}$ ,  $\delta^{11}\text{B}_{\text{borate}}$  calculated according to different  
1013 calibrations (see Table 3 and text), calculated pH based on  $\delta^{11}\text{B}$  ( $\text{pH}_{\delta^{11}\text{B}}$ ) and  $\text{pCO}_2$  calculated from  $\text{pH}_{\delta^{11}\text{B}}$  and  
1014 alkalinity.

1015  
1016 **Figure 10:** Evaluation of the reconstructed parameters,  $\delta^{11}\text{B}_{\text{borate}}$ , pH and  $\text{pCO}_2$  versus *in-situ* parameter. The  
1017 recalculated parameters are consistent with *in-situ* data, except for *G. ruber*. This variability might be explained  
1018 by the different test sizes.

1019 **Table caption**

1020

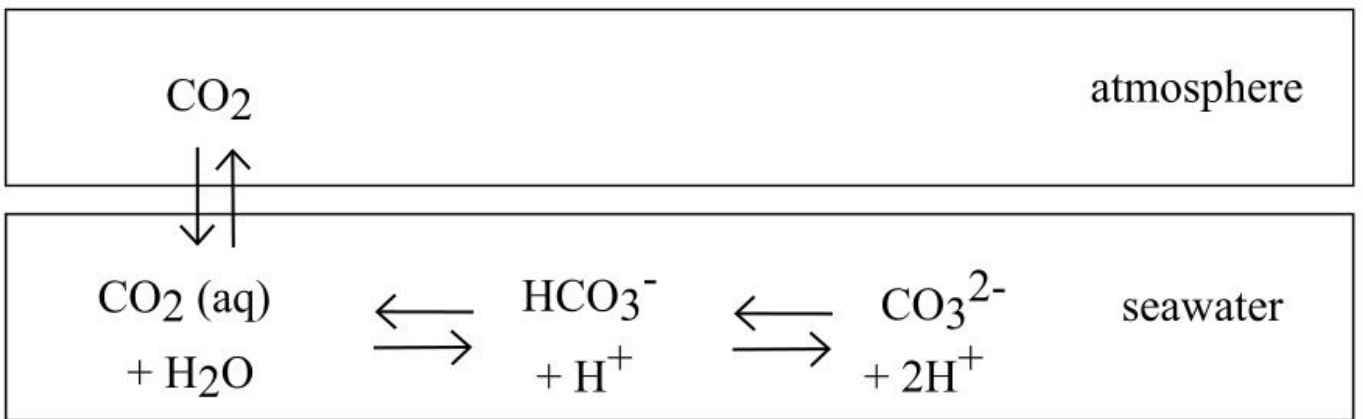
1021 **Table 1:** Box-core information

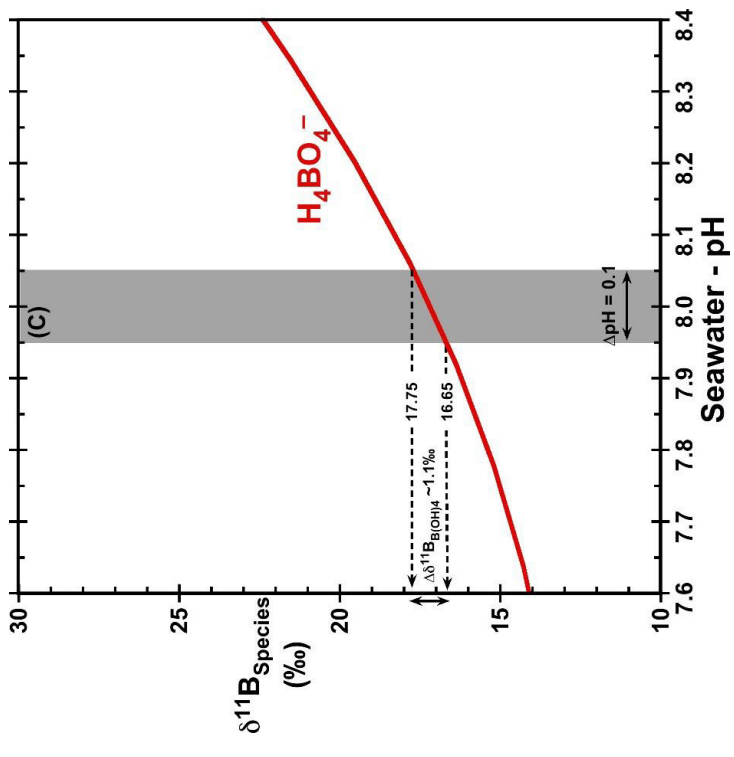
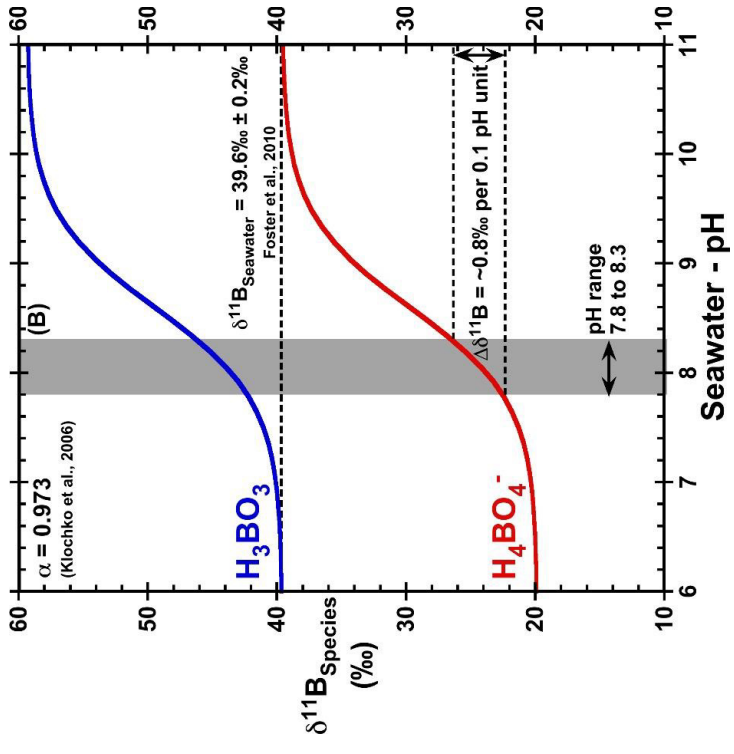
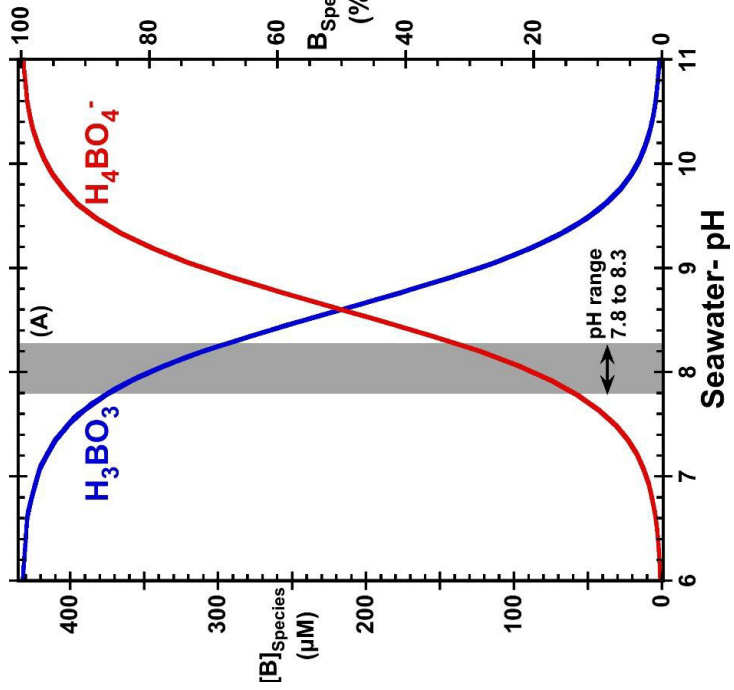
1022

1023 **Table 2:** Analytical results of  $\delta^{13}\text{C}$ ,  $\delta^{18}\text{O}$ ,  $\delta^{11}\text{B}$  and elemental ratios Li/Ca, B/Ca and Mg/Ca

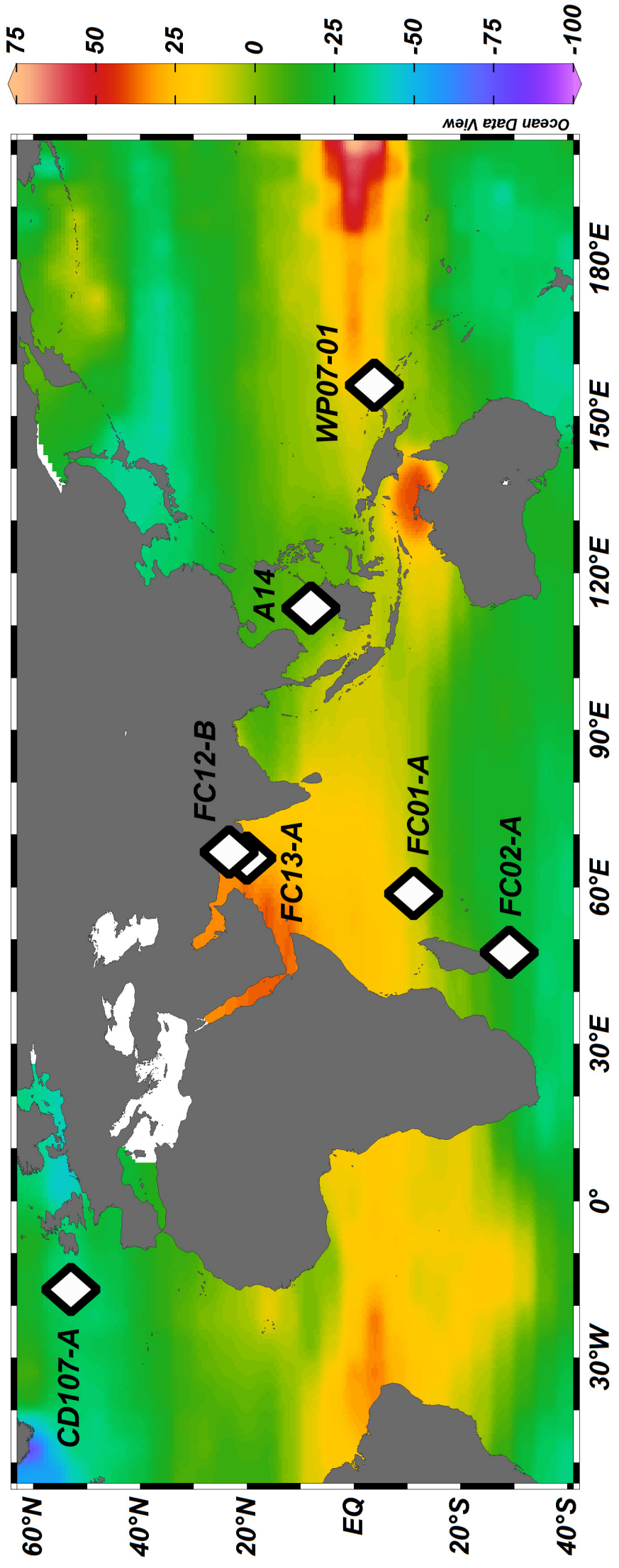
1024

1025 **Table 3:** Species-specific  $\delta^{11}\text{B}_{\text{carbonate}}$  to  $\delta^{11}\text{B}_{\text{borate}}$  calibrations from literature and from our data





**Delta pCO<sub>2</sub> [ $\mu$ atm]**



### Temperature

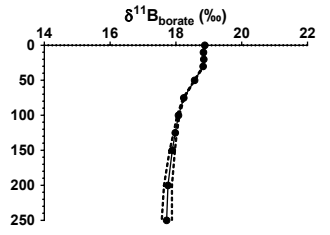
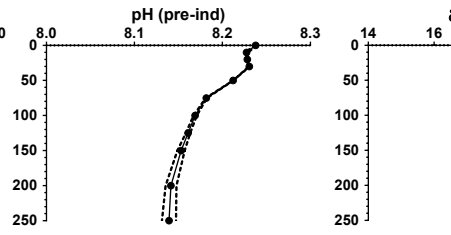
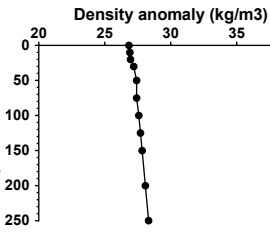
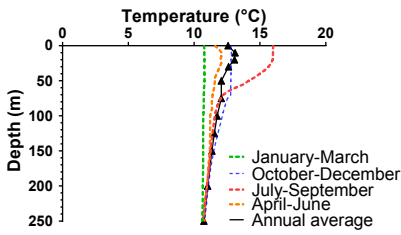
### Density anomaly

### pH (pre-ind)

### $\delta^{11}\text{B}_{\text{borate}}$ (‰)

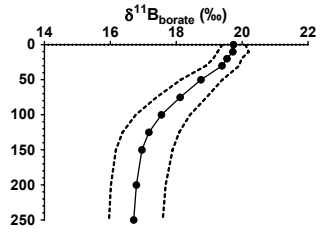
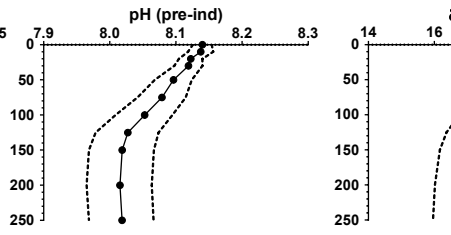
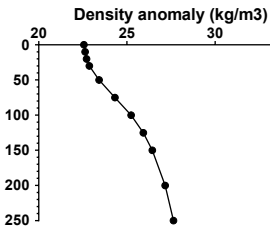
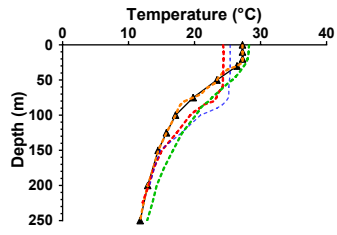
#### Atlantic Ocean

CD107-a  
52.9°N, -16.9°E  
3569 m

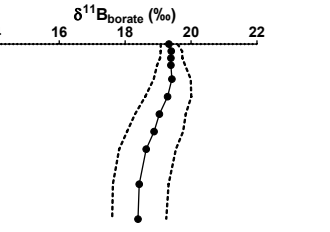
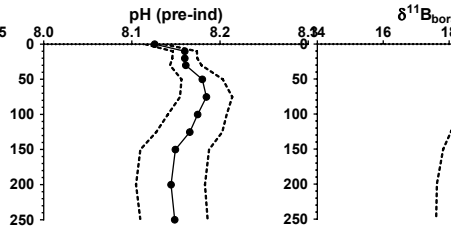
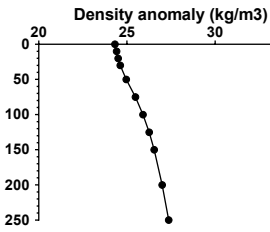
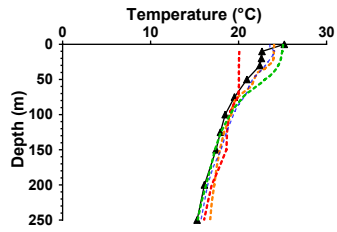


#### Indian Ocean

FC-01a  
-11.2°N, 58.8°E  
3520 m

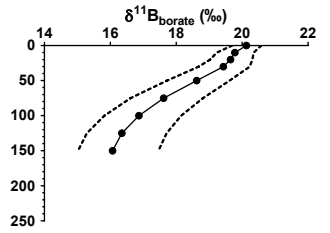
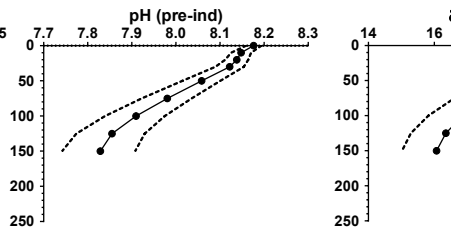
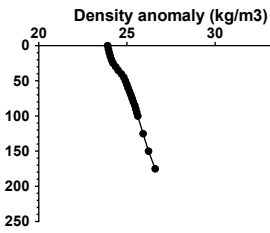
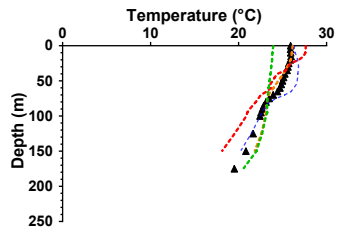


FC-02a  
-29.1°N, 47.5°E  
2871 m

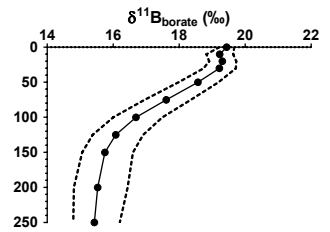
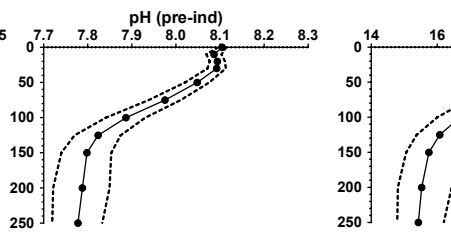
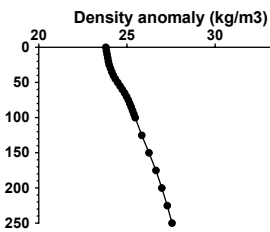
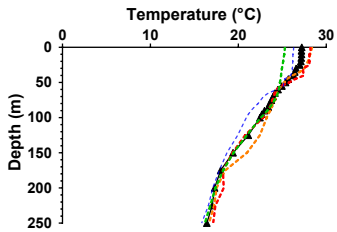


#### Arabian Sea

FC-12b  
23.3°N, 66.7°E  
151 m

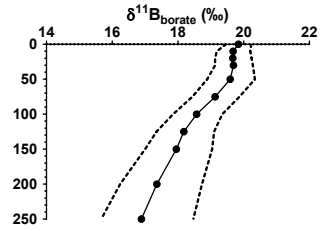
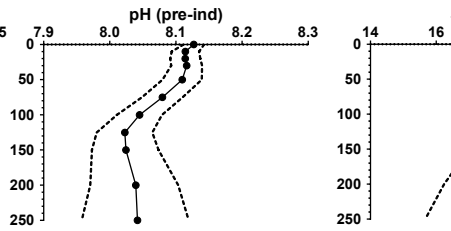
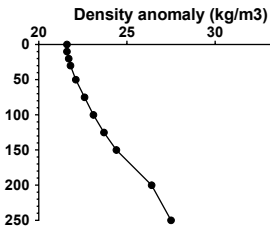
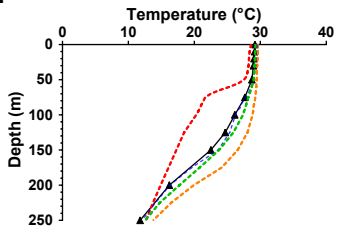


FC-13a  
20.0°N, 65.6°E  
3190 m



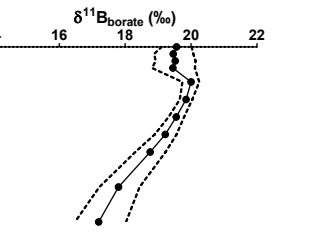
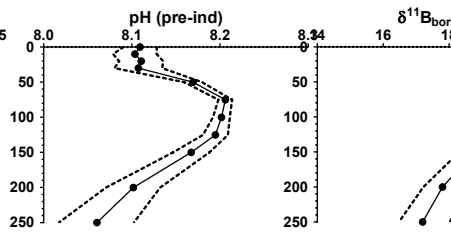
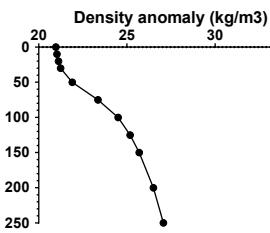
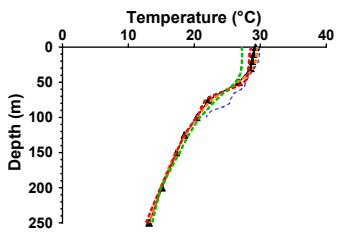
#### Pacific Ocean

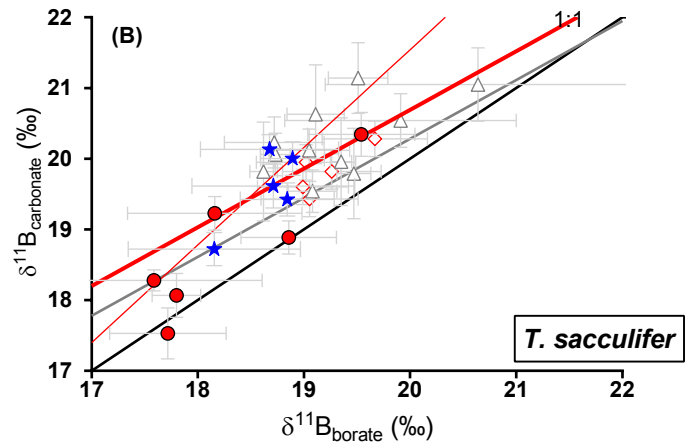
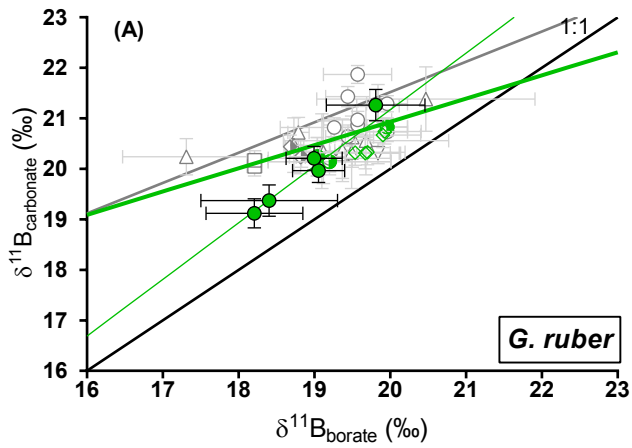
WP07-01  
-3.9°N, 156.0°E  
1800 m



A14

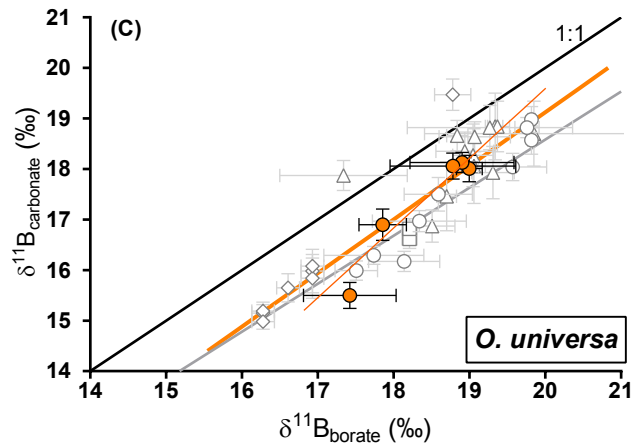
8.0°N, 113.4°E  
1911 m





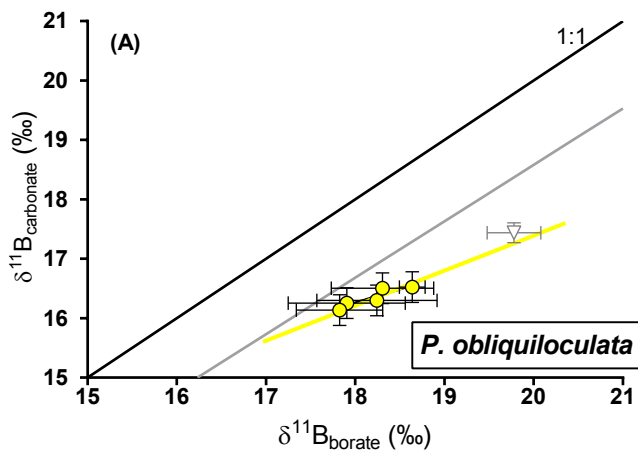
- $\delta^{11}\text{B}_{G. ruber}$  (core-top, this study)
- ◇  $\delta^{11}\text{B}_{G. ruber}$  (core-top, Foster et al., 2008)
- $\delta^{11}\text{B}_{G. ruber}$  (core-top, 250-300 $\mu\text{m}$ , Henehan et al., 2013)
- $\delta^{11}\text{B}_{G. ruber}$  (core-top, Henehan et al., 2013)
- $\delta^{11}\text{B}_{G. ruber}$  (sediment trap, Henehan et al., 2013)
- ◇  $\delta^{11}\text{B}_{G. ruber}$  (tow, Henehan et al., 2013)
- ▽  $\delta^{11}\text{B}_{G. ruber}$  (grab sample, Henehan et al., 2013)
- △  $\delta^{11}\text{B}_{G. ruber}$  (Raizsch et al., 2018)
- $G. ruber$  calibration line (All data, this study)
- $G. ruber$  calibration line (Core-top, this study)
- $G. ruber$  calibration line (Culture, Henehan et al., 2013)

- $\delta^{11}\text{B}_{T. sacculifer}$  (w/o sacc) (core-top, this study)
- △  $\delta^{11}\text{B}_{T. sacculifer}$  (w/o sacc) (core-top, Raizsch et al., 2018)
- ★  $\delta^{11}\text{B}_{T. sacculifer}$  (sacc) (core-top, this study)
- ◇  $\delta^{11}\text{B}_{T. sacculifer}$  (sacc) (core-top, Foster et al., 2008)
- $T. sacculifer$  (w/o sacc and sacc) calibration line (All data, this study)
- $T. sacculifer$  (w/o sacc and sacc) calibration line (Core-top, this study)
- $T. sacculifer$  (s) calibration line (Martinez-Boti et al., 2015)

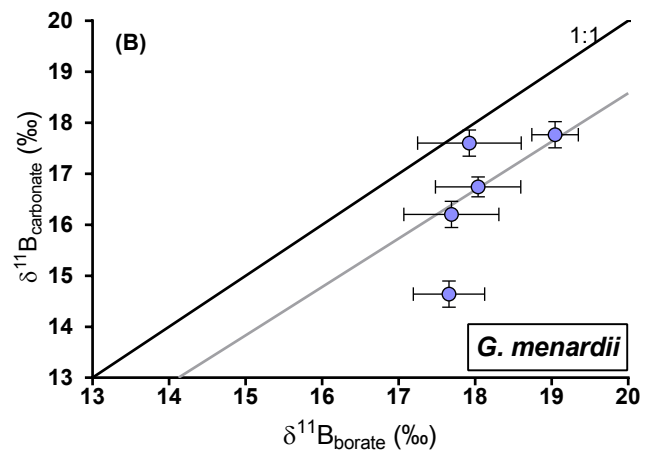


- $\delta^{11}\text{B}_{O. universa}$  (core-top, this study)
- $\delta^{11}\text{B}_{O. universa}$  (core-top, Henehan et al., 2016)
- $\delta^{11}\text{B}_{O. universa}$  (sediment trap, Henehan et al., 2016)
- ◇  $\delta^{11}\text{B}_{O. universa}$  (tow, Henehan et al., 2016)
- △  $\delta^{11}\text{B}_{O. universa}$  (core-top, Raizsch et al., 2018)
- $O. universa$  calibration line (core-top, this study)
- $O. universa$  calibration line (this study, Henehan et al., 2016, Raizsch et al., 2018)
- $O. universa$  calibration line (wild, Henehan et al., 2016)

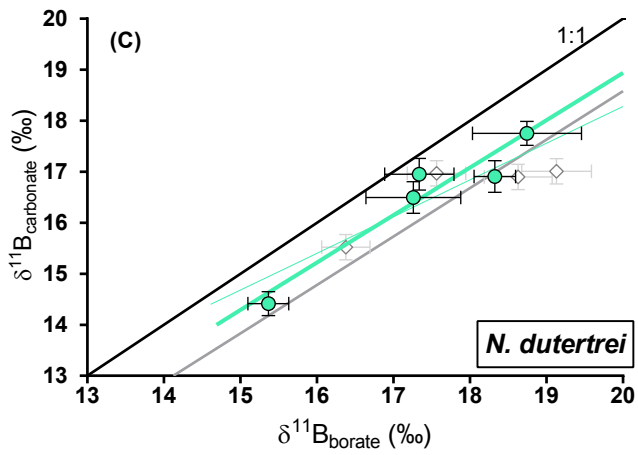




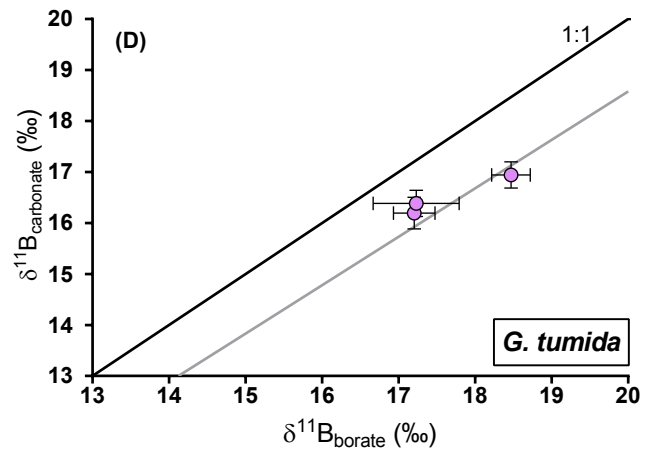
- $\delta^{11}\text{B}_{P.obliquiloculata}$  (Core-top, this study)
- ▽  $\delta^{11}\text{B}_{P.obliquiloculata}$  (Henehan et al., 2016)
- $P.obliquiloculata$  calibration line (this study, Henehan et al., 2016)
- $O.universa$  calibration curve (Henehan et al., 2016)



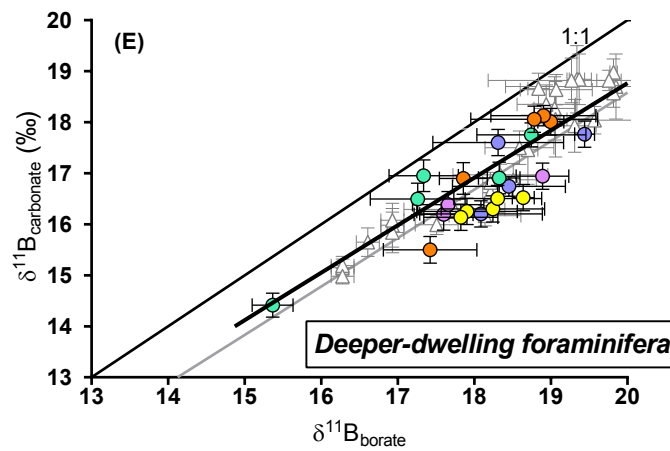
- $\delta^{11}\text{B}_{G.menardii}$  (this study)
- $O.universa$  calibration curve (Henehan et al., 2016)



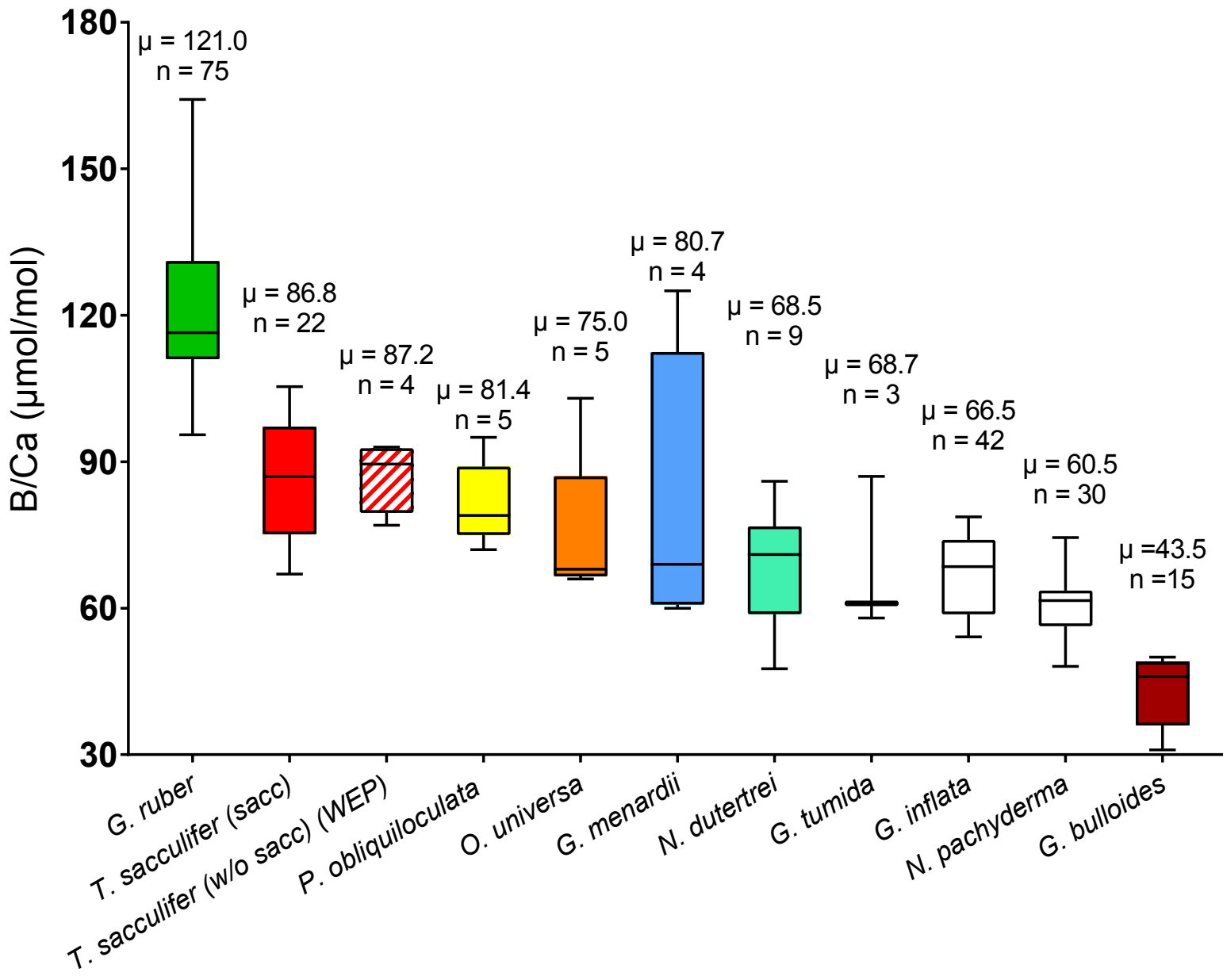
- $\delta^{11}\text{B}_{N.dutertrei}$  (Core-top, this study)
- ◇  $\delta^{11}\text{B}_{N.dutertrei}$  (Core-top, Foster et al., 2008)
- $O.universa$  calibration line (This study)
- $O.universa$  calibration line (This study, Foster et al., 2008)
- $O.universa$  calibration line (Henehan et al., 2016)



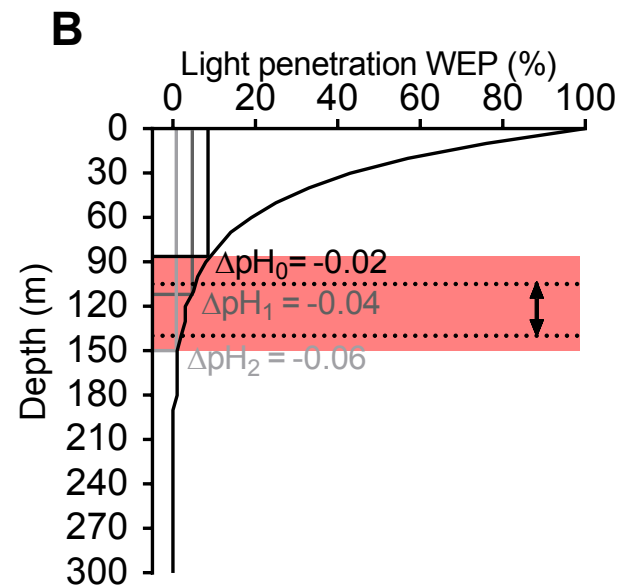
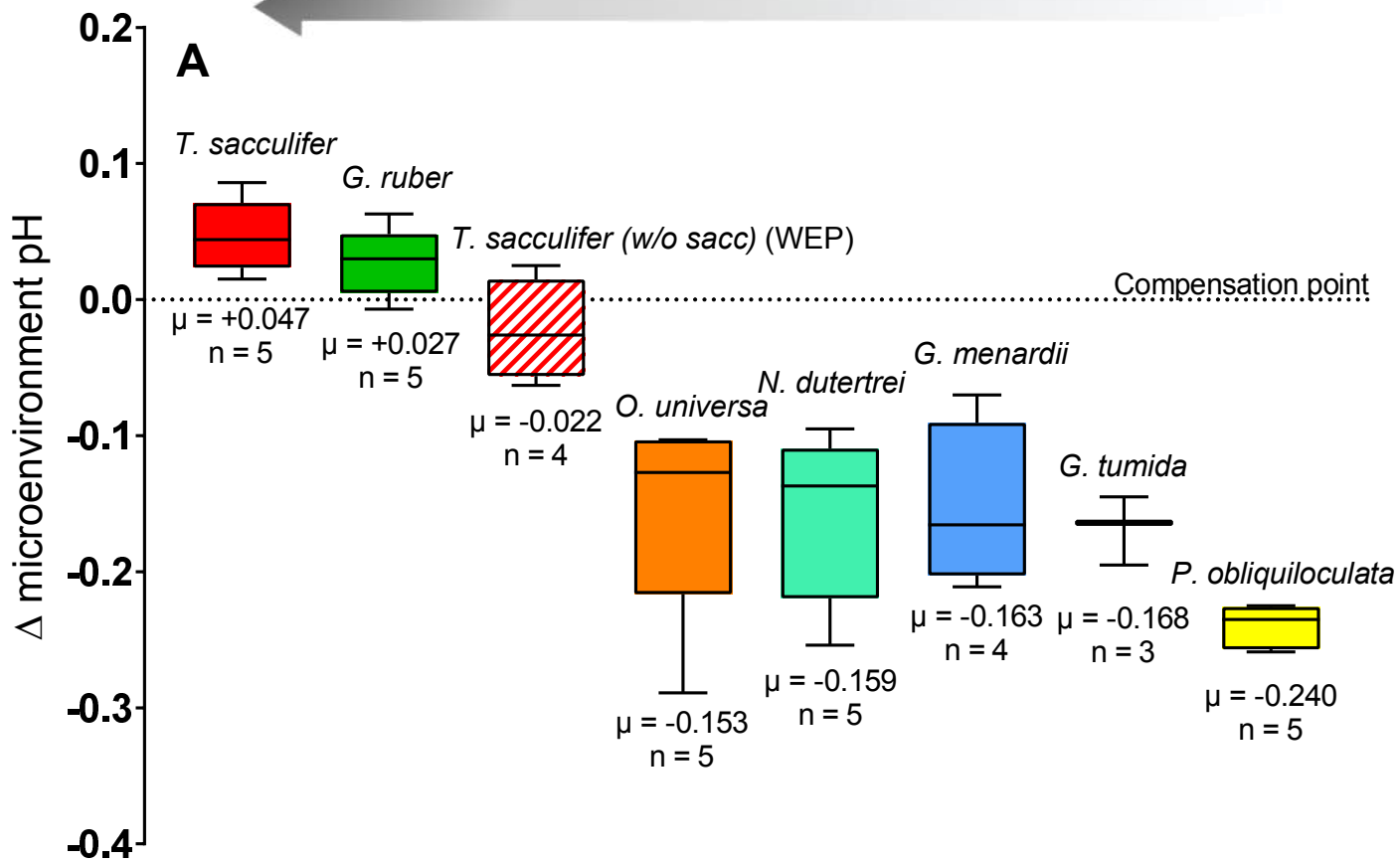
- $\delta^{11}\text{B}_{G.tumida}$  (this study)
- $O.universa$  calibration curve (Henehan et al., 2016)



- $\delta^{11}\text{B}_{O.universa}$
- $\delta^{11}\text{B}_{P.obliquiloculata}$
- $\delta^{11}\text{B}_{N.dutertrei}$
- $\delta^{11}\text{B}_{G.menardii}$
- $\delta^{11}\text{B}_{G.tumida}$
- △  $\delta^{11}\text{B}_{\text{deep-dweller}}$  from literature
- Deep-dweller calibration line
- $O.universa$  calibration line (Henehan et al., 2016)



Photosynthesis/respiration-calcification

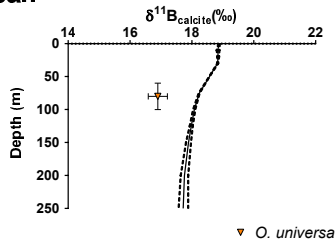
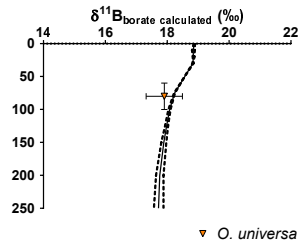
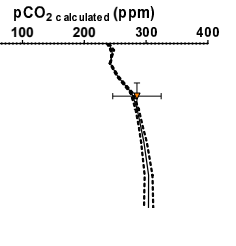
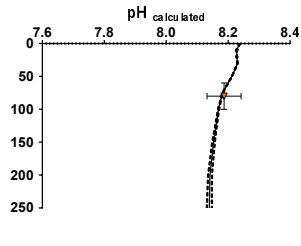


$\delta^{11}\text{B}_{\text{carbonate}}$  $\delta^{11}\text{B}_{\text{borate}}$ 

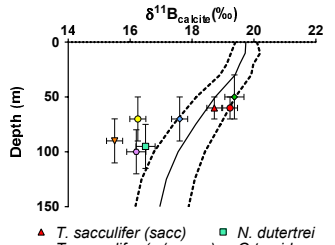
pH

 $\text{pCO}_2$ 

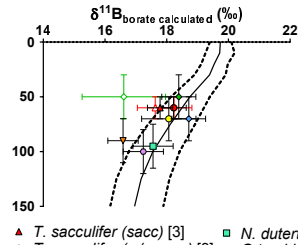
## Atlantic Ocean

CD107-a  
52.9°N, -16.9°E  
3569 m▼ *O. universa*▼ *O. universa*

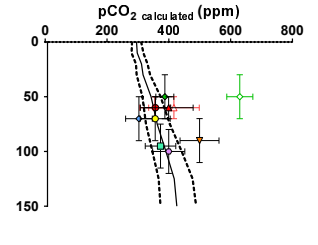
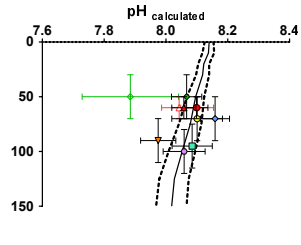
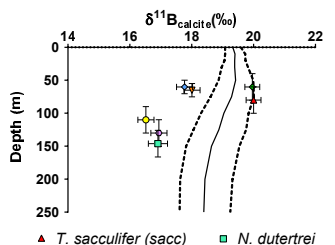
## Indian Ocean

FC-01a  
-11.2°N, 58.8°E  
3520 m

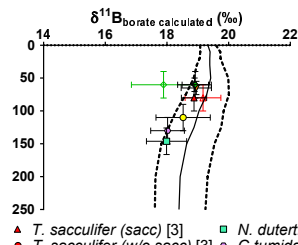
▲ *T. sacculifer* (sacc)    ■ *N. dutertrei*  
● *T. sacculifer* (w/o sacc)    ○ *G. tumida*  
◆ *G. ruber* (white)    ◇ *G. menardii*  
▼ *O. universa*    ○ *P. obliquiloculata*



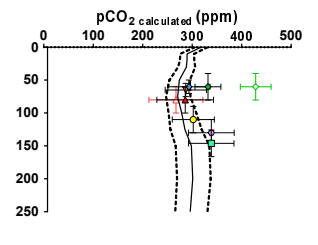
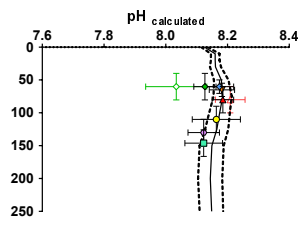
▲ *T. sacculifer* (sacc) [3]    ■ *N. dutertrei*  
● *T. sacculifer* (w/o sacc) [3]    ○ *G. tumida*  
◆ *G. ruber* (white) [1]    ◇ *G. menardii*  
▼ *T. sacculifer* (sacc) [4]    ○ *O. universa*  
○ *T. sacculifer* (w/o sacc) [4]    ○ *P. obliquiloculata*  
◇ *G. ruber* (white) [2]

FC-02a  
-29.1°N, 47.5°E  
2871 m

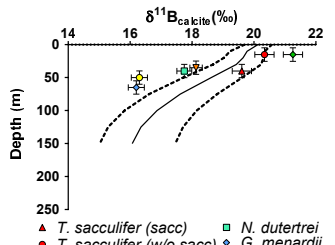
▲ *T. sacculifer* (sacc)    ■ *N. dutertrei*  
● *T. sacculifer* (w/o sacc)    ○ *G. tumida*  
◆ *G. ruber* (white)    ◇ *G. menardii*  
▼ *O. universa*    ○ *P. obliquiloculata*



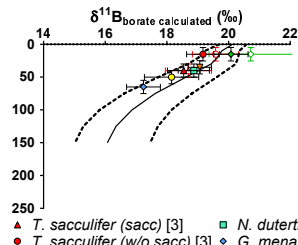
▲ *T. sacculifer* (sacc) [3]    ■ *N. dutertrei*  
● *T. sacculifer* (w/o sacc) [3]    ○ *G. tumida*  
◆ *G. ruber* (white) [1]    ◇ *G. menardii*  
▼ *T. sacculifer* (sacc) [4]    ○ *O. universa*  
○ *T. sacculifer* (w/o sacc) [4]    ○ *P. obliquiloculata*  
◇ *G. ruber* (white) [2]



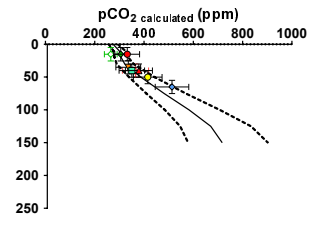
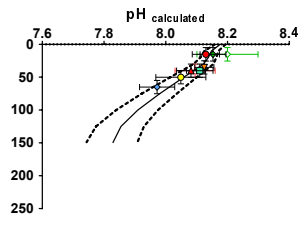
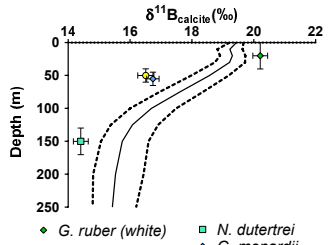
## Arabian Sea

FC-12b  
23.3°N, 66.7°E  
151 m

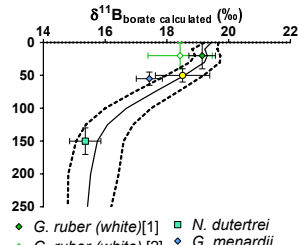
▲ *T. sacculifer* (sacc)    ■ *N. dutertrei*  
● *T. sacculifer* (w/o sacc)    ○ *G. tumida*  
◆ *G. ruber* (white)    ◇ *G. menardii*  
▼ *O. universa*    ○ *P. obliquiloculata*



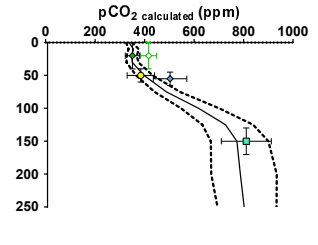
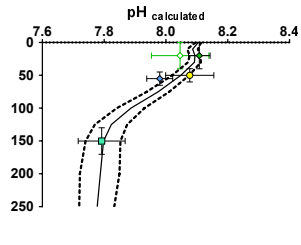
▲ *T. sacculifer* (sacc) [3]    ■ *N. dutertrei*  
● *T. sacculifer* (w/o sacc) [3]    ○ *G. tumida*  
◆ *G. ruber* (white) [1]    ◇ *G. menardii*  
▼ *T. sacculifer* (sacc) [4]    ○ *O. universa*  
○ *T. sacculifer* (w/o sacc) [4]    ○ *P. obliquiloculata*  
◇ *G. ruber* (white) [2]

FC-13a  
20.0°N, 65.6°E  
3190 m

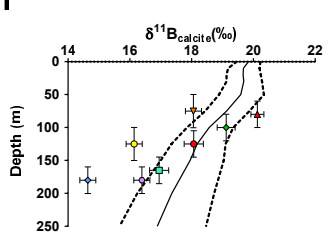
◆ *G. ruber* (white)    ■ *N. dutertrei*  
◇ *G. menardii*    ○ *P. obliquiloculata*



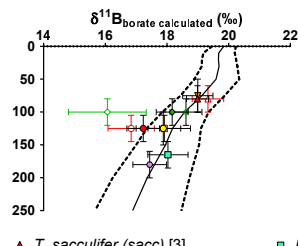
◆ *G. ruber* (white) [1]    ■ *N. dutertrei*  
◇ *G. ruber* (white) [2]    ○ *G. menardii*  
○ *P. obliquiloculata*



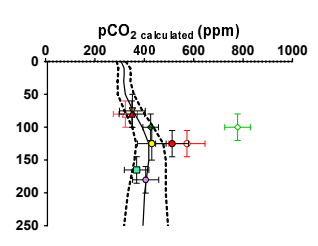
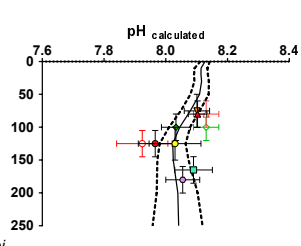
## Pacific Ocean

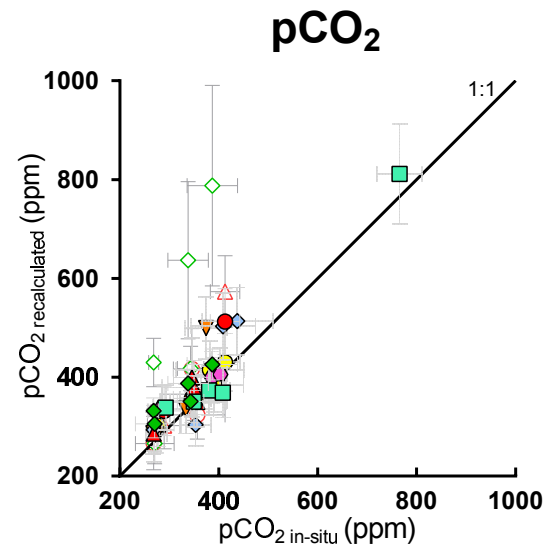
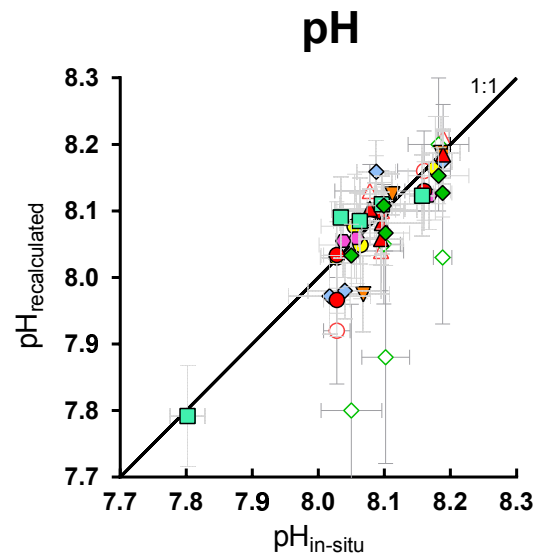
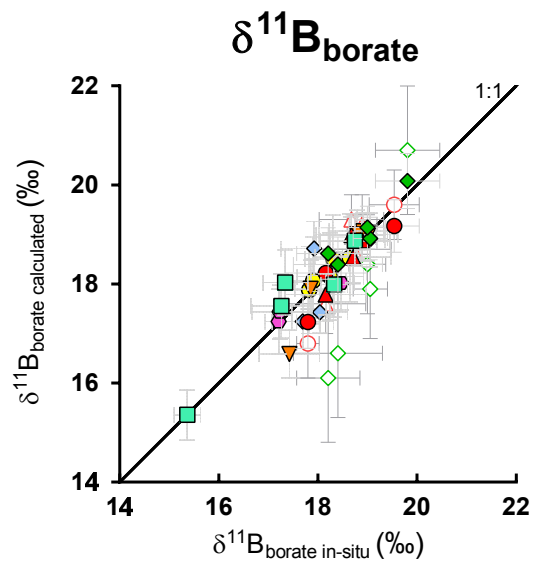
WP07-01  
-3.9°N, 156.0°E  
1800 m

▲ *T. sacculifer* (sacc)    ■ *N. dutertrei*  
● *T. sacculifer* (w/o sacc)    ○ *G. tumida*  
◆ *G. ruber* (white)    ◇ *G. menardii*  
▼ *O. universa*    ○ *P. obliquiloculata*



▲ *T. sacculifer* (sacc) [3]    ■ *N. dutertrei*  
● *T. sacculifer* (w/o sacc) [3]    ○ *G. tumida*  
◆ *G. ruber* (white) [1]    ◇ *G. menardii*  
▼ *T. sacculifer* (sacc) [4]    ○ *O. universa*  
○ *T. sacculifer* (w/o sacc) [4]    ○ *P. obliquiloculata*  
◇ *G. ruber* (white) [2]





- ◆ *G. ruber* (white) [1]
- ▲ *T. sacculifer* (sacc), [3]
- *T. sacculifer* (w/o sacc) [3]
- ◇ *G. ruber* [2]
- *T. sacculifer* (sacc) [4]
- △ *T. sacculifer* (w/o sacc) [4]
- *N. dutertrei*
- ◆ *G. tumida*
- ◆ *G. menardii*
- ▼ *O. universa*
- *P. obliquiloculata*

**Table 1**

<b>Label</b>	<b>Box-Core</b>	<b>Site</b>	<b>Latitude (N)</b>	<b>Longitude (E)</b>	<b>Depth (mbsl)</b>	<b>Oceanic Regime</b>	<b><math>\Delta^{14}\text{C}</math> age (year)</b>
<b><i>Atlantic Ocean</i></b>							
CD107-a	CD107	A	52.92	-16.92	3569	non-upwelling	<3000 <sup>a</sup>
<b><i>Indian Ocean</i></b>							
FC-01a	WIND-33B	I	-11.21	58.77	3520	non-upwelling	
FC-02a	WIND-10B	K	-29.12	47.55	2871	non-upwelling	7252 $\pm$ 27 <sup>b</sup>
<b><i>Arabian Sea</i></b>							
FC-12b	CD145	A150	23.30	66.70	151	seasonal upwelling	
FC-13a	CD145	A3200	20.00	65.58	3190	seasonal upwelling	
<b><i>Pacific Ocean</i></b>							
WP07-01			-3.93	156.00	1800	non-upwelling	7.3-8.6 <sup>c</sup>
A14			8.02	113.39	1911	non-upwelling	7.3-8.6 <sup>c</sup>
806		A	0.32	159.36	2521	equatorial divergence	7.3-8.6 <sup>c</sup>
807		A	3.61	156.62	2804	equatorial divergence	7.3-8.6 <sup>c</sup>

<sup>a</sup>Thomson et al., 2000

<sup>b</sup>Wilson et al., 2012

<sup>c</sup>Age for core-top of site 806B from Lea et al., 2000

Table 2

Core	Species	Fraction size (μm)	Cleaning	$\delta^{13}\text{C}^*$ (‰)	$\delta^{18}\text{O}^*$ (‰)	$\delta^{11}\text{Bc}_1$ (‰)	$\delta^{11}\text{Bc}_2$ (‰)	$\delta^{11}\text{B}_{\text{average}}^{**}$ (‰)	Li/Ca*** (μmol/mol)	B/Ca*** (μmol/mol)	Mg/Ca*** (mmol/mol)	Mn/Ca*** (μmol/mol)	Fe/Ca*** (mmol/mol)
<b>Atlantic Ocean</b>													
CD107a	<i>O. universa</i>	>500	Ox-Red	1.99 ± 0.03	1.25 ± 0.11	16.85 ± 0.31 (2SD, nAE121=11)	16.95 ± 0.31 (2SD, nAE121=11)	16.90 ± 0.22	13.9 ± 0.4	68 ± 7	3.60 ± 0.01	13 ± 7	0.16 ± 0.01
<b>Indian Ocean</b>													
FC-01a	<i>G. ruber</i> (white ss)	250-300	Ox-Red	1.37 ± 0.03	-1.32 ± 0.11	19.33 ± 0.31 (2SD, nAE121=11)	19.41 ± 0.31 (2SD, nAE121=11)	19.37 ± 0.22	15.4 ± 0.4	109 ± 7	3.98 ± 0.01	10 ± 7	0.07 ± 0.01
FC-01a	<i>T. sacculifer</i> (sacc)	300-400	Ox-Red	1.88 ± 0.03	-2.20 ± 0.11	18.71 ± 0.24 (2SD, nAE121=10)	18.73 ± 0.24 (2SD, nAE121=10)	18.72 ± 0.17	12.1 ± 0.4	87 ± 7	3.45 ± 0.01	9 ± 7	0.03 ± 0.01
FC-01a	<i>T. sacculifer</i> (w/o sacc)	300-400	Ox-Red	2.02 ± 0.03	-1.05 ± 0.11	19.13 ± 0.24 (2SD, nAE121=10)	19.32 ± 0.24 (2SD, nAE121=10)	19.23 ± 0.17	12.1 ± 0.4	82 ± 7	3.42 ± 0.01	14 ± 7	0.03 ± 0.01
FC-01a	<i>O. universa</i>	>500	Ox-Red			15.50 ± 0.26 (2SD, nAE121=14)		15.50 ± 0.26					
FC-01a	<i>P. obliquiloculata</i>	300-400	Ox-Red	1.00 ± 0.03	-0.55 ± 0.11	16.40 ± 0.26 (2SD, nAE121=14)	16.10 ± 0.26 (2SD, nAE121=14)	16.25 ± 0.18	15.4 ± 0.4	78 ± 7	2.06 ± 0.01	14 ± 7	0.05 ± 0.01
FC-01a	<i>G. menardii</i>	300-400	Ox-Red	1.64 ± 0.03	0.43 ± 0.11	17.52 ± 0.26 (2SD, nAE121=14)	17.69 ± 0.26 (2SD, nAE121=14)	17.60 ± 0.18	12.7 ± 0.4	63 ± 7	2.26 ± 0.01	8 ± 7	0.07 ± 0.01
FC-01a	<i>N. dutertrei</i>	300-400	Ox-Red	1.28 ± 0.03	-0.43 ± 0.11	16.40 ± 0.31 (2SD, nAE121=11)	16.59 ± 0.31 (2SD, nAE121=11)	16.50 ± 0.22	18.6 ± 0.4	73 ± 7	1.81 ± 0.01	11 ± 7	0.03 ± 0.01
FC-01a	<i>G. tumida</i>	300-400	Ox-Red	1.29 ± 0.03	-0.53 ± 0.11	16.21 ± 0.31 (2SD, nAE121=11)	16.18 ± 0.31 (2SD, nAE121=11)	16.20 ± 0.22	10.0 ± 0.4	61 ± 7	1.79 ± 0.01	11 ± 7	0.02 ± 0.01
FC-02a	<i>G. ruber</i> (white ss)	250-300	Ox-Red	0.30 ± 0.03	-1.40 ± 0.11	20.02 ± 0.24 (2SD, nAE121=10)	19.90 ± 0.24 (2SD, nAE121=10)	19.96 ± 0.17	18.2 ± 0.4	125 ± 7	3.47 ± 0.01	10 ± 7	0.07 ± 0.01
FC-02a	<i>T. sacculifer</i> (sacc)	300-400	Ox-Red	1.43 ± 0.03	-1.60 ± 0.11	20.07 ± 0.24 (2SD, nAE121=10)	19.93 ± 0.24 (2SD, nAE121=10)	20.00 ± 0.17	14.2 ± 0.4	106 ± 7	3.30 ± 0.01	10 ± 7	0.03 ± 0.01
FC-02a	<i>T. sacculifer</i> (w/o sacc)	300-400	Ox-Red	1.52 ± 0.03	-1.40 ± 0.11	23.23 ± 0.24 (2SD, nAE121=10)	23.22 ± 0.24 (2SD, nAE121=10)	23.22 ± 0.17	13.7 ± 0.4	106 ± 7	3.34 ± 0.01	10 ± 7	0.04 ± 0.01
FC-02a	<i>O. universa</i>	>500	Ox-Red	1.79 ± 0.03	0.02 ± 0.11	18.05 ± 0.26 (2SD, nAE121=14)	17.97 ± 0.26 (2SD, nAE121=14)	18.01 ± 0.18	14.8 ± 0.4	67 ± 7	4.40 ± 0.01	11 ± 7	0.05 ± 0.01
FC-02a	<i>P. obliquiloculata</i>	300-400	Ox-Red	0.34 ± 0.03	0.56 ± 0.11	16.35 ± 0.26 (2SD, nAE121=14)	16.69 ± 0.26 (2SD, nAE121=14)	16.52 ± 0.18	16.6 ± 0.4	83 ± 7	2.33 ± 0.01	7 ± 7	0.03 ± 0.01
FC-02a	<i>G. menardii</i>	300-400	Ox-Red	1.73 ± 0.03	-0.51 ± 0.11	17.77 ± 0.26 (2SD, nAE121=14)	17.77 ± 0.26 (2SD, nAE121=14)	17.77 ± 0.26	15.8 ± 0.4	125 ± 7	2.21 ± 0.01	17 ± 7	0.03 ± 0.01
FC-02a	<i>N. dutertrei</i>	300-400	Ox-Red	1.03 ± 0.03	-0.55 ± 0.11	16.78 ± 0.31 (2SD, nAE121=11)	17.03 ± 0.31 (2SD, nAE121=11)	16.91 ± 0.22	18.6 ± 0.4	82 ± 7	2.13 ± 0.01	13 ± 7	0.07 ± 0.01
FC-02a	<i>G. tumida</i>	300-400	Ox-Red	1.64 ± 0.03	-0.28 ± 0.11	16.93 ± 0.26 (2SD, nAE121=14)	16.95 ± 0.26 (2SD, nAE121=14)	16.94 ± 0.18	15.6 ± 0.4	87 ± 7	1.90 ± 0.01	17 ± 7	0.04 ± 0.01
<b>Arabian Sea</b>													
FC-12b	<i>G. ruber</i> (white ss)	250-300	Ox-Red	0.58 ± 0.03	-2.82 ± 0.11	21.30 ± 0.31 (2SD, nAE121=11)	21.23 ± 0.31 (2SD, nAE121=11)	21.26 ± 0.22	19.5 ± 0.4	164 ± 7	5.76 ± 0.01	14 ± 7	0.16 ± 0.01
FC-12b	<i>G. sacculifer</i> (s)	300-400	Ox-Red	1.76 ± 0.03	-2.15 ± 0.11	19.65 ± 0.31 (2SD, nAE121=11)	19.57 ± 0.31 (2SD, nAE121=11)	19.61 ± 0.22	14.6 ± 0.4	101 ± 7	4.28 ± 0.01	17 ± 7	0.14 ± 0.01
FC-12b	<i>T. sacculifer</i> (w/o sacc)	300-400	Ox-Red	1.97 ± 0.03	-2.19 ± 0.11	20.32 ± 0.31 (2SD, nAE121=11)	20.37 ± 0.31 (2SD, nAE121=11)	20.34 ± 0.22	16.7 ± 0.4	116 ± 7	4.90 ± 0.01	20 ± 7	0.26 ± 0.01
FC-12b	<i>O. universa</i>	>500	Ox-Red	1.89 ± 0.03	-1.59 ± 0.11	18.13 ± 0.20 (2SD, nAE121=6)		18.13 ± 0.20	13.6 ± 0.4	103 ± 7	6.91 ± 0.01	10 ± 7	0.06 ± 0.01
FC-12b	<i>P. obliquiloculata</i>	300-400	Ox-Red	0.5 ± 0.03	-1.58 ± 0.11	16.45 ± 0.26 (2SD, nAE121=14)	16.15 ± 0.26 (2SD, nAE121=14)	16.30 ± 0.18	16.7 ± 0.4	95 ± 7	3.61 ± 0.01	69 ± 7	0.38 ± 0.01
FC-12b	<i>G. menardii</i>	300-400	Ox-Red	1.05 ± 0.03	-0.97 ± 0.11	16.2 ± 0.26 (2SD, nAE121=14)		16.20 ± 0.26	14.8 ± 0.4	75 ± 7	3.44 ± 0.01	52 ± 7	0.17 ± 0.01
FC-12b	<i>N. dutertrei</i>	300-400	Ox-Red	1.35 ± 0.03	-1.57 ± 0.11	17.77 ± 0.24 (2SD, nAE121=10)	17.73 ± 0.24 (2SD, nAE121=10)	17.75 ± 0.17	17.1 ± 0.4	75 ± 7	3.25 ± 0.01	46 ± 7	0.25 ± 0.01
FC-13a	<i>G. ruber</i> (white ss)	250-300	Ox-Red	0.08 ± 0.03	-3.71 ± 0.11	20.27 ± 0.24 (2SD, nAE121=10)	20.15 ± 0.24 (2SD, nAE121=10)	20.21 ± 0.17	16.4 ± 0.4	147 ± 7	4.52 ± 0.01	13 ± 7	0.08 ± 0.01
FC-13a	<i>T. sacculifer</i> (s)	300-400	Ox-Red	1.59 ± 0.03	-2.46 ± 0.11	17.85 ± 0.29 (2SD, nAE121=12)		17.85 ± 0.29	15.7 ± 0.4	121 ± 7	5.49 ± 0.01	21 ± 7	0.49 ± 0.01
FC-13a	<i>P. obliquiloculata</i>	300-400	Ox-Red	0.00 ± 0.03	-0.97 ± 0.11	16.51 ± 0.26 (2SD, nAE121=14)	16.50 ± 0.26 (2SD, nAE121=14)	16.51 ± 0.18	18.7 ± 0.4	79 ± 7	4.43 ± 0.01	30 ± 7	0.43 ± 0.01
FC-13a	<i>G. menardii</i>	300-400	Ox-Red	0.75 ± 0.03	-1.07 ± 0.11	16.74 ± 0.20 (2SD, nAE121=6)		16.74 ± 0.20	9.2 ± 0.4	60 ± 7	1.99 ± 0.01	19 ± 7	0.07 ± 0.01
FC-13a	<i>N. dutertrei</i>	300-400	Ox-Red	0.71 ± 0.03	-1.41 ± 0.11	14.43 ± 0.24 (2SD, nAE121=10)	14.40 ± 0.24 (2SD, nAE121=10)	14.41 ± 0.17	15.7 ± 0.4	69 ± 7	1.98 ± 0.01	15 ± 7	0.06 ± 0.01
<b>Pacific Ocean</b>													
WP07-a	<i>G. ruber</i> (white ss)	250-400	Ox-Red			19.12 ± 0.29 (2SD, nAE121=12)		19.12 ± 0.29	14.5 ± 0.4	144 ± 7	4.32 ± 0.01	15 ± 7	0.16 ± 0.01
WP07-a	<i>T. sacculifer</i> (sacc)	250-400	Ox-Red			20.13 ± 0.21 (2SD, nAE121=11)		20.13 ± 0.21	12.7 ± 0.4	92 ± 7	4.44 ± 0.01	22 ± 7	0.05 ± 0.01
WP07-a	<i>T. sacculifer</i> (w/o sacc)	250-400	Ox-Red			18.10 ± 0.31 (2SD, nAE121=11)	18.04 ± 0.31 (2SD, nAE121=11)	18.07 ± 0.22	12.3 ± 0.4	192 ± 7	4.51 ± 0.01	21 ± 7	0.08 ± 0.01
WP07-a	<i>O. universa</i>	500-630	Ox-Red			18.13 ± 0.26 (2SD, nAE121=14)	17.99 ± 0.26 (2SD, nAE121=14)	18.06 ± 0.18	11.9 ± 0.4	71 ± 7	7.52 ± 0.01	11 ± 7	0.02 ± 0.01
WP07-a	<i>P. obliquiloculata</i>	250-400	Ox-Red			16.08 ± 0.26 (2SD, nAE121=14)	16.19 ± 0.26 (2SD, nAE121=14)	16.14 ± 0.18	13.4 ± 0.4	72 ± 7	3.02 ± 0.01	7 ± 7	0.03 ± 0.01
WP07-a	<i>G. menardii</i>	250-400	Ox-Red			14.74 ± 0.26 (2SD, nAE121=14)	14.53 ± 0.26 (2SD, nAE121=14)	14.64 ± 0.18	13.5 ± 0.4	85 ± 7	2.68 ± 0.01	26 ± 7	0.08 ± 0.01
WP07-a	<i>N. dutertrei</i>	250-400	Ox-Red			16.91 ± 0.31 (2SD, nAE121=11)	16.99 ± 0.31 (2SD, nAE121=11)	16.95 ± 0.22	21.7 ± 0.4	86 ± 7	3.66 ± 0.01	42 ± 7	0.63 ± 0.01
WP07-a	<i>G. tumida</i>	250-400	Ox-Red			16.45 ± 0.26 (2SD, nAE121=14)	16.32 ± 0.26 (2SD, nAE121=14)	16.39 ± 0.18	10.6 ± 0.4	58 ± 7	2.55 ± 0.01	16 ± 7	0.10 ± 0.01
806A	<i>T. sacculifer</i> (w/o sacc)	250-400	Ox-Red			17.53 ± 0.36 (2SD, nAE121=11)		17.53 ± 0.36	14.40 ± 0.4	77 ± 7	3.89 ± 0.01	7 ± 7	0.15 ± 0.01
807A	<i>T. sacculifer</i> (w/o sacc)	250-400	Ox-Red			18.38 ± 0.21 (2SD, nAE121=11)	18.17 ± 0.21 (2SD, nAE121=11)	18.28 ± 0.15	12.54 ± 0.4	87 ± 7	4.24 ± 0.01	17 ± 7	0.09 ± 0.01
A14	<i>G. ruber</i> (white ss)	250-400	Ox-Red			18.91 ± 0.24 (2SD, nAE121=10)	19.17 ± 0.24 (2SD, nAE121=10)	19.04 ± 0.17					
A14	<i>T. sacculifer</i> (sacc)	250-400	Ox-Red			19.53 ± 0.24 (2SD, nAE121=10)	19.32 ± 0.24 (2SD, nAE121=10)	19.42 ± 0.17	12.0 ± 0.4	102 ± 7	3.91 ± 0.01	22 ± 7	0.02 ± 0.01
A14	<i>T. sacculifer</i> (w/o sacc)	250-400	Ox-Red			18.93 ± 0.24 (2SD, nAE121=10)	18.84 ± 0.24 (2SD, nAE121=10)	18.88 ± 0.17	12.3 ± 0.4	93 ± 7	3.76 ± 0.01	25 ± 7	0.06 ± 0.01
A14	<i>O. universa</i>	500-560	Ox-Red			17.33 ± 0.26 (2SD, nAE121=14)	17.08 ± 0.26 (2SD, nAE121=14)	17.20 ± 0.18	11.3 ± 0.4	66 ± 7	6.59 ± 0.01	10 ± 7	0.02 ± 0.01
A14	<i>N. dutertrei</i>	250-400	Ox-Red			14.39 ± 0.31 (2SD, nAE121=11)		14.39 ± 0.31	16.9 ± 0.4	75 ± 7	1.99 ± 0.01	35 ± 7	0.04 ± 0.01

\* uncertainties given in 1SD (see text)

\*\* When two measurements were carried out uncertainty was calculated with  $\Delta a = \sqrt{1/\sum(1/\Delta a_i^2)}$ ; with only one measurement the error was determined on reproducibility of the AE121 standard

\*\*\*Uncertainty given in 2SD, calculated on the reproducibility of CamWuellestorf (see text and table S3, ref in Misra et al., 2014)

Table 3

Species	Size fraction (µm)	Material	Instrument (original)	Regression method	$\delta^{11}\text{B}_{\text{borate}} = f(\delta^{11}\text{B}_{\text{calcite}})$	n	Calibration number	Reference
<i>G. ruber</i>	~380	Culture/core tops/plankton tows	MC-ICP-MS		$\delta^{11}\text{B}_{\text{borate}} = [\delta^{11}\text{B}_{\text{calcite}} - 9.52 (\pm 2.02)]/0.6 (\pm 0.11)$			Henehan et al., 2013
<i>G. ruber</i>	315-355	Core-tops	MC-ICP-MS		$\delta^{11}\text{B}_{\text{borate}} = [\delta^{11}\text{B}_{\text{calcite}} - 11.78 (\pm 3.20)]/0.45 (\pm 0.16)$			Raitzsch et al., 2018
<i>T. sacculifer</i>	n.d.	Culture/artificial seawater enriched in B	N-TIMS		$\delta^{11}\text{B}_{\text{borate}} = [\delta^{11}\text{B}_{\text{calcite}} - 3.94 (\pm 4.02)]/0.82 (\pm 0.22)$			Sanyal et al., 2001 refitted Martinez-Boti et al., 2015
<i>T. sacculifer</i>	315-355	Core-tops	MC-ICP-MS		$\delta^{11}\text{B}_{\text{borate}} = [\delta^{11}\text{B}_{\text{calcite}} - 8.86 (\pm 5.27)]/0.59 (\pm 0.21)$			Raitzsch et al., 2018
<i>O. universa</i>	no effect	Core-tops/plankton tows/sediment traps	MC-ICP-MS		$\delta^{11}\text{B}_{\text{borate}} = [\delta^{11}\text{B}_{\text{calcite}} + 0.42 (\pm 2.85)]/0.95 (\pm 0.17)$			Henehan et al., 2016
<i>O. universa</i>	>425	Core-tops	MC-ICP-MS		$\delta^{11}\text{B}_{\text{borate}} = [\delta^{11}\text{B}_{\text{calcite}} + 5.69 (\pm 7.51)]/1.26 (\pm 0.39)$			Raitzsch et al., 2018
<i>G. bulloides</i>	300-355	Core-top/sediment trap	MC-ICP-MS		$\delta^{11}\text{B}_{\text{borate}} = [\delta^{11}\text{B}_{\text{calcite}} + 3.440 (\pm 4.584)]/1.074 (\pm 0.252)$			Martinez-Boti et al., 2015
<i>G. bulloides</i>	315-355	Core-tops	MC-ICP-MS		$\delta^{11}\text{B}_{\text{borate}} = [\delta^{11}\text{B}_{\text{calcite}} + 3.81 (\pm 13.17)]/1.13 (\pm 0.72)$			Raitzsch et al., 2018
<i>N. pachyderma</i>	150-200	Core-tops	MC-ICP-MS		$\delta^{11}\text{B}_{\text{borate}} = \delta^{11}\text{B}_{\text{calcite}} + 3.38$			Yu et al., 2013
<i>G. ruber</i>	250-400	Core-tops	MC-ICP-MS	Bootstrap	$\delta^{11}\text{B}_{\text{borate}} = [\delta^{11}\text{B}_{\text{calcite}} + 1.23 (\pm 0.59)]/1.12 (\pm 1.67)$	5	1	This study
<i>G. ruber</i>	250-400	Core-tops	MC-ICP-MS	Bootstrap	$\delta^{11}\text{B}_{\text{borate}} = [\delta^{11}\text{B}_{\text{calcite}} - 11.73 (\pm 0.83)]/0.46 (\pm 0.34)$	40	2	This study; Foster et al., 2008; Henehan et al., 2016; Raitzsch et al., 2018
<i>T. sacculifer (sacc and w/o sacc)</i>	250-400	Core-tops	MC-ICP-MS	Bootstrap	$\delta^{11}\text{B}_{\text{borate}} = [\delta^{11}\text{B}_{\text{calcite}} + 6.06 (\pm 0.25)]/1.38 (\pm 1.33)$	11	3	This study
<i>T. sacculifer (sacc and w/o sacc)</i>	250-400	Core-tops	MC-ICP-MS	Bootstrap	$\delta^{11}\text{B}_{\text{borate}} = [\delta^{11}\text{B}_{\text{calcite}} - 4.09 (\pm 0.86)]/0.83 (\pm 0.48)$	27	4	This study; Foster et al., 2008; Raitzsch et al., 2018
<i>N. duterrei</i>	300-400	Core-tops	MC-ICP-MS	Bootstrap	$\delta^{11}\text{B}_{\text{borate}} = [\delta^{11}\text{B}_{\text{calcite}} - 0.34 (\pm 1.83)]/0.93 (\pm 0.55)$	5	5	This study
<i>N. duterrei</i>	300-400	Core-tops	MC-ICP-MS	Bootstrap	$\delta^{11}\text{B}_{\text{borate}} = [\delta^{11}\text{B}_{\text{calcite}} - 3.88 (\pm 0.65)]/0.72 (\pm 0.74)$	9	6	This study; Foster et al., 2008
<i>O. universa</i>	400-600	Core-tops	MC-ICP-MS	Bootstrap	$\delta^{11}\text{B}_{\text{borate}} = [\delta^{11}\text{B}_{\text{calcite}} + 8.01 (\pm 2.3)]/1.38 (\pm 2.67)$	5	7	This study
<i>O. universa</i>	400-600	Core-tops	MC-ICP-MS	Bootstrap	$\delta^{11}\text{B}_{\text{borate}} = [\delta^{11}\text{B}_{\text{calcite}} + 2.08 (\pm 0.59)]/1.06 (\pm 0.13)$	36	8	This study; Henehan et al., 2016; Raitzsch et al., 2018
<i>G. menardii</i>	400-600	Core-tops	MC-ICP-MS	Bootstrap	$\delta^{11}\text{B}_{\text{borate}} = [\delta^{11}\text{B}_{\text{calcite}} - 5.36 (\pm 1.36)]/0.65 (\pm 0.76)$	5	9	This study
<i>G. tumida</i>	400-600	Core-tops	MC-ICP-MS	Bootstrap	$\delta^{11}\text{B}_{\text{borate}} = [\delta^{11}\text{B}_{\text{calcite}} - 6.33 (\pm 2.52)]/0.57 (\pm 1.2)$	3	10	This study
<i>P. obliquiloculata</i>	300-400	Core-tops	MC-ICP-MS	Bootstrap	$\delta^{11}\text{B}_{\text{borate}} = [\delta^{11}\text{B}_{\text{calcite}} - 5.59 (\pm 4.16)]/0.59 (\pm 0.65)$	6	11	This study; Henehan et al., 2016
<i>Deep-dweller</i>	300-600	Core-tops	MC-ICP-MS	Bootstrap	$\delta^{11}\text{B}_{\text{borate}} = [\delta^{11}\text{B}_{\text{calcite}} - 1.99 (\pm 0.13)]/0.82 (\pm 0.27)$	22	12	This study
<i>Deep-dweller</i>	300-600	Core-tops	MC-ICP-MS	Bootstrap	$\delta^{11}\text{B}_{\text{borate}} = [\delta^{11}\text{B}_{\text{calcite}} - 0.18 (\pm 0.6)]/0.95 (\pm 0.13)$	54	13	This study; Foster et al., 2008; Henehan et al., 2016; Raitzsch et al., 2018



## Supplemental information

Seawater pH reconstruction using boron isotopes in multiple planktonic foraminifera species with different depth habitats and their potential to constrain pH and pCO<sub>2</sub> gradients

Maxence Guillermic<sup>1,2</sup>, Sambuddha Misra<sup>3,4</sup>, Robert Eagle<sup>2,5</sup>, Alexandra Villa<sup>2,6</sup>, Fengming Chang<sup>7</sup>,  
Aradhna Tripathi<sup>1,2,5</sup>

<sup>1</sup> Department of Earth, Planetary, and Space Sciences, UCLA, University of California – Los Angeles, Los Angeles, CA 90095 USA

<sup>2</sup> Laboratoire Géosciences Océan UMR6538, UBO, Institut Universitaire Européen de la Mer, Rue Dumont d'Urville, 29280, Plouzané, France

<sup>3</sup> Indian Institute of Science, Centre for Earth Sciences, Bengaluru, Karnataka 560012, India

<sup>4</sup> The Godwin Laboratory for Palaeoclimate Research, Department of Earth Sciences, University of Cambridge, UK

<sup>5</sup> Institute of the Environment and Sustainability, Department of Atmospheric and Oceanic Sciences, University of California – Los Angeles, CA 90095, USA

<sup>6</sup> Department of Geology, University of Wisconsin-Madison, Madison, WI 53706 USA

<sup>7</sup> Key Laboratory of Marine Geology and Environment, Institute of Oceanology, Chinese Academy of Sciences, Qingdao 266071, China

## Supplemental Figures

**Figure S1:** An example of the impact of seasonality on results. Based on data from GLODAP used for site FC13-a. Seasonality has less of an impact than a change in the depth habitats.

**Figure S2:** Figure showing the offset  $\Delta^{11}\text{B} = \delta^{11}\text{B}_{\text{carbonate}} - \delta^{11}\text{B}_{\text{borate}}$  versus calcification depth, red symbols are from Arabian Sea, green from Indian Ocean and Blue from the WEP, blue with black line symbols are data from site A14. This figure highlights a decrease of  $\delta^{11}\text{B}_{\text{carbonate}}$  for *T. sacculifer* and *G. ruber* with a deeper depth habitat.

**Figure S3:** Multi-panels figure showing the correlation between B/Ca and boron geochemistry and different variables. A to C show comparison of B/Ca and A)  $[\text{B}(\text{OH})_4^-]/[\text{HCO}_3^-]$ , B)  $\delta^{11}\text{B}_{\text{carbonate}}$  and C) temperature. Panel D) shows the correlation between  $\delta^{11}\text{B}_{\text{carbonate}}$  and temperature. Symbol in brackets is high B/Ca; this point is included in the linear regressions. Linear regression (LR - black line) is when compiling *G. ruber* and *T. sacculifer*, LR of *G. ruber* (dotted line green), *T. sacculifer* (red line –  $p < 0.05$ ), *T. sacculifer* (w/o sacc – red dotted line).

**Figure S4:** Boron geochemistry against water depth. A)  $\delta^{11}\text{B}_{\text{carbonate}}$  versus water depth, B) B/Ca against water depth and C)  $\delta^{11}\text{B}_{\text{carbonate}}$  versus calcification depth and linear regressions for *G. ruber*, *T. sacculifer* (w/o sacc), *T. sacculifer* (sacc) and *O. universa*.

**Figure S5:** Figure evaluating the circularity of our reconstructions. It is showing in the y-axis the difference between reconstruction utilizing calibrations derived from the entire dataset and compared to *in-situ* values and in the x-axis the difference between the reconstruction utilizing the species-specific calibrations derived excluding the site of interest (no circularity) compared to *in-situ* values. Results show that difference is not significant between the two reconstruction methods (e.g. following the 1:1 line), validating the method and the calibrations.

## **Supplemental Tables**

**Table S1:** Elemental ratios of multi-elemental standards utilized in this study.

**Table S2:** Reproducibility of boron isotope standards.

**Table S3:** Reproducibility of elemental ratios for CamWuellestorfi standard.

**Table S4:** Seasonality of foraminifera utilized in this study.

**Table S5:** Mg/Ca-T calibrations used for reconstructions and  $\delta^{18}\text{O}_w$ -T calibrations used for calcification depth reconstructions.

**Table S6:** Calcification depth (CD) calculations from  $\delta^{18}\text{O}$  (CD1), Mg/Ca (CD2) and literature (CD3).

**Table S7:** Pre-industrial in-situ parameters estimated using calcification depths for each species and calculated parameters based on analytical results.

### Trace element standards

A series of multi-element standards (Table S1) with fixed Ca concentration and variable B, Mg, Sr, Mn, Ba, Zn, Cd, U, Li, Al and Fe concentrations were prepared for elemental ratios analysis in Brest following the method developed by Yu et al., (2005). Multi-element stock standard mixtures were prepared gravimetrically by spiking a 10,000 ppm Ca standard with appropriate amounts of Li, B, Al, Mn, Zn, Sr, Cd and U mono-elemental 1,000 ppm (SCP Science). They were diluted with OPTIMA grade HNO<sub>3</sub> acid and 18.2 MΩ.cm-1 water to reach a 0.28M HNO<sub>3</sub> final solution. The stock standards (1500 ppm Ca) were prepared in 500mL cleaned PFA bottles. Working standards were made by diluting the stock solutions to a final concentration of 100 ppm Ca. The multi-element standards were calibrated at the University of Cambridge, elemental ratios are presented in Table S1. An external standard CamWuellestorf (Misra et al., 2014a) was used in Brest for cross-calibration and reproducibility (Table S3).

### Potential contaminations

Possible contamination of samples due to presence of silicate minerals was monitored with the Fe/Mg ratio. Samples with Fe/Mg > 0.1 mol/mol would be rejected due to potential contamination by silicate minerals (Barker et al., 2003). Samples (site E035 excluded) have an average Fe/Mg of  $0.03 \pm 0.05$  mol/mol (2SD, n=42), meaning that silicate minerals have been efficiently removed during our cleaning.

Contribution of Mn-Fe-oxide coatings to Mg/Ca ratio has been calculated to be 0.5 μmol/mol Mg/Ca (change for 5 μmol/mol Mn/Ca ratio Barker et al., 2003). The maximum Mn/Ca ratio in our samples is 89 μmol/mol which can lead to a potential contribution of ~9 μmol/mol Mg/Ca or in other words a decrease of 0.1°C in our reconstructed temperatures. However, the calibration error is much larger and is estimated to be ~1.4°C (Dekens et al., 2002). The range in Mn/Ca values in our samples is  $0.021 \pm 0.033$  mmol/mol (2SD, n=42) which allows us to not be ignore *Mn-Fe-oxide* coating related complications. Additionally, no correlations were found between Mg/Ca and Fe/Ca ( $R^2=0.006$ ) or with Mn/Ca ( $R^2=0.008$ ), and between B/Ca ratio and Mn/Ca ( $R^2=0.003$ ) or Fe/Ca ( $R^2=0.062$ ) ratios.

Contamination by clays was monitored with Ti/Ca calculated from blank corrected intensities. Al/Ca ratios were not reliable as we are using an alumina injector for HF matrix in our lab. A minor correlation was found between Ti/Ca and Mg/Ca ( $R^2=0.1388$ ) but none with B/Ca ( $R^2=0.0887$ ).

### Calcification depth determination

The first approach involves comparing measured  $\delta^{18}O_c$  with theoretical predictions of  $\delta^{18}O_c$  based on vertical profiles of temperature and the  $\delta^{18}O$  of seawater ( $\delta^{18}O_w$ ). We assume  $\delta^{18}O_c$  is in equilibrium with seawater. First,  $\delta^{18}O_w$  was calculated using location-specific  $\delta^{18}O_w$ -salinity relationships and salinity profiles. We used salinity values from the World Ocean Atlas database (Boyer et al., 2013). Oxygen isotopes may be affected by both temperature and salinity. As our sites present different hydrographic settings and freshwater inputs, location-specific  $\delta^{18}O_w$ -salinity relationship relationships are utilized for accurate  $\delta^{18}O_w$  reconstructions. For Site CD107-a, we used a  $\delta^{18}O_w$ -salinity relationship of  $0.56*S-19.3$  (Duplessy et al., 1991). For FC01-a and FC02-a, we used a  $\delta^{18}O_w$ -salinity relationship of  $0.24*S-7.8$  (Sime et al., 2005), and for FC13-a and FC12-b, we used a  $\delta^{18}O_w$ -salinity relationship of  $0.28*S-9.24-0.27$  (Rosteket al., 1993). Then, we used the calculated ambient  $\delta^{18}O_w$  in concert with: (1) temperature profiles from the World Ocean Atlas database (Boyer et al., 2013), and (2) published calcite-water oxygen isotope fractionation factors, to calculate theoretical values for  $\delta^{18}O_c$ . Species-

specific relationships were used when available, including for *T. sacculifer* (Mulitza et al., 2003), *G. ruber* (Mulitza et al., 2003), and *O. universa* (Bemis et al., 2002, medium light). For all other, species we used the calcite equation from Kim and O’Niel (1997), adapted to a quadratic form by Bemis et al., (1998) following the approach of Sime et al., (2005). To take into account the ecology of each species, theoretical  $\delta^{18}\text{O}_c$  profiles were made for the season of maximum abundance (Table S4). Therefore spring and summer profiles were used for *T. sacculifer*, summer profiles used for *G. ruber*, and winter and annual average profiles was used for *N. dutertrei*. Annual average profiles were used for the other species.

For the two sites WP07-1 and A14, a different approach was necessary because  $\delta^{18}\text{O}_c$  data is sparse. At these sites, and for our other sites, we utilized Mg/Ca-derived temperatures to estimate calcification depths (Table S6).  $T_{\text{Mg/Ca}}$  was derived using species-specific Mg/Ca-temperature calibrations (Table S6) along with the Mg/Ca ratios determined in this study. Calcification depth was estimated by comparing  $T_{\text{Mg/Ca}}$  to modern temperature profiles from the World Ocean atlas database 2013 (Boyer et al., 2013) in light of the ecology (seasonality of growth) of the species of interest. A caveat is that in certain cases  $T_{\text{Mg/Ca}}$  may be partially biased by a carbonate ion effect or salinity effect (Russell et al., 2004; Elderfield et al., 2006; Ferguson et al., 2008; Arbuszewski et al., 2010; Martinez-Boti et al., 2011). These artifacts on  $T_{\text{Mg/Ca}}$  may be significant at high-latitude sites such as CD107-a which is located in the North Atlantic Ocean.

### **Depth habitat**

Planktonic foraminifera live in the upper 500 m of the water column. Their preferred depth habitat depends on their ecology, which in turn relies on the hydrographic conditions. For example, *G. ruber* is commonly found in the mixed layer (Fairbanks and Wiebe, 1980; Dekens et al., 2002; Farmer et al., 2007) during summer (Deuser et al., 1981) whereas *T. sacculifer* (n or ns) is present in the mixed layer until the mid-thermocline depth (Farmer et al., 2007) during spring and summer (Deuser et al., 1981, 1989). Specimens of *P. obliquiloculata* and *N. dutertrei* are found during winter (Deuser et al., 1989), in the mixed layer (~60m) for *P. obliquiloculata*, and at mid-thermocline depth for *N. dutertrei* (Farmer et al., 2007). Whereas, *O. universa* tends to record annual average conditions and is living within the mixed layer. Specimens of *G. menardii* calcify within the seasonal thermocline (Fairbanks et al., 1982, Farmer et al., 2007, Regenberg et al., 2009) even upper thermocline (Farmer et al., 2007) and records annual temperatures. And specimens of *G. tumida* are found at the lower thermocline or below the thermocline and record annual average conditions (Fairbanks and Wiebe, 1980; Farmer et al., 2007, Birch et al., 2013). Our calcification depth reconstructions are summarized in Table 3, also see Table S6 for comparison.

### **Atlantic Ocean**

Farmer et al., (2007) determined the depth habitat for *O. universa* to be ranging from 0 to 60m (LL, Bemis et al., 1998). Our calculation, through  $\delta^{18}\text{O}$  measurement, suggests a deeper habitat of around 70m (LL, Bemis et al., 1998), 80m (ML, Bemis et al., 2002). Whereas, the Mg/Ca method derived depth habitat calculation yields a depth habitat of 50 m. The lower habitat depth can also come from the different size fractions, as our size fraction is lower than Farmer’s. *O.universa* is thought to migrate to shallower depth along its ontogeny (Emiliani et al., 1954) younger individuals are thus living deeper but smaller individuals might also have a

deeper habitat as already suggested by Hönisch and Heming, (2004). Since most of the published studies have used the  $\delta^{18}\text{O}$ -based depth calcification, we will preferentially adopt this method.

### ***Indian Ocean***

Calcification depths for the Indian Ocean cores have already been determined for majority of the species by Sime et al., (2005). Additionally, Birch et al., (2013) have reconstructed the depth habitat of multiple species from a core collected in the offshore region of Tanzania (Glow 3). In Indian Ocean specimens of *G. ruber* is found in the top 50m (Birch et al., 2013) and until 60 m (Sime et al., 2005), *T. sacculifer* is found in the surface mixed layer (SML) but also in the upper thermocline between 50-70 m for Birch et al., (2013) and between 60 to 80 m for Sime et al., (2005). Our results are consistent with these reported depth habitats. We calculate that specimens of *G. ruber*, *T. sacculifer* with and without sac are living in the top 80m; *O. universa* lives between 50 to 90 m (Sime et al., 2005, Birch et al., 2013). For *N. dutertrei* we calculate a depth habitat of 90m at site FC01a, calcification depths derived from both  $\delta^{18}\text{O}$  and Mg/Ca methods agree with the 93 m estimate by Sime et al., (2005). At site FC02a the calculated calcification depth based on  $\delta^{18}\text{O}$  method is 65 m, and, the Mg/Ca derived depth is 100m; however, Sime et al., (2005) proposed a calcification depth of 146 m. A deeper depth habitat than site FC01a seems to be in line with the weaker stratification of the water column at site FC02a. The depth habitat for *P. obliquiloculata*'s was determined to be 106–120m by Sime et al., (2005); however, our calculations predict a lower and narrower depth habitat of 60 – 70m. Calcification depth for *G. menardii* has been calculated to be 60 – 70m, which is consistent with an upper thermocline depth habitat. Specimens of *G. tumida* is commonly found at the bottom of the thermocline which is around 200-250m at our Indian Ocean sites, Birch et al., (2013) found this species ranging from 100 to 200 m but our  $\delta^{18}\text{O}$  based habitat reconstruction suggests a shallower depth of 70m at both sites. It seems that the calcification derived Mg/Ca for *G. tumida* is more realistic than with our  $\delta^{18}\text{O}_c$  reconstructions, the Mg/Ca based calculation predicts a depth habitat of 100 – 130 m.

### ***Arabian Sea***

In the Arabian Sea foraminifera are affected by changes in local hydrology caused by the Indian summer and winter monsoons. The specimens of different species collectively record a shallower habitat during SW monsoon (e.g., upwelling) and a deeper habitat during NE monsoon (Peeters and Brummer, 2002). Except for *N. dutertrei*, our two methods of calcification depth reconstruction closely agree with each other within their respective uncertainties. The depth habitat reconstructions for *G. ruber* and for *T. sacculifer* are consistent with species living in the shallow mixed layer (SML) at a depth of 30m for *G. ruber* and 40 m for *T. sacculifer*. Specimens of *O. universa* are calculated to live at 30m depth; *N. dutertrei* at site FC12-b (water depth 151m) is living around 40m and at 150m at site FC13-b (water depth 3200m), which is consistent with the hydrography at this site (Fig. 4). The depth habitat of *P. obliquiloculata* is calculated to be 50m at both sites. Specimens of *G. menardii* is found at depths of 60m, consistent with Peeters and Brummer, (2002) estimate of 50 – 130m.

### ***Pacific Ocean***

For Pacific Ocean samples the Mg/Ca derived calcification depths were used in absence of  $\delta^{18}\text{O}_c$  values. The Sites WP07-01 and A14 are located in the Western Equatorial Pacific with Site WP07-01

characterized by a deep thermocline. At these sites *G. ruber* and *T. sacculifer* have deep depth habitat of around 100m for *G. ruber* (Elderfield and Ganssen, 2000) and around 125m for *T. sacculifer* (Rickaby et al., 2005). The depth habitat for specimens of *O. universa* was determined to be 75m depth at site WP07-01 and at 55m depth at site A14. We calculate that *P. obliquiloculata* is living at 125m deep. Rickaby et al., (2005) estimated the living depth of *N. dutertrei* at 165m in agreement with our calculated depths (~125m). Specimens of *G. menardii* were determined to live at 180m like *G. tumida* (Rickaby et al., 2005).

### **The data are not consistent with a dissolution effect to explain the low $\delta^{11}\text{B}$ *T. sacculifer* in the WEP**

Documented dissolution effects have been attributed to the preferential dissolution of ontogenic calcite relative to the light  $\delta^{11}\text{B}$  of gametogenic calcite (Ni et al., 2007; Seki et al., 2010; Henehan et al., 2016). *T. sacculifer* (w/o sacc) should be less impacted compared to the *T. sacculifer* (sacc). Hönisch and Hemming, (2004) and Ni et al., (2007) reported a dissolution effect at site 806 (close to our WP07-01 site) for *T. sacculifer* (sacc), however, in our data the  $\delta^{11}\text{B}_{\text{carbonate}}$  for *T. sacculifer* (sacc) is not decreasing with water depth when *T. sacculifer* (w/o sacc) is which suggests that at these sites and at the same size-fraction no dissolution is observed (eg. different water depth).  $\Delta^{11}\text{B}$  for *T. sacculifer* (w/o sacc) and for *G. ruber* shift to lighter with higher calcification depth, a trend that does not support a dissolution effect. The lethal temperature for *T. sacculifer* is 14°C, which at site WP07-01 corresponds to a  $\delta^{11}\text{B}_{\text{borate}}$  of 17.5 ‰ which makes our low  $\delta^{11}\text{B}_{\text{carbonate}}$  realistic. If no dissolution is observed, a deep depth habitat inducing a respiration-driven microenvironment might explain the low  $\delta^{11}\text{B}$  of the measured carbonate.

### **Microenvironment calculations**

We observe a trend between  $\Delta^{11}\text{B}$  (eg.  $\Delta^{11}\text{B} = \delta^{11}\text{B}_{\text{carbonate}} - \delta^{11}\text{B}_{\text{borate}}$ ) with derived calcification depth (Fig. S2). In order to verify why the WEP  $\delta^{11}\text{B}_{\text{carbonate}}$  of *T. sacculifer* (w/o sacc) is low and to test the hypothesis of the depth habitat we try to recalculate independently the theoretical water depth habitat based on culture results from Jorgensen et al., (1985) and our microenvironment pH results. A change of microenvironment pH for *T. sacculifer* will change the theoretical light intensity needed to reach this microenvironment pH. The compensation light intensity ( $E_c$ ) for *T. sacculifer* has been calculated by Jorgensen et al., (1985) to be  $\sim 30 \mu\text{Eistn.m}^{-2}.\text{s}^{-1}$ ,  $E_c$  corresponds to the energy where photosynthesis compensates respiration or where  $\delta^{11}\text{B}_{\text{carbonate}}$  reaches the 1:1 theoretical line. We tested two microenvironment pH,  $\Delta\text{pH}_1 = -0.04$  and  $\Delta\text{pH}_2 = -0.06$  (Fig S3). We've recalculated the light energy needed to decrease the pH of  $\Delta\text{pH}_1$  and  $\Delta\text{pH}_2$  and apply these changes to the light penetration profile determined with an insolation  $E_0$  in the WEP of  $220 \text{ J.s}^{-1}.\text{m}^{-2}$  (Weare et al., 1981) and a light attenuation coefficient of 0.028 (Wang et al., 2008). A decrease of  $\Delta\text{pH}_1$  would lead to a decrease of  $15 \mu\text{Eistn.m}^{-2}.\text{s}^{-1}$  and a decrease of  $\Delta\text{pH}_2$  would lead to a decrease of  $24 \mu\text{Eistn.m}^{-2}.\text{s}^{-1}$  (Jorgensen et al., 1985). These results correspond in our case of a light penetration of 12% to reach  $E_c$ , 5% for a decrease of  $\Delta\text{pH}_1$  and 1% for a decrease of  $\Delta\text{pH}_2$ . This means that in the WEP if *T. sacculifer* calcifies below 75m where  $E_c$  is reached the  $\delta^{11}\text{B}_{\text{carbonate}}$  is below the theoretical 1:1 line. *T. sacculifer* (w/o sacc) in the WEP is decreasing its pH of  $\sim \Delta\text{pH}_1$  which would imply a calcification depth of 110m consistent with the reconstruction of Rickaby et al., (2005).

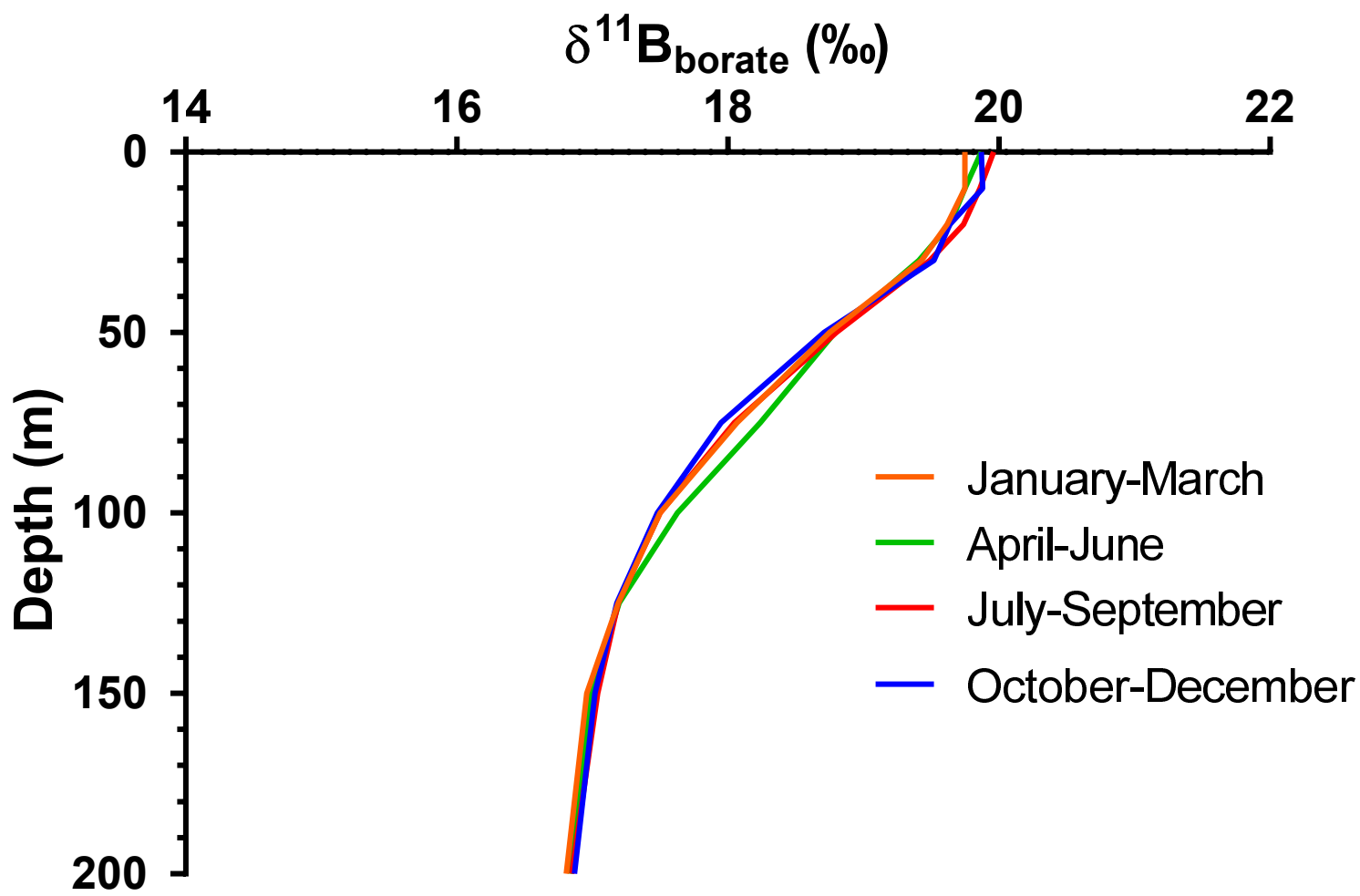
$$\Delta\text{microenvironment pH} = -\log\left(\frac{(\delta^{11}\text{B}_{\text{seawater}} - \delta^{11}\text{B}_{\text{carbonate}}) \times K_b^*}{\varepsilon - \delta^{11}\text{B}_{\text{seawater}} + \delta^{11}\text{B}_{\text{carbonate}}}\right) - \text{pH}_{\text{seawater}}$$

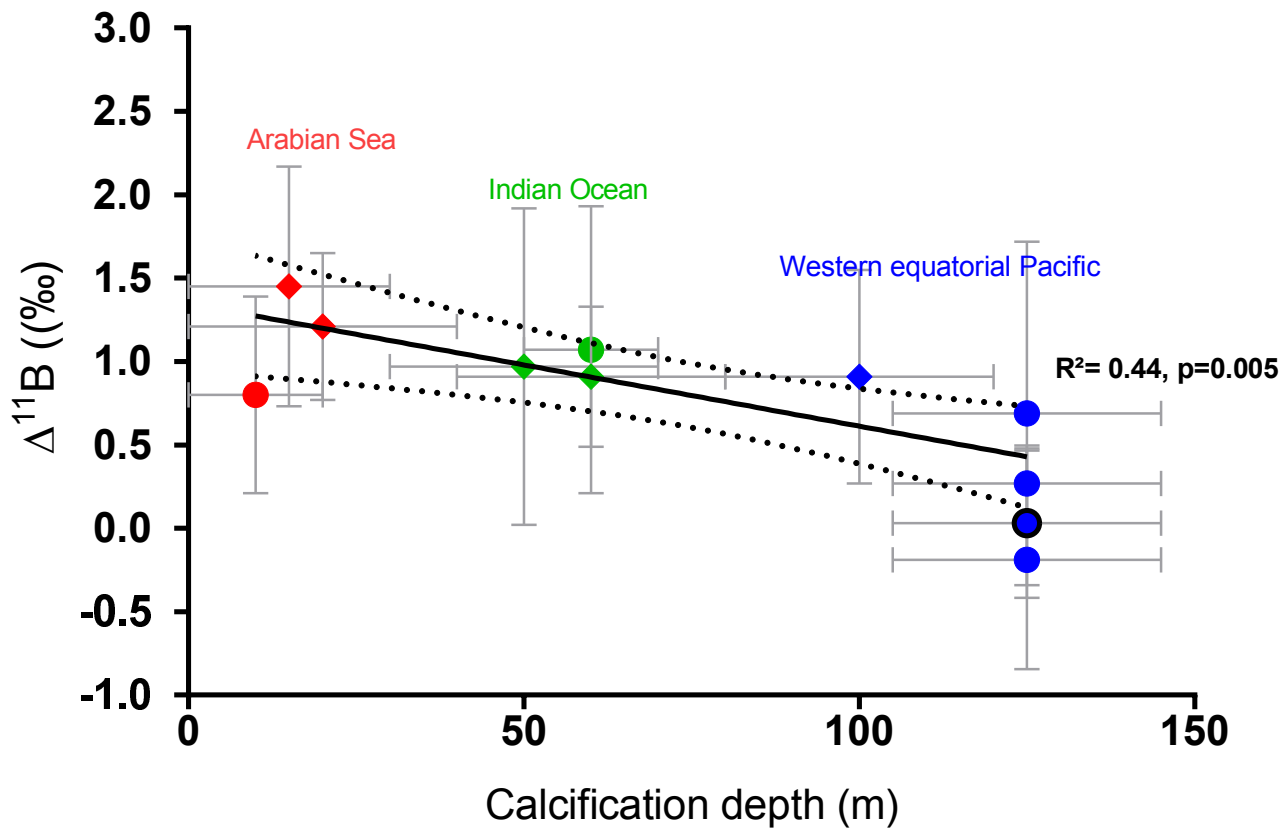
## References

- Arbuszewski, J., DeMenocal, P., Kaplan, A. and Farmer, E. C.: On the fidelity of shell-derived  $\delta^{18}\text{O}$  seawater estimates, *Earth Planet. Sci. Lett.*, 300, 185–196, 2010.
- Barker, S., Greaves, M. and Elderfield, H.: A study of cleaning procedures used for foraminiferal Mg/Ca paleothermometry, *Geochemistry, Geophys. Geosystems* 4, 1–20, 2003.
- Bemis, B. E., Spero, H. J. and Thunell, R. C.: Using species-specific paleotemperature equations with foraminifera: a case study in the Southern California Bight, *Mar. Micropaleontol.*, 46, 405–430, 2002.
- Bemis, B. E., Spero, H. J., Bijma, J. and Lea, D. W.: Reevaluation of the oxygen isotopic composition of planktonic foraminifera: Experimental results and revised paleotemperature equations, *Paleoceanography*, 13, 150–160, 1998.
- Birch, H., Coxall, H. K., Pearson, P. N., Kroon, D. and O'Regan, M.: Planktonic foraminifera stable isotopes and water column structure: Disentangling ecological signals, *Mar. Micropaleontol.*, 101, 127–145, 2013.
- Boyer, T.P., J. I. Antonov, O. K. Baranova, C. Coleman, H. E. Garcia, A. Grodsky, D. R. Johnson, R. A. Locarnini, A. V. Mishonov, T.D. O'Brien, C.R. Paver, J.R. Reagan, D. Seidov, I. V. Smolyar, and M. M. Zweng: World Ocean Database 2013, NOAA Atlas NESDIS 72, S. Levitus, Ed., A. Mishonov, Technical Ed.; Silver Spring, 2013
- Dekens, P. S., Lea, D. W., Pak, D. K. and Spero, H. J.: Core top calibration of Mg/Ca in tropical foraminifera: Refining paleotemperature estimation, *Geochemistry, Geophys. Geosystems*, 3, 1–29, 2002.
- Deuser, W.G., Ross, E.H., Hemleben, Ch., Spindler, M.: Seasonal changes in species composition, numbers, mass, size, and isotopic composition of planktonic foraminifera settling into the deep Sargasso Sea, *Palaeogeogr., Palaeoclimat., Palaeoecol.*, 33:103-127, 1981.
- Deuser, W. G. and Ross, E. H., Seasonally abundant planktonic foraminifera of the Sargasso Sea; succession, deep-water fluxes, isotopic compositions, and paleoceanographic implications, *J. Foraminifer. Res.*, 19, 268–293, 1989.
- Duplessy, J., Labeyrie, L., Juilletleclerc, A., Maitre, F., Duprat, J. and Sarnthein, M., Surface salinity reconstruction of the north-atlantic ocean during the last glacial maximum, *Oceanol. Acta*, 14, 311–324, 1991.
- Elderfield, H., Yu, J., Anand, P., Kiefer, T. and Nyland, B.: Calibrations for benthic foraminiferal Mg/Ca paleothermometry and the carbonate ion hypothesis, *Earth Planet. Sci. Lett.*, 250, 633–649, 2006.
- Farmer, E. C., Kaplan, A., de Menocal, P. B. and Lynch-Stieglitz, J.: Corroborating ecological depth preferences of planktonic foraminifera in the tropical Atlantic with the stable oxygen isotope ratios of core top specimens, *Paleoceanography*, 22, 1–14, 2007.
- Fairbanks, R. G., Sverdrlove, M., Free, R., Wiebe, P. H. and Bé, A. W. H.: Vertical distribution and isotopic fractionation of living planktonic foraminifera from the Panama Basin, *Nature*, 298, 841–844, 1982.
- Fairbanks, R. G. and Wiebe, P. H., Foraminifera and Chlorophyll Maximum: Vertical Distribution, Seasonal Succession, and Paleoceanographic Significance, *Science*, 209, 1524–1526, 1980.
- Ferguson, J. E., Henderson, G. M., Kucera, M. and Rickaby, R. E. M.: Systematic change of foraminiferal Mg/Ca ratios across a strong salinity gradient, *Earth Planet. Sci. Lett.*, 265, 153–166, 2008.
- Henehan, M. J., Foster, G. L., Bostock, H. C., Greenop, R., Marshall, B. J. and Wilson, P. A.: A new boron isotope-pH calibration for *Orbulina universa*, with implications for understanding and accounting for 'vital effects.', *Earth Planet. Sci. Lett.*, 454, 282–292, 2016.

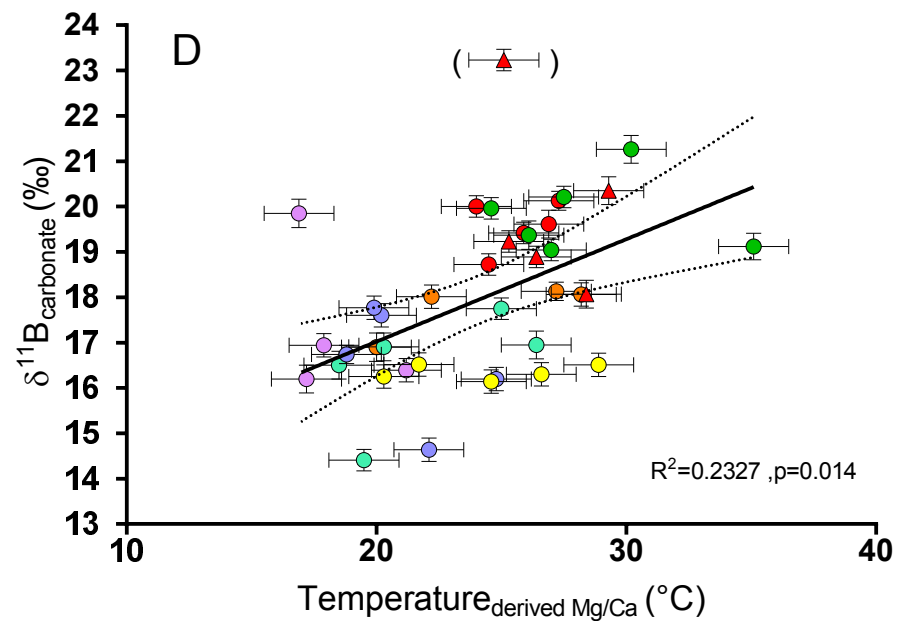
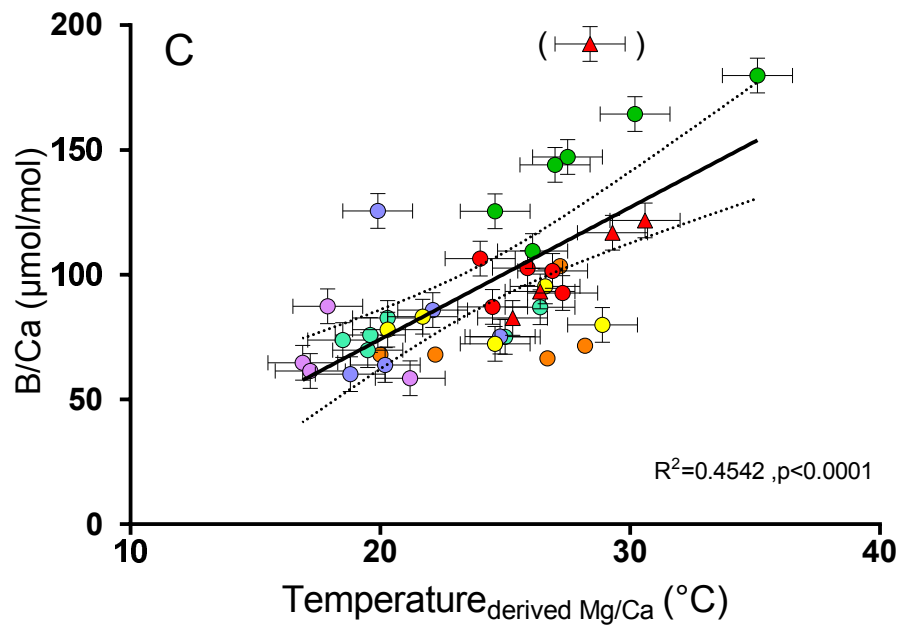
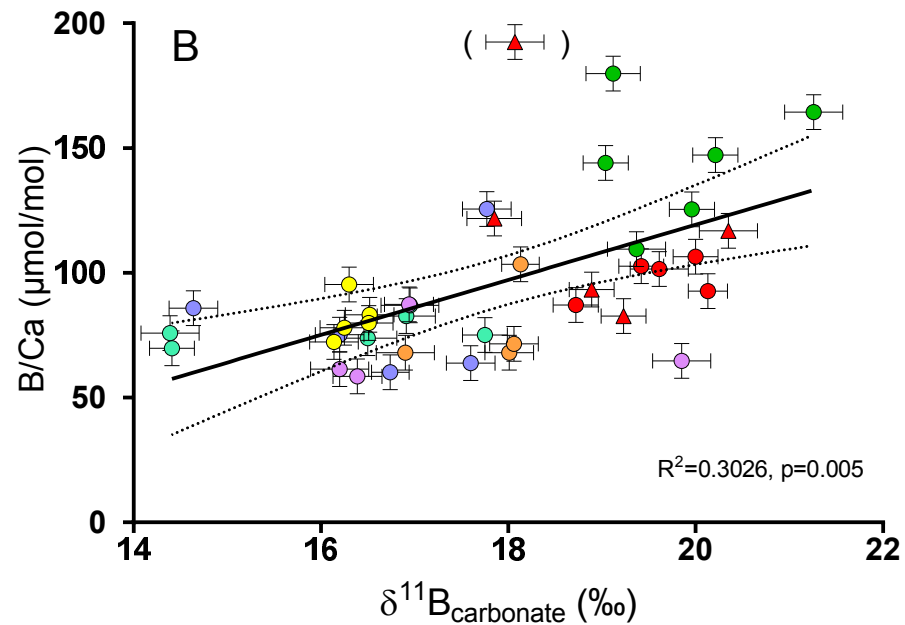
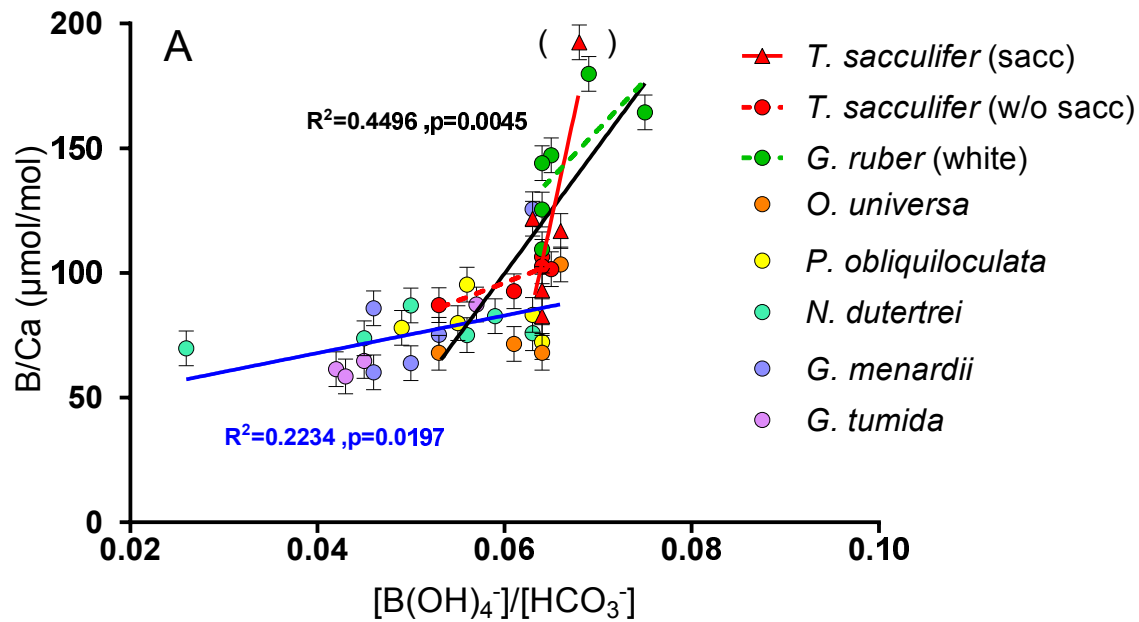


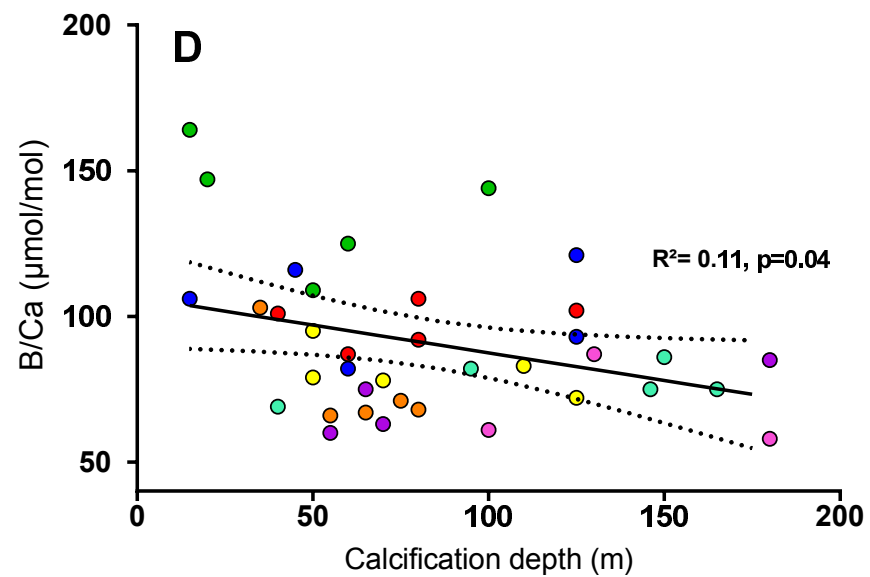
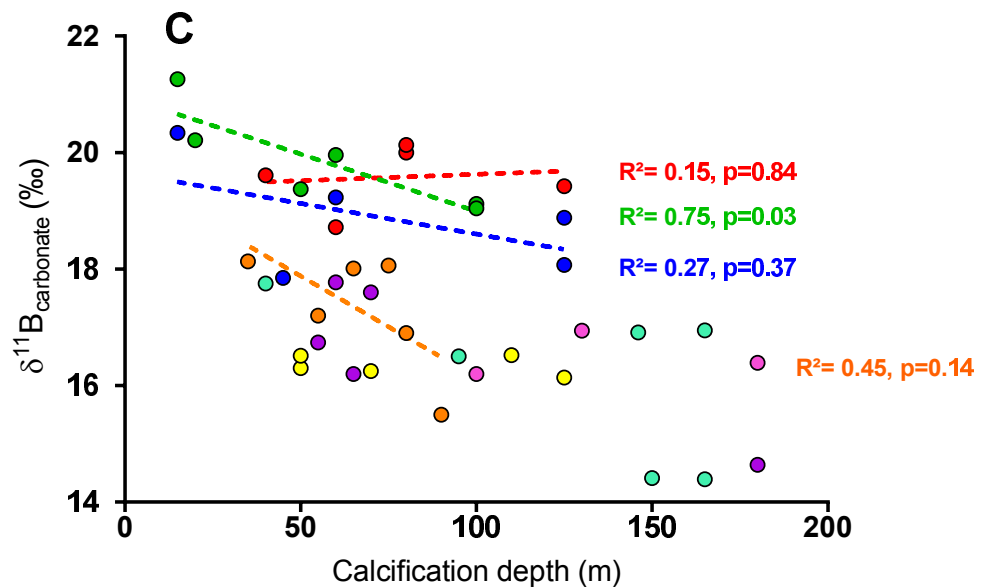
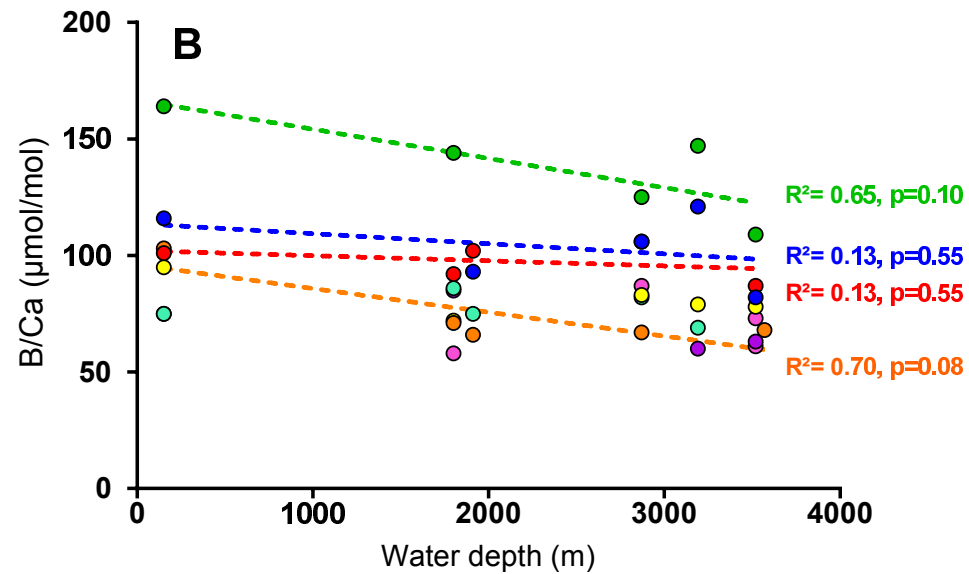
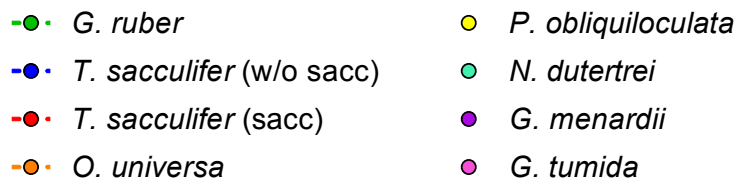
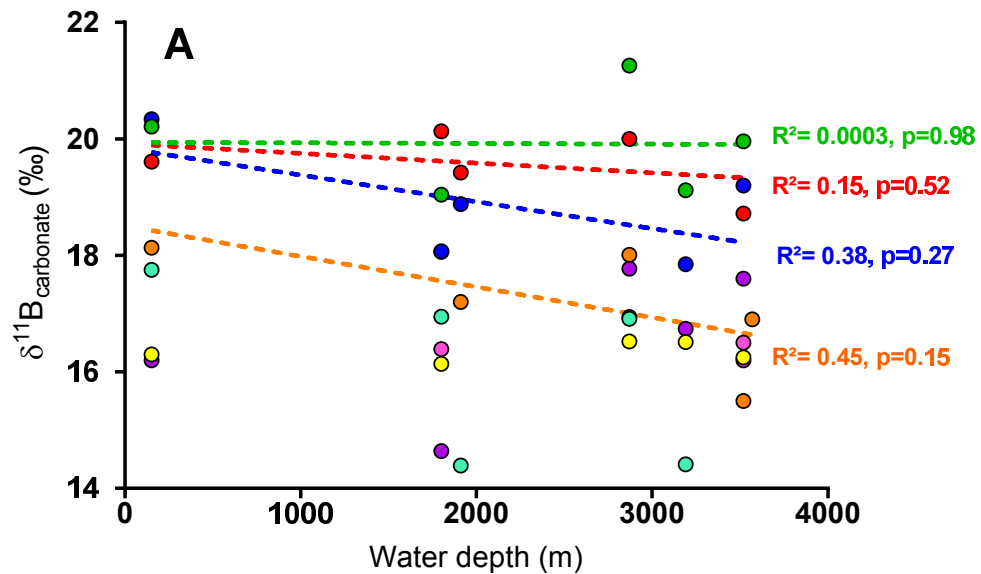
- Hönisch, B. and Hemming, N. G.: Ground-truthing the boron isotope-paleo-pH proxy in planktonic foraminifera shells: Partial dissolution and shell size effects, *Paleoceanography*, 19, 1–13, 2004.
- Jørgensen, B. B., Erez, J., Revsbech, P. and Cohen, Y.: Symbiotic photosynthesis in a planktonic foraminiferan, *Globigerinoides sacculifer* (Brady), studied with microelectrodes, *Limnol. Oceanogr.* 30, 1253–1267, 1985.
- Kim, S.-T. and O’Neil, J. R.: Equilibrium and nonequilibrium oxygen isotope effects in synthetic carbonates, *Geochim. Cosmochim. Acta*, 61, 3461–3475, 1997.
- Martínez-Botí, M. A., Mortyn, P. G., Schmidt, D. N., Vance, D. and Field, D. B.: Mg/Ca in foraminifera from plankton tows: Evaluation of proxy controls and comparison with core tops, *Earth Planet. Sci. Lett.*, 307, 113–125, 2011.
- Misra, S., Greaves, M., Owen, R., Kerr, J., Elmore, A. C. and Elderfield, H.: Determination of B/Ca of natural carbonates by HR-ICP-MS, *Geochemistry, Geophys. Geosystems*, 15, 1617–1628, 2014.
- Mulitza, S., Boltovskoy, D., Donner, B., Meggers, H., Paul, A. and Wefer, G.: Temperature:δ18O relationships of planktonic foraminifera collected from surface waters, *Palaeogeogr. Palaeoclimatol. Palaeoecol.* 202, 143–152, 2003.
- Ni, Y., Foster, G. L., Bailey, T., Elliott, T., Schmidt, D. N., Pearson, P., Haley, B. and Coath, C.: A core top assessment of proxies for the ocean carbonate system in surface-dwelling foraminifers, *Paleoceanography*, 22, 2007.
- Peeters, F. J. C. and Brummer, G.-J. a.: The seasonal and vertical distribution of living planktic foraminifera in the NW Arabian Sea, *Geol. Soc. London, Spec. Publ.*, 195, 463–497, 2002.
- Rostek, F., Ruhland, G., Bassinot, F. C., Muller, P. J., Labeyrie, L. D., Lancelot, Y. and Bard, E.: Reconstructing Sea-Surface Temperature and Salinity Using δ18O and Alkenone Records, *Nature*, 364, 319–321, 1993.
- Russell, A. D., Hönisch, B., Spero, H. J. and Lea, D. W.: Effects of seawater carbonate ion concentration and temperature on shell U, Mg, and Sr in cultured planktonic foraminifera, *Geochim. Cosmochim. Acta*, 68, 4347–4361, 2004.
- Seki, O., Foster, G. L., Schmidt, D. N., Mackensen, A., Kawamura, K. and Pancost, R. D.: Alkenone and boron-based Pliocene pCO<sub>2</sub> records, *Earth Planet. Sci. Lett.*, 292, 201–211, 2010.
- Sime, N. G., De La Rocha, C. L. and Galy, A.: Negligible temperature dependence of calcium isotope fractionation in 12 species of planktonic foraminifera, *Earth Planet. Sci. Lett.*, 232, 51–66, 2005.
- Yu, J., Day, J., Greaves, M. and Elderfield, H.: Determination of multiple element/calcium ratios in foraminiferal calcite by quadrupole ICP-MS, *Geochemistry, Geophys. Geosystems* 6, 2005.
- Rickaby, R. E. M. and Halloran, P.: Cool La Nina During the Warmth of the Pliocene?, *Science*, 307, 1948–1952, 2005.
- Wang, G., Cao, W., Yang, D. and Xu, D. Variation in downwelling diffuse attenuation coefficient in the northern South China Sea, *Chinese J. Oceanol. Limnol.*, 26, 323–333, 2008.
- Weare, B. C., Strub, P. T. and Samuel, M. D.: Annual Mean Surface Heat Fluxes in the Tropical Pacific Ocean, *J. Phys. Oceanogr.*, 11, 705–717, 1981.



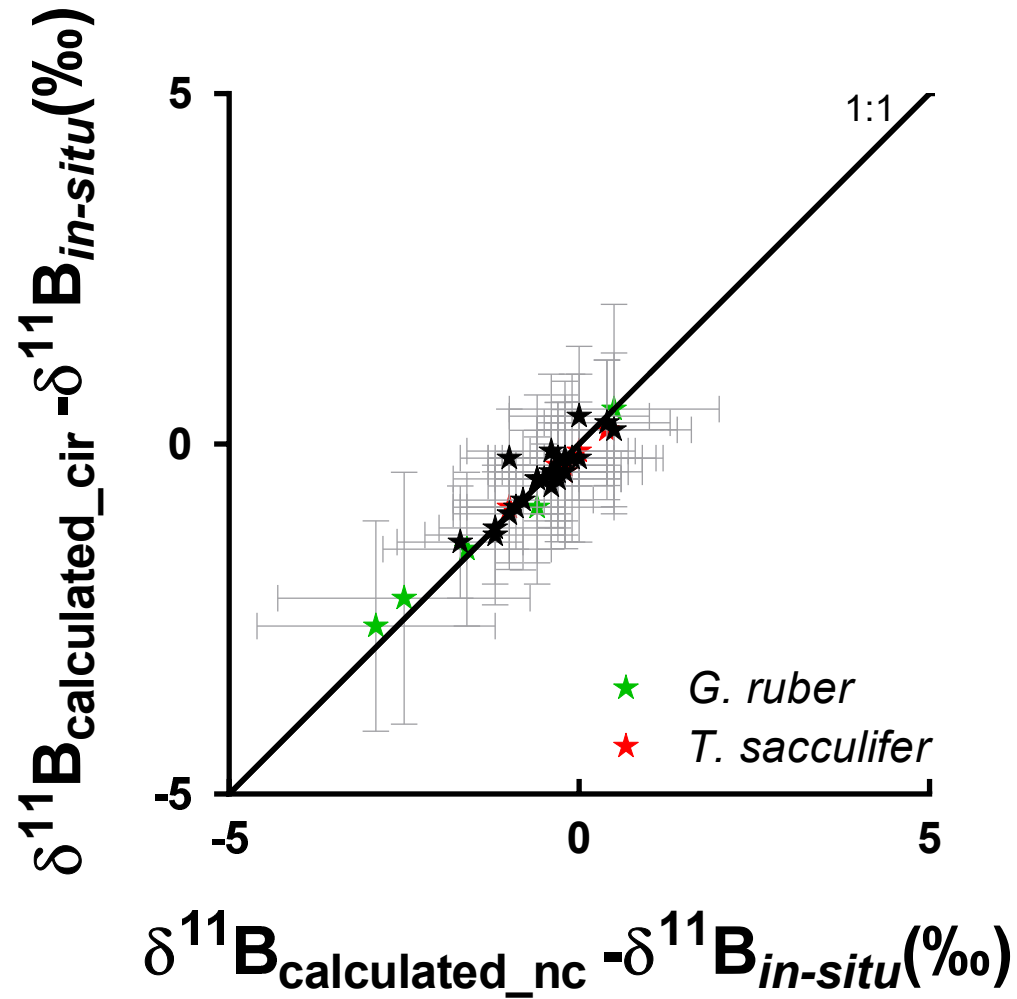


- ◆ *G. ruber* (Arabian Sea)
- *T. sacculifer* (w/sacc) (Arabian Sea)
- ◆ *G. ruber* (Indian Ocean)
- *T. sacculifer* (w/o sacc) (Indian Ocean)
- ◆ *G. ruber* (WEP)
- *T. sacculifer* (w/o sacc) (WEP)
- Linear reg. All





$\delta^{11}\text{B}_{\text{borate}}$



pH

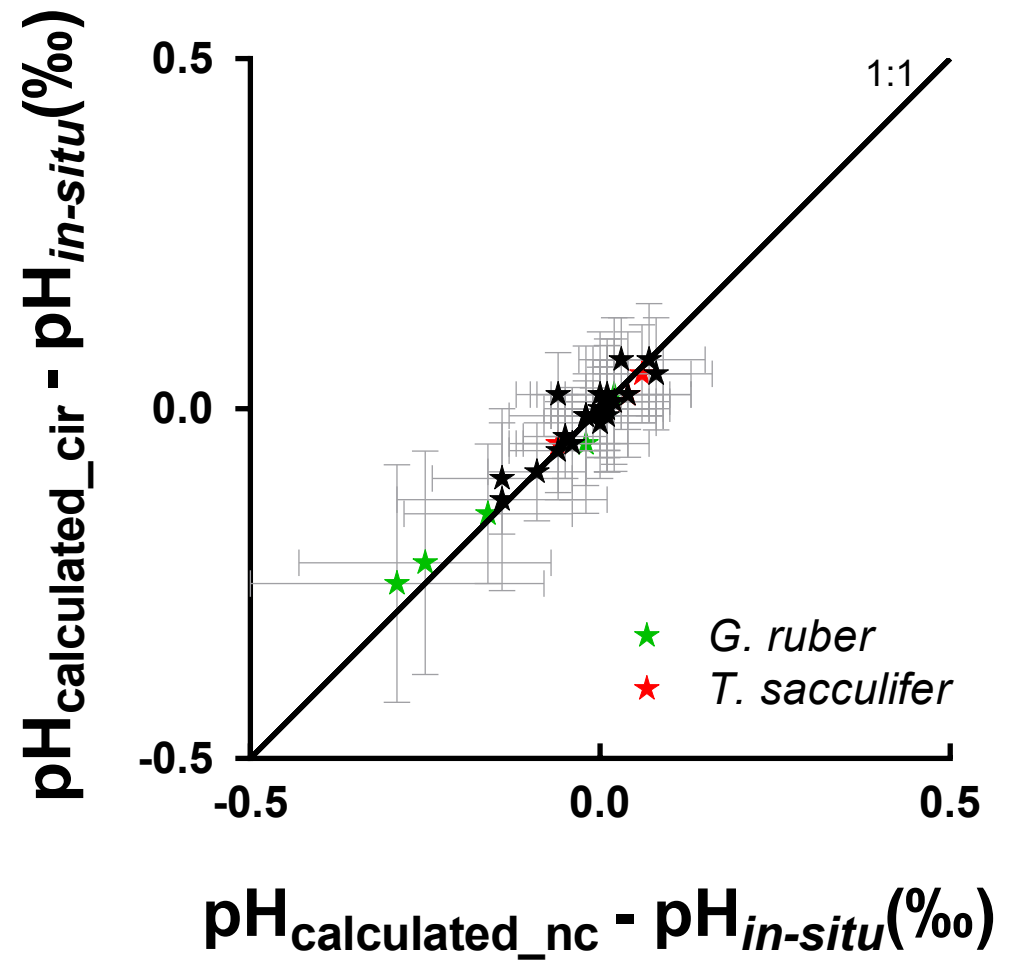


**Table S1**

<b>Elemental ratios</b>	<b>Li/Ca</b> μmol/mol	<b>B/Ca</b> μmol/mol	<b>Mg/Ca</b> mmol/mol	<b>Al/Ca</b> mmol/mol	<b>Sr/Ca</b> mmol/mol	<b>Cd/Ca</b> μmol/mol	<b>Ba/Ca</b> μmol/mol	<b>U/Ca</b> nmol/mol	<b>Mn/Ca</b> μmol/mol	<b>Fe/Ca</b> mmol/mol
Standard solution 0	0.8	9	0.10	0.131	0.00	0.03	0.6	31	1	0.01
Standard solution 1	2.3	38	0.31	0.112	0.49	0.05	1.9	38	12	0.02
Standard solution 3	6.8	108	1.31	0.177	1.06	0.13	3.0	53	39	0.04
Standard solution 5	14.6	216	3.17	0.223	1.57	0.23	5.1	62	129	0.08
Standard solution 6	19.0	278	5.23	0.352	1.97	0.28	5.5	74	196	0.11
Standard solution 8	25.0	281	6.07	0.602	2.99	0.50	20.1	390	501	0.50
Standard solution 9		408			4.89					
Standard solution 10		519			8.01					
Standard solution 11		607			9.93					

**Table S2**

<b>Standard</b>	<b><math>\delta^{11}\text{B}_1</math> (‰)</b>	<b><math>2\text{SD}_{\text{AEI21}}</math></b>	<b><math>n_{\text{AEI21}}</math></b>	<b><math>\delta^{11}\text{B}_2</math> (‰)</b>	<b><math>2\text{SD}_{\text{AEI21}}</math></b>	<b><math>n_{\text{AEI21}}</math></b>	<b>Reference</b>
NEP1	25.21	0.25	11	25.22	0.25	11	This study
NEP2	25.00	0.30	12				This study
NEP3	24.70	0.30	12				This study
NEP4	25.40	0.21	11				This study
NEP5	25.32	0.21	11	25.33	0.21	11	This study
NEP6	25.22	0.21	11				This study
NEP7	25.26	0.26	15				This study
NEP8	25.39	0.26	15				This study
NEP9	26.15	0.26	15				This study
NEP10	25.97	0.26	15				This study
NEP11	26.09	0.26	15	26.09	0.26	15	This study
NEP12	26.22	0.26	15	26.29	0.26	15	This study
NEP13	26.19	0.26	15	26.21	0.26	15	This study
NEP14	26.12	0.26	15	26.13	0.26	15	This study
NEP15	26.00	0.26	15				This study
NEP16	26.04	0.26	15				This study
NEP17	26.02	0.29	12				This study
NEP18	25.86	0.29	12	25.86	0.26	14	This study
NEP19	25.78	0.26	14				This study
NEP20	25.42	0.15	3	25.32	0.15	3	This study
NEP21	25.54	0.22	6	26.16	0.22	6	This study
NEP22	26.42	0.22	6				This study
JCP-1-1	24.07	0.10					This study
JCP-1-2	24.17	0.11		24.17	0.10		This study
JCP-1-3	24.01	0.11					This study
JCP-1-4	23.92	0.26					This study
JCP-1-5	24.03	0.26		24.05	0.39		This study
JCP-1-6	24.18	0.36		24.16	0.36		This study
<b>Standard</b>	<b>Average <math>\delta^{11}\text{B}</math></b>	<b><math>2\text{SD}</math></b>	<b><math>n</math></b>	<b>Reference</b>			
NEP	25.70	0.93	22	This study			
NEP	26.20	0.88	27	Holcomb et al., 2015			
NEP	25.80	0.89	6	Sutton et al., 2018			
JCP-1	24.06	0.20	6	This study			
JCP-1	24.37	0.32	57	Holcomb et al., 2015			
JCP-1	24.42	0.28	7	Sutton et al., 2018			





**Table S4**

<b>Specie</b>	<b>Seasonality</b>
<i>T. sacculifer (sacc)</i>	Spring
<i>T. sacculifer (w/o sacc)</i>	Spring
<i>G. ruber (white)</i>	Summer
<i>N. dutertrei</i>	Winter
<i>G. tumida</i>	Annual average
<i>G. menardii</i>	Annual average
<i>O. universa</i>	Annual average
<i>P. obliquiloculata</i>	Winter

Table S5

Species	B	A	Reference
<i>T. sacculifer (sacc)</i>	0.377	0.090	Anand et al., 2003
<i>T. sacculifer (w/o sacc)</i>	0.347	0.090	Anand et al., 2003
<i>G. ruber (white)</i>	0.300	0.089	Dekens et al., 2002
<i>N. dutertrei</i>	0.600	0.008	Dekens et al., 2002
<i>G. tumida</i>	0.380	0.090	Anand et al., 2003
<i>G. menardii</i>	0.360	0.091	Regenberg et al., 2009
<i>O. universa</i>	0.595	0.090	Anand et al., 2003
<i>P. obliquiloculata</i>	0.328	0.090	Anand et al., 2003

Species	A	B	C	dw correction	Condition	Reference	Equation
<i>O. universa</i>	16.500	4.800		-0.27	LL	Bemis et al., 1998	$T=A-B*(\delta^{18}O_c-\delta^{18}O_w)$
<i>O. universa</i>	15.700	4.460	0.35	-0.27	ML	Bemis et al., 2002	$T=A-B*(\delta^{18}O_c-\delta^{18}O_w)+C*(\delta^{18}O_c-\delta^{18}O_w)^2$
<i>O. universa</i>	14.900	4.800		-0.27	HL	Bemis et al., 1998	$T=A-B*(\delta^{18}O_c-\delta^{18}O_w)$
<i>T. sacculifer</i>	14.910	4.350		-0.27		Mulitza et al., 2003	$T=A-B*(\delta^{18}O_c-\delta^{18}O_w)$
<i>G. ruber</i>	14.200	4.440		-0.27		Mulitza et al., 2003	$T=A-B*(\delta^{18}O_c-\delta^{18}O_w)$
All	16.900	4.380	0.1	-0.2		Shackleton et al., 1974	$T=A-B*(\delta^{18}O_c-\delta^{18}O_w)+C*(\delta^{18}O_c-\delta^{18}O_w)^2$
All	17.000	4.520	0.03	-0.22		Erez and Luz, 1983	$T=A-B*(\delta^{18}O_c-\delta^{18}O_w)+C*(\delta^{18}O_c-\delta^{18}O_w)^2$
All	16.100	4.640	0.09	-0.27		Kim and O'Neil 1997	$T=A-B*(\delta^{18}O_c-\delta^{18}O_w)+C*(\delta^{18}O_c-\delta^{18}O_w)^3$

Table S6

Core	Species	CD <sub>1</sub>	CD <sub>2</sub>	CD <sub>3</sub>	Reference
FC-01a	<i>G. ruber</i> (white ss)	83 ± 20	30 ± 10	50 ± 20	Sime thesis 2006
FC-02a	<i>G. ruber</i> (white ss)	56 ± 10	15 ± 10	60 ± 20	Sime thesis 2006
FC-12b	<i>G. ruber</i> (white ss)	Surface ± 10	0-30	60 ± 10	Peeters and Brumer, 2012 (non upwelling station Arabian sea)
FC-13a	<i>G. ruber</i> (white ss)	Surface ± 10	20 ± 20	60 ± 10	Peeters and Brumer, 2012 (non upwelling station Arabian sea)
WP7-01	<i>G. ruber</i> (white ss)			100±20	Elderfield and Ganssen, 2000
A14	<i>G. ruber</i> (white ss)		60 ± 10	100±20	Elderfield and Ganssen, 2000
FC-01a	<i>T. sacculifer</i> (sacc)	48 ± 10	50 ± 10	60 ± 10	Sime et al., 2005
FC-02a	<i>T. sacculifer</i> (sacc)	7 ± 10	30 ± 10	80 ± 20	Sime et al., 2006
FC-12b	<i>T. sacculifer</i> (sacc)	15 ± 10	40 ± 10		
WP7-01	<i>T. sacculifer</i> (sacc)		80 ± 20	125 ± 15	Rickaby et al., 2005
A14	<i>T. sacculifer</i> (sacc)		60 ± 10	125 ± 15	
FC-01a	<i>T. sacculifer</i> (w/o sacc)	88 ± 20	50 ± 10	60 ± 10	Sime thesis 2006 (Wind22-b)
FC-02a	<i>T. sacculifer</i> (w/o sacc)	32 ± 10	10 ± 10	80 ± 20	Sime thesis 2006
FC-12b	<i>T. sacculifer</i> (w/o sacc)	0-15 ± 10	30 ± 10	45 ± 20	Peeters and Brumer, 2012 (non upwelling station Arabian sea)
WP7-01	<i>T. sacculifer</i> (w/o sacc)		80 ± 20	125 ± 15	Rickaby et al., 2005
A14	<i>T. sacculifer</i> (w/o sacc)		60 ± 10	125 ± 15	Rickaby et al., 2005
CD107a	<i>O. universa</i>	80 ± 20	50 ± 20	0-50	Farmer et al., 2007
FC-01a	<i>O. universa</i>	45 ± 10	60 ± 10	90 ± 20	Sime et al., 2005
FC-02a	<i>O. universa</i>	127 ± 20	45 ± 15	65 ± 10	Birshe et al., 2013
FC-12b	<i>O. universa</i>	35 ± 10	30 ± 20		
WP7-01	<i>O. universa</i>		75 ± 25		
A14	<i>O. universa</i>		55 ± 15		
FC-01a	<i>P. obliquiloculata</i>	70 ± 20	75 ± 15	106 ± 20	Sime et al., 2005
FC-02a	<i>P. obliquiloculata</i>	226 ± 20	60 ± 10		
FC-12b	<i>P. obliquiloculata</i>	40 ± 10	50 ± 10		
FC-13a	<i>P. obliquiloculata</i>	65 ± 10	50 ± 10		
WP7-01	<i>P. obliquiloculata</i>		125 ± 25		
FC-01a	<i>N. dutertrei</i>	95 ± 20	90 ± 20	93 ± 20	Sime et al., 2005
FC-02a	<i>N. dutertrei</i>	65 ± 10	100 ± 20	146 ± 20	Sime et al., 2005
FC-12b	<i>N. dutertrei</i>	40 ± 10	50 ± 10		
FC-13a	<i>N. dutertrei</i>	45 ± 10	150 ± 20		
WP7-01	<i>N. dutertrei</i>		125 ± 25	165	Rickaby et al., 2005
A14	<i>N. dutertrei</i>		110 ± 20	165	Rickaby et al., 2005
FC-01a	<i>G. menardii</i>	135 ± 20	70 ± 20		
FC-02a	<i>G. menardii</i>	60 ± 10	60 ± 10		
FC-12b	<i>G. menardii</i>	65 ± 10	55 ± 15	60 ± 10	Peeters and Brumer, 2012 (non upwelling station Arabian sea)
FC-13a	<i>G. menardii</i>	55 ± 10	70 ± 10	60 ± 10	Peeters and Brumer, 2012 (non upwelling station Arabian sea)
WP7-01	<i>G. menardii</i>		180 ± 20		
FC-01a	<i>G. tumida</i>	70 ± 20	100 ± 10	160 ± 20	Birshe et al., 2013
FC-02a	<i>G. tumida</i>	70 ± 20	130 ± 20	160 ± 20	Birshe et al., 2013
WP7-01	<i>G. tumida</i>		180 ± 20	210 - 240	Rickaby et al., 2005

CD<sub>1</sub>: Depth habitat estimated from δ<sup>18</sup>O<sub>c</sub>

CD<sub>2</sub>: Depth habitat estimated from Mg/Ca derived temperature

CD<sub>3</sub>: Depth habitat from literature

Table S7

Core	Species	Depth habitat (m)	PRE INDUSTRIAL IN-SITU PARAMETERS																		CALCULATED PARAMETERS														
			Temperature (°C)	2sd*	Salinity	2sd*	pH (pre-ind)	2sd*	pCO <sub>2</sub>	2sd*	HCO <sub>3</sub> <sup>-</sup>	2sd*	CO <sub>3</sub> <sup>2-</sup>	2sd*	DIC	2sd*	ALK	2sd*	δ <sup>11</sup> B <sub>bratate</sub>	2sd*	T <sub>Mg/Ca</sub>	2sd	pH <sub>d11B</sub>	2sd**	pCO <sub>2</sub>	2sd***	Calibration	pH <sub>d11B</sub>	2sd**	pCO <sub>2</sub>	2sd***	Calibration			
<b>Atlantic Ocean</b>																																			
CD107a	<i>O. universa</i>	80 ± 20	12.0	0.3	35.6	0.01	8.19	0.03	274	21	1856	29	192	12	2059	18	2333	1	17.86	0.31	20.0	1.4	8.19	0.06	285	39	[8]								
<b>Indian Ocean</b>																																			
FC-01a	<i>G. ruber</i> (white ss)	50 ± 20	23.4	5.9	35.0	0.4	8.10	0.04	338	41	1743	138	226	48	1979	93	2299	22	18.40	0.90	26.1	1.4	8.07	0.05	387	29	[1]	7.88	0.16	630	42	[2]			
FC-01a	<i>T. sacculifer</i> (sacc)	60 ± 10	21.9	5.7	35.1	0.3	8.09	0.03	346	38	1773	126	215	45	1998	84	2303	18	18.15	0.81	24.5	1.4	8.06	0.04	400	79	[3]	8.04	0.06	417	82	[4]			
FC-01a	<i>T. sacculifer</i> (w/o sacc)	60 ± 10	21.9	5.7	35.1	0.3	8.09	0.03	346	38	1773	126	215	45	1998	84	2303	18	18.16	0.82	25.3	1.4	8.10	0.04	357	49	[3]	8.10	0.05	356	49	[4]			
FC-01a	<i>O. universa</i>	90 ± 20	18.2	4.0	35.2	0.0	8.07	0.04	374	43	1856	94	184	35	2053	62	2311	9	17.42	0.61			7.98	0.06	499	63	[8]								
FC-01a	<i>P. obliquiloculata</i>	106 ± 20	20.5	4.6	35.2	0.1	8.09	0.03	353	32	1802	99	204	36	2018	65	2306	11	17.91	0.66	20.3	1.4	8.10	0.08	356	48	[11]								
FC-01a	<i>G. menardii</i>	70 ± 20	20.5	4.6	35.2	0.1	8.09	0.03	353	32	1802	99	204	36	2018	65	2306	11	17.93	0.68	20.2	1.4	8.16	0.05	304	43	[13]								
FC-01a	<i>N. dutertrei</i>	95 ± 20	17.7	4.0	35.1	0.0	8.06	0.04	380	43	1868	94	180	35	2061	62	2313	9	17.26	0.62	18.5	1.4	8.09	0.06	373	49	[13]								
FC-01a	<i>G. tumida</i>	100 ± 20	17.1	1.6	35.1	0.0	8.06	0.02	386	22	1881	41	175	15	2070	27	2314	3	17.21	0.27	17.2	1.4	8.06	0.07	400	52	[13]								
FC-02a	<i>G. ruber</i> (white ss)	60 ± 20	20.4	2.4	35.5	0.0	8.19	0.01	268	10	1724	26	246	10	1979	17	2332	2	19.06	0.34	24.6	1.4	8.13	0.04	332	26	[1]	8.03	0.10	428	31	[2]			
FC-02a	<i>T. sacculifer</i> (sacc)	80 ± 20	19.3	1.9	35.6	0.1	8.19	0.01	268	7	1741	38	240	15	1989	24	2333	3	18.89	0.30	24.0	1.4	8.18	0.03	286	57	[3]	8.21	0.05	267	54	[4]			
FC-02a	<i>T. sacculifer</i> (w/o sacc)	80 ± 20	19.3	1.9	35.6	0.1	8.19	0.01	268	7	1741	38	240	15	1989	24	2333	3	18.90	0.30	25.1	1.4													
FC-02a	<i>O. universa</i>	65 ± 10	20.1	1.1	35.5	0.0	8.19	0.00	268	2	1728	15	245	6	1981	9	2332	1	19.00	0.17	22.2	1.4	8.18	0.04	287	42	[8]								
FC-02a	<i>P. obliquiloculata</i>	60 ± 10	18.3	0.5	35.6	0.0	8.18	0.01	277	8	1769	17	228	7	2007	10	2334	1	18.64	0.14	21.7	1.4	8.16	0.08	302	43	[11]								
FC-02a	<i>G. menardii</i>	60 ± 10	20.4	1.9	35.5	0.0	8.19	0.01	268	10	1724	19	246	7	1979	12	2332	2	19.05	0.30	19.9	1.4	8.17	0.05	293	42	[13]								
FC-02a	<i>N. dutertrei</i>	146 ± 20	17.5	1.0	35.6	0.1	8.16	0.02	292	14	1798	31	216	13	2024	18	2333	2	18.33	0.27	20.3	1.4	8.12	0.06	339	46	[13]								
FC-02a	<i>G. tumida</i>	130 ± 20	17.8	0.8	35.6	0.0	8.17	0.02	284	17	1784	32	222	14	2015	19	2334	1	18.47	0.25	17.9	1.4	8.12	0.05	339	46	[13]								
<b>Arabian Sea</b>																																			
FC-12b	<i>G. ruber</i> (white ss)	0-30	25.9	0.3	36.6	0.1	8.18	0.05	271	39	1655	53	292	23	1954	31	2374	8	19.81	0.65	30.2	1.4	8.15	0.04	305	28	[1]	8.20	0.10	265	26	[2]			
FC-12b	<i>T. sacculifer</i> (sacc)	40 ± 10	25.3	0.6	36.5	0.0	8.10	0.06	350	64	1756	75	249	31	2015	46	2369	2	18.71	0.77	26.9	1.4	8.09	0.04	374	54	[3]	8.10	0.06	366	53	[4]			
FC-12b	<i>T. sacculifer</i> (w/o sacc)	15 ± 10	25.9	0.0	36.5	0.1	8.16	0.04	290	34	1681	45	281	19	1970	28	2374	8	19.54	0.50	29.3	1.4	8.13	0.04	332	50	[3]	8.16	0.06	302	47	[4]			
FC-12b	<i>O. universa</i>	35 ± 10	25.5	0.6	36.5	0.0	8.11	0.06	334	56	1738	68	257	28	2004	41	2369	1	18.90	0.69	27.2	1.4	8.13	0.03	336	50	[8]								
FC-12b	<i>P. obliquiloculata</i>	50 ± 10	25.0	0.9	36.5	0.1	8.06	0.06	382	69	1794	75	233	32	2038	45	2368	3	18.24	0.67	26.6	1.4	8.05	0.08	415	58	[11]								
FC-12b	<i>G. menardii</i>	65 ± 10	24.1	1.1	36.4	0.1	8.02	0.06	438	72	1850	75	209	32	2072	45	2365	4	17.69	0.62	24.8	1.4	7.97	0.06	514	68	[13]								
FC-12b	<i>N. dutertrei</i>	40 ± 10	25.3	0.6	36.5	0.0	8.10	0.06	350	64	1756	75	249	31	2015	46	2369	2	18.75	0.71	25.0	1.4	8.11	0.04	350	52	[13]								
FC-13a	<i>G. ruber</i> (white ss)	20 ± 20	27.1	1.1	36.7	0.1	8.10	0.03	343	27	1724	43	263	17	1996	26	2371	2	19.00	0.37	27.5	1.4	8.11	0.04	351	29	[1]	8.05	0.09	417	32	[2]			
FC-13a	<i>T. sacculifer</i> (w/o sacc)	45 ± 20	25.7	0.7	36.6	0.0	8.07	0.03	380	34	1782	38	239	16	2032	23	2371	2	18.86	0.45	30.6	1.4													
FC-13a	<i>P. obliquiloculata</i>	50 ± 10	25.4	1.2	36.6	0.1	8.06	0.05	391	59	1797	66	233	29	2041	40	2370	4	18.31	0.57	28.9	1.4	8.08	0.08	385	55	[11]								
FC-13a	<i>G. menardii</i>	55 ± 10	25.1	1.3	36.6	0.1	8.04	0.05	409	65	1815	69	225	30	2052	41	2369	5	18.04	0.56	18.8	1.4	7.98	0.04	503	68	[13]								
FC-13a	<i>N. dutertrei</i>	150 ± 20	19.4	2.3	36.0	0.1	7.80	0.03	766	45	2056	37	118	15	2199	25	2348	1	15.37	0.27	19.5	1.4	7.79	0.08	811	101	[13]								
<b>Pacific Ocean</b>																																			
WP07-a	<i>G. ruber</i> (white ss)	100±20	26.1	2.4	35.2	0.4	8.05	0.05	387	51	1753	81	224	31	1988	52	2305	7	18.21	0.64	27.0	1.4	8.03	0.05	426	32	[1]	7.80	0.16	778	52	[2]			
WP07-a	<i>T. sacculifer</i> (sacc)	80 ± 20	27.4	2.2	35.0	0.5	8.08	0.05	357	56	1708	89	242	33	1960	58	2303	10	18.68	0.65	27.3	1.4	7.99	0.04	478	63	[3]	8.13	0.04	324	49	[4]			
WP07-a	<i>T. sacculifer</i> (w/o sacc)	125 ± 20	24.7	1.8	35.4	0.2	8.03	0.00	413	30	1797	31	209	9	2017	23	2311	10	17.80	0.23	28.4	1.4	8.03	0.05	427	58	[3]	7.92	0.08	573	73	[4]			
WP07-a	<i>O. universa</i>	75 ± 25	27.7	2.6	34.9	0.6	8.09	0.07	349	68	1696	110	247	39	1953	73	2303	15	18.78	0.83	28.2	1.4	8.10	0.04	352	52	[8]								
WP07-a	<i>P. obliquiloculata</i>	125 ± 25	24.7	3.6	35.4	0.4	8.03	0.02	413	30	1797	80	209	26	2017	56	2311	18	17.82	0.48	24.6	1.4	8.03	0.08	430	58	[11]								
WP07-a	<i>N. dutertrei</i>	165 ± 20	20.6	3.8	35.5	0.2	8.03	0.01	408	10	1855	44	189	18	2057	26	2322	0	17.34	0.45	26.4	1.4	8.09	0.06	369	50	[13]								
WP07-a	<i>G. tumida</i>	180 ± 20	18.7	5.0	35.4	0.2	8.04	0.01	403	13	1877	58	180	24	2070	35	2322	0	17.23	0.56	21.2	1.4	8.05	0.06	406	53	[13]								

\* uncertainties calculated using Henehan's 2016 R code

\*\* propagated uncertainty on pH including d11B, temperature, salinity uncertainties

\*\*\* propagated uncertainty on pCO<sub>2</sub> including d11B, temperature, salinity, Alk uncertainties